

Springer Theses

Recognizing Outstanding Ph.D. Research

Simone Milanolo

Sources and Transport of Inorganic Carbon in the Unsaturated Zone of Karst



Springer

Springer Theses

Recognizing Outstanding Ph.D. Research

Aims and Scope

The series “Springer Theses” brings together a selection of the very best Ph.D. theses from around the world and across the physical sciences. Nominated and endorsed by two recognized specialists, each published volume has been selected for its scientific excellence and the high impact of its contents for the pertinent field of research. For greater accessibility to non-specialists, the published versions include an extended introduction, as well as a foreword by the student’s supervisor explaining the special relevance of the work for the field. As a whole, the series will provide a valuable resource both for newcomers to the research fields described, and for other scientists seeking detailed background information on special questions. Finally, it provides an accredited documentation of the valuable contributions made by today’s younger generation of scientists.

Theses are accepted into the series by invited nomination only and must fulfill all of the following criteria

- They must be written in good English.
- The topic should fall within the confines of Chemistry, Physics, Earth Sciences, Engineering and related interdisciplinary fields such as Materials, Nanoscience, Chemical Engineering, Complex Systems and Biophysics.
- The work reported in the thesis must represent a significant scientific advance.
- If the thesis includes previously published material, permission to reproduce this must be gained from the respective copyright holder.
- They must have been examined and passed during the 12 months prior to nomination.
- Each thesis should include a foreword by the supervisor outlining the significance of its content.
- The theses should have a clearly defined structure including an introduction accessible to scientists not expert in that particular field.

More information about this series at <http://www.springer.com/series/8790>

Simone Milanolo

Sources and Transport of Inorganic Carbon in the Unsaturated Zone of Karst

Doctoral Thesis accepted by
University of Nova Gorica, Slovenia

 Springer

Author

Dr. Simone Milanolo
Hydro-Engineering Institute
Sarajevo
Bosnia and Herzegovina

Supervisors

Prof. Frank McDermott
School of Earth Sciences, Science Centre
University College Dublin
Belfield, Dublin 4
Ireland

Prof. Franci Gabrovšek
Karst Research Institute ZRC SAZU
Postojna
Slovenia

Thesis endorsed by Prof. Wolfgang Dreybrodt

ISSN 2190-5053

Springer Theses

ISBN 978-3-319-29307-3

DOI 10.1007/978-3-319-29308-0

ISSN 2190-5061 (electronic)

ISBN 978-3-319-29308-0 (eBook)

Library of Congress Control Number: 2015960777

© Springer International Publishing Switzerland 2016

This work is subject to copyright. All rights are reserved by the Publisher, whether the whole or part of the material is concerned, specifically the rights of translation, reprinting, reuse of illustrations, recitation, broadcasting, reproduction on microfilms or in any other physical way, and transmission or information storage and retrieval, electronic adaptation, computer software, or by similar or dissimilar methodology now known or hereafter developed.

The use of general descriptive names, registered names, trademarks, service marks, etc. in this publication does not imply, even in the absence of a specific statement, that such names are exempt from the relevant protective laws and regulations and therefore free for general use.

The publisher, the authors and the editors are safe to assume that the advice and information in this book are believed to be true and accurate at the date of publication. Neither the publisher nor the authors or the editors give a warranty, express or implied, with respect to the material contained herein or for any errors or omissions that may have been made.

Printed on acid-free paper

This Springer imprint is published by SpringerNature

The registered company is Springer International Publishing AG Switzerland

Parts of this thesis have been published in the following journal articles:

Milanolo, S., Gabrovšek, F., 2015. Estimation of carbon dioxide flux degassing from percolating waters in a karst cave: Case study from Bijambare cave, Bosnia and Herzegovina. *Chemie Erde—Geochemistry* 75(4), 465–474. DOI:[10.1016/j.chemer.2015.10.004](https://doi.org/10.1016/j.chemer.2015.10.004)

Milanolo, S., Gabrovšek, F., 2009. Analysis of Carbon Dioxide Variations in the Atmosphere of Srednja Bijambarska Cave, Bosnia and Herzegovina. *Boundary-Layer Meteorology* 131, 479–493. DOI:[10.1007/s10546-009-9375-5](https://doi.org/10.1007/s10546-009-9375-5)

Milanolo S., Mulaomerović J., 2008. Speleološka istraživanja na području “Zaštićenog pejzaža Bijambare” (Speleological researches on the territory of the “Protected landscape Bijambare”). *Naš Krš* 40–41, 3–24.

Supervisors' Foreword

Karst encompasses a significant part of our planet's surface. This is a large territory fraction with specific hydrological conditions, morphologies, landscapes, and an outstanding surface and underground biodiversity. It is the primary source of drinking water for many populations worldwide and an archive of data about our past climatic conditions which are stored layer after layer in cave stalagmites. Inorganic carbon, in the form of carbon dioxide in the gas phase, carbonate–bicarbonate ions in water solution, and calcium carbonate in the limestone rock, is the key player in shaping surface and underground karst features. Mass transport phenomena, storage, and chemical equilibriums govern the fluxes between air–water–rock compartments and along the vertical profile of an idealized karst massif. This thesis provides an overview of these fluxes and the underlining governing mechanisms linking together different scientific topics into a unique conceptual framework. However, it provides not only a review of the existing state of the art and available literature but also important new experimental evidence, and it develops and tests new modeling approaches to quantify these fluxes and dynamics. Overall, this thesis represents a valuable reference for scholars interested in karst and in the details of hydrology and hydrogeology, paleoclimate studies on cave speleothems, cave climate and show cave management, and on aspects of global carbon cycle involving the weathering of carbonate rocks.

Dublin, Ireland
Postojna, Slovenia
January 2016

Prof. Frank McDermott
Prof. Franci Gabrovšek

Acknowledgements

This Ph.D. would not be possible without the support, more or less formal, of many organizations, colleagues, and friends. To all of them I owe a lot.

The present work and speleological researches in Bijambare region have been started within the project lead by COOR/CESD in collaboration with Sarajevo Šume: “Construction of Bijambare vacation complex: Phase I.” The project has been financed by the European Community and Kanton Sarajevo. My Ph.D. study was also co-financed by the Slovenian Ministry of Education, Science and Sport. I would like to thank also the Bijambare protected area management (JU Zašticena prirodna područja Kantona Sarajevo) and rangers for allowing to access and work in the cave and surrounding area. Outside temperature data were obtained as part of the project C6 (Climatic Changes and Carbon Cycle in Canyons and Caves) for which I have to thank Paolo Madonia (Istituto Nazionale di Geofisica e Vulcanologia—Palermo). Handheld carbon dioxide meter was kindly borrowed from “Speleološka udruga Vjetrenica–Popovo polje” thanks to Ivo Lučić. Centre for Research and Sustainable Development of Karst within the Academy of Sciences and Arts of Bosnia and Herzegovina contributed by providing a field pH meter and few temperature loggers. The determination of Radon concentrations and other microclimatic characteristics of the cave were possible thanks to the cooperation with Prof. Vanja Radolić, Department of Physics, University of Osijek; Doc. Dalibor Paar, Department of Physics, Faculty of Science, University of Zagreb; and Doc. Nenad Buzjak, Department of Geography, Faculty of Science, University of Zagreb. Isotope analysis has been performed by Doc. Sonja Lojen at the Department of Environmental Sciences, Jožef Stefan Institute (Ljubljana–Slovenia). I’m grateful to the Federal Hydro-meteorological Institute of Bosnia and Herzegovina for providing meteorological data from the Sarajevo station. I’m thankful to Prof. Tarik Kupusović, director of the Hydro-Engineering Institute Sarajevo, the place where I work, for the kind support since the very beginning of this work, and because he allowed me to use the laboratory for all necessary chemical analyses. I’m also grateful to all my colleagues at HEIS for the help and fruitful discussions. A special thanks to Prof. Galiba Sijarić for the help and

enthusiasm during most of the sampling campaign. I want to especially thank Prof. Franci Gabrovšek, Karst Research Institute (Postojna–Slovenia), and Prof. Frank McDermott, University College Dublin (Dublin–Ireland), both Mentors of this thesis, for the assistance and patience during these long years of ups and downs.

I cannot forget to mention here the speleological groups where my passion for underground researches matured: Gruppo Grotte Novara (Novara–Italy) and the Centar za krš i speleologiju (Center for karst and speleology, former Speleo Dodo, Sarajevo) and especially to Cella Giandomenico and Jasminko Mulaomerović, a kind of twin mentors for my speleological career.

I have to admit that if I arrived to these points it is mostly because my parents never had any doubts about my capacities and never stop supporting me even when I took decisions apparently “unconventional” or I was almost ready to give up everything. I hope I will be able to live up to their example with my young daughters.

Last but not least, I would like to dedicate a special acknowledgement to my wife Amila, for being the one who pushed me into and through all of this. I know she is the happiest person (after me) knowing that this Ph.D. is finally over. At the very end came Nadia and Senem: I’m happy my daughters arrived just on time to enjoy the end of this adventure.

Contents

1	Introduction	1
1.1	Thesis Background	1
1.2	Thesis Goals and Approach	3
1.2.1	Thesis Objective	3
1.2.2	Project Goals	3
1.2.3	Beneficiary Fields of Research	3
1.2.4	Timeframe	4
1.2.5	Spatial Framework	4
1.2.6	Thesis Approach	4
1.3	Thesis Structure	5
	References	6
2	Site Description	7
2.1	General Overview of the Area	7
2.1.1	Bijambare Protected Landscape	7
2.1.2	Geology	9
2.1.3	Hydrology	12
2.1.4	Climatic Characteristics	13
2.2	Caves	17
2.2.1	Speleological Explorations	17
2.2.2	Srednja Bijambarska Pećina	19
	References	22
3	Materials and Methods	23
3.1	Introduction	23
3.2	Atmospheric Parameters	24
3.2.1	Cave Monitoring System	24
3.2.2	Gemini Tinytag Data Loggers	24
3.2.3	USB Stick Sensors	27
3.2.4	Diver and Baro Sensors	28
3.2.5	Air Velocity Sensor	29
3.2.6	Handheld Carbon Dioxide Sensors	29

- 3.2.7 Radon Detectors 30
- 3.2.8 Air Sensors Location 31
- 3.3 Water Analysis 31
 - 3.3.1 Sampling and Sample Handling 31
 - 3.3.2 Discharge Rate. 33
 - 3.3.3 Chemical Analysis 35
 - 3.3.4 The Location of Water Sampling Sites 37
- 3.4 Calcite Deposition 38
 - 3.4.1 Determination of Calcite Deposition Rate 38
 - 3.4.2 Location of Measurement Sites for Calcite Deposition. 41
- 3.5 Isotopic Composition 42
- References 42
- 4 A Conceptual Model of the Inorganic Carbon Transport Within a Karst Massif 43**
 - 4.1 Karst and the Global Carbon Cycle 44
 - 4.2 The Equilibria of the H₂O–CO₂–CaCO₃ System. 45
 - 4.3 Open and Closed Systems. 47
 - 4.4 The Calcium Carbonate Dissolution and Precipitation 48
 - 4.5 Water and Inorganic Carbon in a Karst Massif. 50
 - 4.5.1 The Soil 50
 - 4.5.2 The Epikarst and Vadose Zone 51
 - 4.5.3 The Phreatic Zone 52
 - 4.6 Conclusions. 54
 - References 55
- 5 Cave Climate 59**
 - 5.1 Introduction. 59
 - 5.2 Results and Discussion 60
 - 5.2.1 Historical Data. 60
 - 5.2.2 Temperature 61
 - 5.2.3 Climatic Regimes. 63
 - 5.2.4 Developing an Internal–External Temperature Semi Empiric Relationship 65
 - 5.2.5 Linear Regression Results 66
 - 5.2.6 Relative Humidity 68
 - 5.2.7 Carbon Dioxide 69
 - 5.2.8 Radon Concentration 70
 - 5.3 Conclusions. 71
 - References 71

6 Carbon Dioxide Sources, Storage and Transport in the Cave Atmosphere 73

6.1 Introduction 73

6.2 Carbon Dioxide Concentration Variability in the Cave Atmosphere 74

6.2.1 Seasonal and Diurnal Variability 74

6.2.2 Spatial Variability 75

6.2.3 Vertical Distribution 77

6.3 Modelling 78

6.3.1 Model Description 78

6.3.2 Model Regression 79

6.4 Discussion 83

6.4.1 Ventilation Rate 83

6.4.2 Natural Input 84

6.4.3 Concentration in the Inlet Stream 85

6.4.4 Anthropogenic Input 86

6.4.5 Model Sensibility to Data Selection 86

6.5 Conclusions 87

References 87

7 Cave Atmosphere Response to Artificial Input of Carbon Dioxide 89

7.1 Introduction 89

7.2 The Experimental Set-Up 90

7.3 Results 93

7.3.1 Temperature Records 93

7.3.2 Pressure Records 93

7.3.3 Air Velocity 94

7.3.4 Carbon Dioxide Concentration Records 94

7.3.5 Results Interpretation by Cave Climatic Regimes 94

7.4 Modeling 96

7.4.1 The Dynamics of Carbon Dioxide Release 96

7.4.2 Modelling Approaches 97

7.4.3 Approach 1 98

7.4.4 Approach 2 98

7.5 Discussion 101

7.5.1 Diffusion, Turbulence and Cave Atmosphere Mixing 101

7.5.2 Model Results 103

7.5.3 Model Sensitivity to “Music Hall” Volume 104

7.6 Conclusions 105

References 106

8	From Soil to Cave: The Inorganic Carbon in Drip Water	107
8.1	Introduction.	107
8.2	Results	108
8.2.1	Drip Sites	108
8.2.2	Pool Water	110
8.3	Discussion.	112
8.3.1	The Characteristics and Classification of Drip Sites . . .	112
8.3.2	The Evolution from Soil to Sampling Point	115
8.3.3	The Evolution from Dripping Site to the Equilibrium with Cave Environment	118
8.3.4	The Fluxes of Carbon Dioxide.	119
8.4	Conclusions.	122
	References	123
9	Calcite Deposition	125
9.1	Introduction.	125
9.2	Precipitation Rate Theory	126
9.3	Results	129
9.4	Discussion.	131
9.4.1	Parameters Controlling Calcite Deposition	131
9.4.2	Predicted Growth Rates.	132
9.4.3	Impact of Droplet Splashing on the Measured Deposition Rates	134
9.4.4	Impact of the Incomplete Solution Equilibration Process on the Measured Deposition Rates	140
9.5	Conclusions.	140
	References	141
10	The Isotopic Imprint	143
10.1	Introduction.	143
10.2	The Carbon Stable Isotopic Composition of Drip Water	144
10.3	Results	145
10.4	Discussion.	146
10.5	Conclusions.	149
	References	150
11	General Conclusions.	153
11.1	Summary of the Inorganic Carbon Fluxes in the Unsaturated Zone	153
11.2	Scale-Up to Global Level	155
11.3	Open Questions and Further Research Possibilities	155
	Reference	157

Chapter 1

Introduction

Abstract Karst is a distinctive landscape with specific surface morphologies and underground water drainage systems created by the fast dissolution of the rock (carbonate based rocks such as limestone, dolomite, marble and evaporite rocks). Worldwide, it accounts for around 20 % of the dry surface (excluding that part of the Earth covered by ice caps). Carbonate karst alone extends over around 10–15 % of the continental area, and provides water supply for approximately one fourth of the world’s population. In the case of carbonate rocks such as limestone, formation of karst features involves a complex interaction between the calcium carbonate in the rock, the carbonate and bicarbonate ions, carbonic acid, dissolved carbon dioxide in the percolating water and carbon dioxide in the gas phase. The total carbon in these forms is referred to as Inorganic Carbon (IC), while the IC fraction in water species is named Dissolved Inorganic Carbon (DIC). The main aim of this thesis is to contribute to a better understanding of the inorganic carbon path inside a limestone massif. This is achieved by identifying the functional compartments and mechanisms for its transport and by quantifying the different fluxes, assessing their relative contributions and their seasonal variations. This work has potential implications in several related fields of research such as Earth’s carbon cycle, paleoclimate studies, anthropogenic impact on the karst environment and cave genesis.

1.1 Thesis Background

Karst is defined as: “*A terrain with distinctive landforms and drainage arising from greater rock solubility in natural water that is found elsewhere*” (Jennings 1985) or “*... a special style of landscape containing caves and extensive underground water systems that is developed on especially soluble rocks such as limestone, marble, and gypsum*” (Ford and Williams 2007, p. 1). In general, the majority of definitions available in the literature stress on the link between the peculiar surface morphologies the underground water drainage system and their genesis processes due to fast dissolution of the rock.

Two families of rocks have been traditionally considered the substrate for developing of karst processes: carbonate rocks (limestone, dolomite, marble) and evaporites (mostly gypsum and to a minor extent, halite). However, in extreme cases, with enough time available and specific climatic conditions, other barely soluble rocks can also develop morphologies typical of a karst region (as proven for example by the exploration of large caves in quartzite on the Venezuelan Tepuis).

Worldwide, relatively soluble rocks comprise around 20 % of the dry surface (excluding that part of the Earth's surface covered by ice caps), while carbonate karst alone accounts for around 10–15 % of continental area (Ford and Williams 2007, p. 5). It can be further estimated that almost one fourth of the world's population depends directly or indirectly on karst aquifers for their drink water supply (Ford and Williams 2007, p. 441).

The word karst was originally used to describe stony desert landscapes or barren grounds (specifically, in its classical definition, the northern region of the Dinaric Alps across the Italian and Slovenian border), sometimes associated with a negative connotation due to unproductiveness or harsh living conditions. Nowadays, thanks to the expanding of knowledge, the perception of the value of this kind of territory shifted towards *“a unique, non-renewable resource with significant biological, hydrological, mineralogical, scientific, cultural, recreational, and economic values”* (British Columbia, Ministry of Forestry 2003, p. 6).

Karst specific surface morphologies have dimensions covering several orders of magnitudes: from a scale of centimeters to several kilometers. These include features such as: runnels, flutes, clints, dolines, ponors, blind valleys and poljes. Below the ground, karst presents a highly developed, hierarchically structured, drainage network which often completely replaces the surface hydrology. Caves are the largest branches of these systems, very often abandoned by water in favor of other channels located to lower levels. More generally, caves are defined from a slightly anthropocentric biased standpoint as *“a natural opening formed in the rocks below the surface of the ground large enough for a man to enter”* (Field 2002). Caves are valuable repositories of information on geological, morphological, climatic and human history as well as for the evolution of species. For example, researchers have used caves sediments as proxies to retrieve paleoclimate evidences of past ages, or to investigate species living in their highly specialized habitats and environments.

As mentioned before, in karst, both surface forms and underground voids are generated by the fast dissolution of the rock. In the case of carbonate rocks such as limestones, mechanisms involve a complex system of chemical equilibria between the calcium carbonate in the rock, carbonate ion, bicarbonate ion, carbonic acid and dissolved carbon dioxide in the percolating water and carbon dioxide in the gas phase (usually the carbon dioxide rich gas phase generated by plant root respiration and organic matter biodegradation in the soil layer and in the rock voids). The carbon included in all these compounds is named “Inorganic Carbon” (IC) to distinguish it from the “Organic Carbon” contained in biological matter (OC). The fraction of carbon contained by a filtered water solution is termed “Dissolved Inorganic Carbon” (DIC).

1.2 Thesis Goals and Approach

1.2.1 Thesis Objective

The main aim of this thesis is to contribute to a better understanding of the inorganic carbon path inside a limestone massif by identifying the functional compartments and mechanisms for its transport and then by quantifying the different fluxes, assessing their relative contributions and their seasonal variations.

1.2.2 Project Goals

The thesis objectives divide into three main goals as follows:

- A. To identify the main inorganic carbon functional compartments and their relationships within a karst massif.
- B. To identify the physical and chemical mechanisms responsible for the transport of inorganic carbon between the compartments identified above but with special emphasis on the unsaturated zone.
- C. To develop conceptual and mathematical models to describe the mechanisms identified in point B above and then to quantitatively estimate several of the fluxes of inorganic carbon in the unsaturated zone.

1.2.3 Beneficiary Fields of Research

This work has potential implications in several related fields of research:

- *Earth carbon cycle*: providing qualitative and quantitative data on the role of karst and specific karst processes in the global carbon balance.
- *Paleoclimate studies*: providing insights on mechanisms potentially effecting speleothems growth rates and composition, thereby helping to build a more robust relationship between the analyzed proxies and climatic conditions.
- *Anthropogenic impact on the cave environment*: The contribution of CO₂ from tourist respiration will be evaluated within the model of CO₂ balance in the cave atmosphere.
- *Caves genesis*: In addition to contribution on the study of speleothems growth controlling factors, this thesis, provide insights into carbon dioxide distribution within a limestone massif, it may also be relevant for studies of early underground conduits network evolution and cave development models.

1.2.4 Timeframe

The project is based on 4 years and 4 months of field data (October 2006 to February 2011), and therefore it encompasses near-past to present-day conditions only. The quantitative results may be projected into the past only as long as the climatic and morphological conditions have been similar to the present day settings. However, it is expected that conceptual models developed in this thesis are of more general validity and may also be adapted in other conditions theoretically up to early stages of karst development and caves genesis.

1.2.5 Spatial Framework

Due to easy access and its central location within the karst vertical profile most of measurements and experiments have been performed in a cave (Srednja Bijambarska pećina—Bosnia and Herzegovina). For this reason the unsaturated zone of karst will be the core of this thesis and the soil and phreatic regions will be included, but only where necessary to define the boundary conditions.

1.2.6 Thesis Approach

The thesis primary aim is to analyze the inorganic carbon path through a limestone massif entirely, following an ideal path of water infiltrating into the soil, penetrating through the first layer of highly fissured rock deep into the unsaturated zone, and then entering the phreatic zone. Of course the analysis can only be carried out in detail by delineating sub regions and boundaries within the vertical profile and studying them separately. Unfortunately most of the sections of a karst massif are hardly if not accessible at all for direct measurements, and they can only be studied indirectly. Models and results obtained under these conditions are consequently very often based on hypothesis and assumptions affecting the overall confidence in the outcome. To partially overcome this problem, after studying separately different sections of the overall inorganic path across the limestone massif, a holistic approach can be used to test the validity of obtained results. In fact, the analyzed regions needs to be re-connected to each other in order to exchange inorganic carbon, and therefore the results obtained from independent models developed for different regions or compartments must be coherent at these interfaces. Assessing this level of consistency can give insight on the overall validity of the approach. The experimental part of this thesis was mainly focused at three different compartments covering the three different “forms” of inorganic carbon:

- Air (cave and soil atmospheres): carbon dioxide.
- Water (dripping and cave pools water): mainly bicarbonate anion.
- Rock (limestone rock and speleothems): calcium carbonate.

1.3 Thesis Structure

Based on the approach described in the previous paragraph, the main goals given in Sect. 1.2.2 are further divided into several subtasks representing the thesis structure skeleton:

- Review of the existing literature on carbon dioxide in the soil, epikarst, cave atmosphere and saturated zone. This also includes references on other sources or sinks of inorganic carbon, such as dissolution of limestone and precipitation of speleothems.
- Development of a conceptual model for carbon dioxide and inorganic carbon transport within a karst massif.
- Air compartment which has been further breakdown into:
 - Collection of data on cave air quality;
 - Development of a conceptual model of cave climate;
 - Development of a mathematical model based on the CO_2 balance;
 - Validation of the model and estimation of the fluxes of CO_2 sources and sinks.
- Water compartment which has been further breakdown into:
 - Collection of data on the chemical composition of water at drip sites and pools;
 - Development of a method to estimate the initial carbon dioxide concentration in the soil and in the percolating water;
 - Estimation of the amount of inorganic carbon transported towards the saturated zone;
 - Estimation of the amount of carbon dioxide release to the cave environment.
- Rock compartment which has been further breakdown into:
 - Collection of data on limestone precipitation using glass tablets;
 - Estimation of the amount of inorganic carbon transferred to the water by limestone dissolution based on the drip water analysis;
 - Estimation of the amount of inorganic carbon fixed by speleothems deposition.

- Mass balance:
 - Based on the general conceptual model and the results obtained by “air”, “water” and “rock” analysis, the creation of a draft balance of carbon dioxide applied to the cave environment.
 - Assessment of the level of consistency of results obtained by different models.

References

- British Columbia, Ministry of Forestry (2003) Karst management handbook for British Columbia
- Field MS (2002) A lexicon of cave and karst terminology with special reference to environmental karst hydrology. U.S. Environmental Protection Agency National, Center for Environmental Assessment, Washington
- Ford DC, Williams PW (2007) Karst hydrology and geomorphology. Wiley, Hoboken
- Jennings JN (1985) Karst geomorphology. Basil Blackwell, Oxford

Chapter 2

Site Description

Abstract The Bijambare protected area is located around 25 km north of Sarajevo, and nowadays encompasses 490 ha of coniferous forest and meadows as well as several karst features. The average elevation is between 900 and 950 m. Available climatic data are limited, but based on a few partial sources an average temperature of 6.2 °C and precipitation of 917 mm year⁻¹ can be estimated. At the contact between Triassic impermeable quartz sandstone and limestone, waters from two main streams sink underground before re-emerging at the Orlja spring. In the area there are 8 known caves and, among them, Srednja Bijambarska cave is the longest (533 m of explored passages) and adapted as show cave. Srednja Bijambarska cave has a relatively simple morphology that for the scope of this work can be divided into 4 elements: the entrance section, the main channel, the narrow passage and the “Music hall”.

2.1 General Overview of the Area

2.1.1 *Bijambare Protected Landscape*

Bosnia and Herzegovina (BiH) shares a large portion of Dinaric karst and carbonate rocks cover around 65 % of its territory (Čičić 1998). Nevertheless, karst and karst features represent at present the most undervalued and understudied portion of this country (excluding places where hydropower, forestry and ore extraction interests prevail).

The Bijambare area (Fig. 2.1) is located around 25 km due north of Sarajevo, and around 40 km by car. The region represents the North edge of the Nišići highland (around 900–950 m a.s.l.) and at the same time one of the last carbonate

Material from this chapter has been originally published in Milanolo S, Mulaomerović J (2008) Speleološka istraživanja na području “Zaštićenog pejzaža Bijambare” (Speleological researches on the territory of the “Protected landscape Bijambare”). Naš Krš 40-41: 3–24.

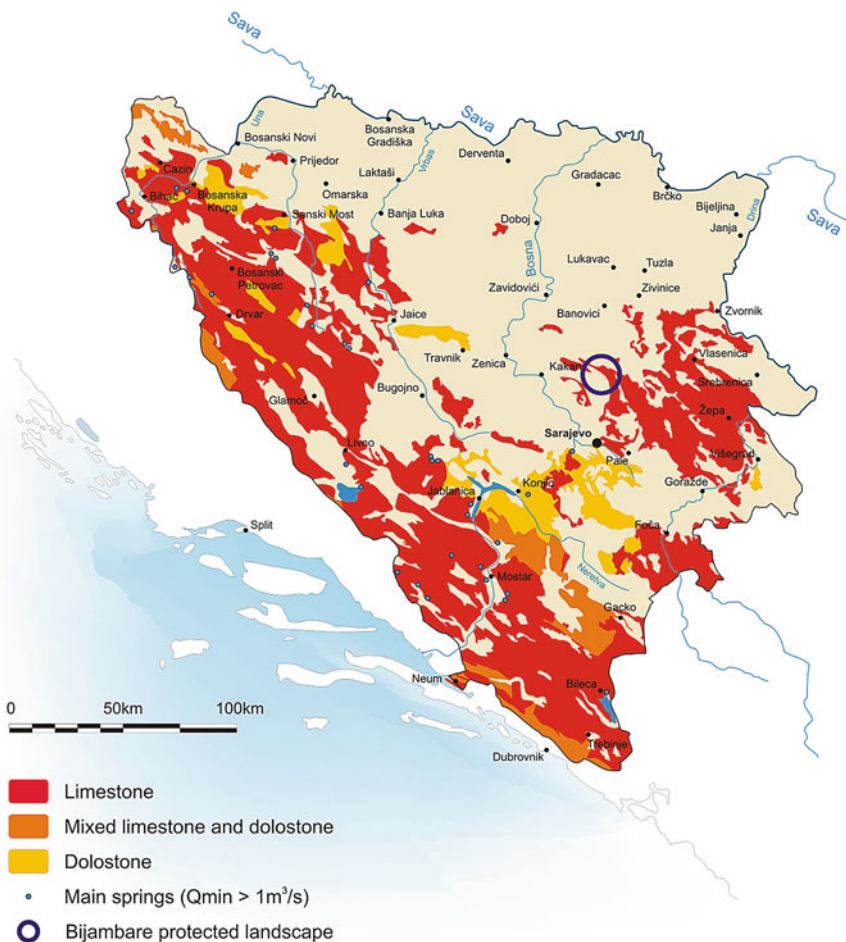


Fig. 2.1 Overview of main carbonate outcrops in Bosnia and Herzegovina. Redesigned and simplified from the 1:500,000 hydrogeological map of former Yugoslavia

outcrops of the large karst area North-East of Sarajevo (mainly centered on the Romanija massif).

In late 2003, around 367 ha of coniferous forest, marshes, pastures, including several caves, swallow holes, dolines and other karst features were declared protected (see Figs. 2.2 and 2.3). This early surface has been expanded in 2009 to 490 ha.

Bijambare is at present one of the three protected areas within Sarajevo region (Kanton Sarajevo) and, based on protection level and aims it is classified as fifth level of IUCN scale: protected landscape (Dudley 2008).



Fig. 2.2 View of Bijambare protected landscape area from Gornja Bijambarska pećina (Upper Bijambare cave)

2.1.2 Geology

Based on the 1:100,000 geological map (Vareš and Vlasenica sheets), the area is characterized by almost parallel geological structures with approximate direction NNW-SSE. Starting from the west, up to 2 km from Bijambare caves, the bedrock is composed by chert—carbonate rocks from Jurassic-Cretaceous age, extending over large part of Nišići highland. Towards the Bijambare protected area, Triassic rocks trusted over the Jurassic-Cretaceous and therefore, proceeding east, it can be found Triassic quartz sandstones with few outcrops of middle Trias (Ladinic) limestone. Further east, Bijambare caves develop close to the hidden passage between quartz sandstone and lower Triassic (Anisic) limestone. This carbonate rocks strip has an average width of 1–2 km and it is further confined to the east by Jurassic marlstones and calcarenites and by another occurrence of Triassic quartz sandstone. Along current path of Bijelila creek, recent quaternary fluvial material has been deposited. A general overview of the Bijambare area geological settings is given in Fig. 2.4.

The Bijambare caves are located close to the hidden passage between the impermeable quartz sandstone and the limestone along a fault that dictates the direction of the last tract of Bijelila valley and as well of the touristic cave.

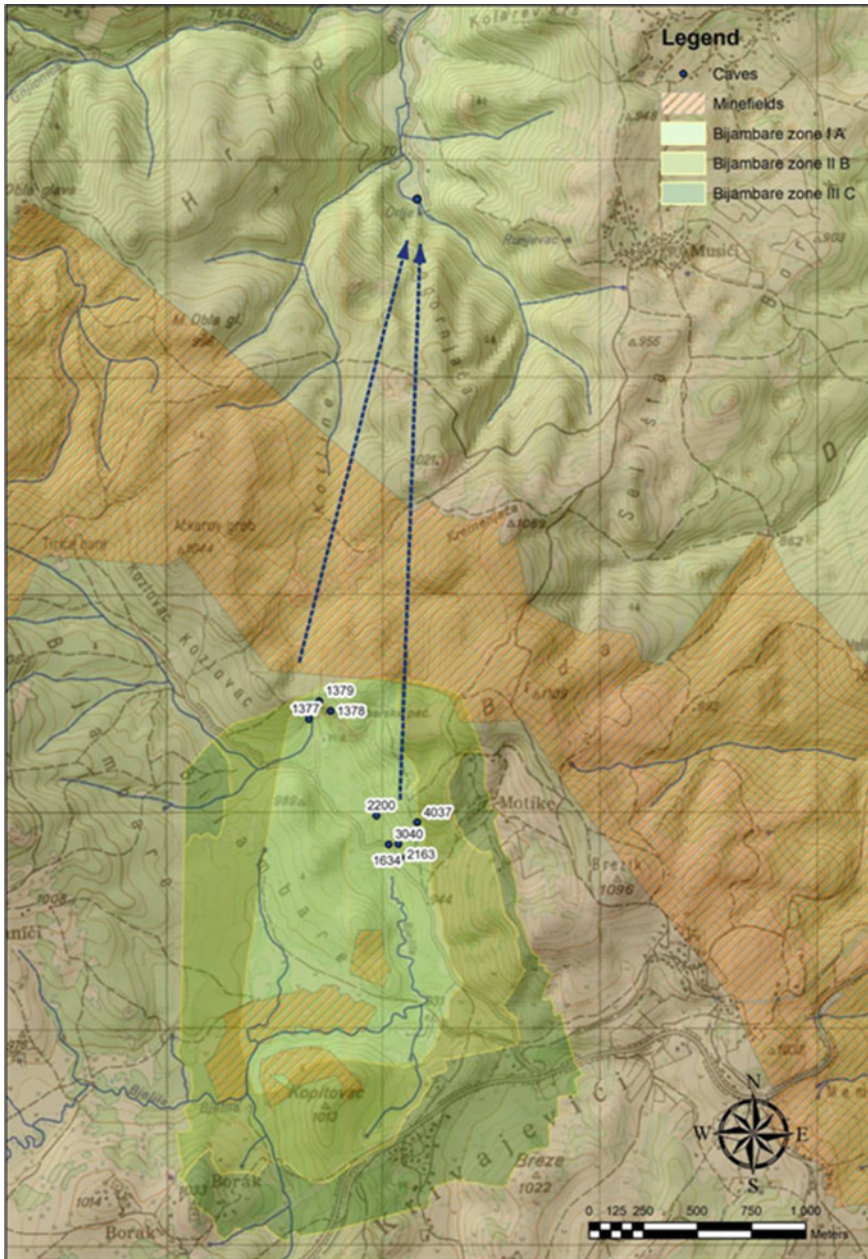


Fig. 2.3 The 2003 border of Bijambare protected area with internal zoning. Known caves are shown and labeled by their cadaster number. *Two dot lines* connect the main sinking streams to the Orlja spring

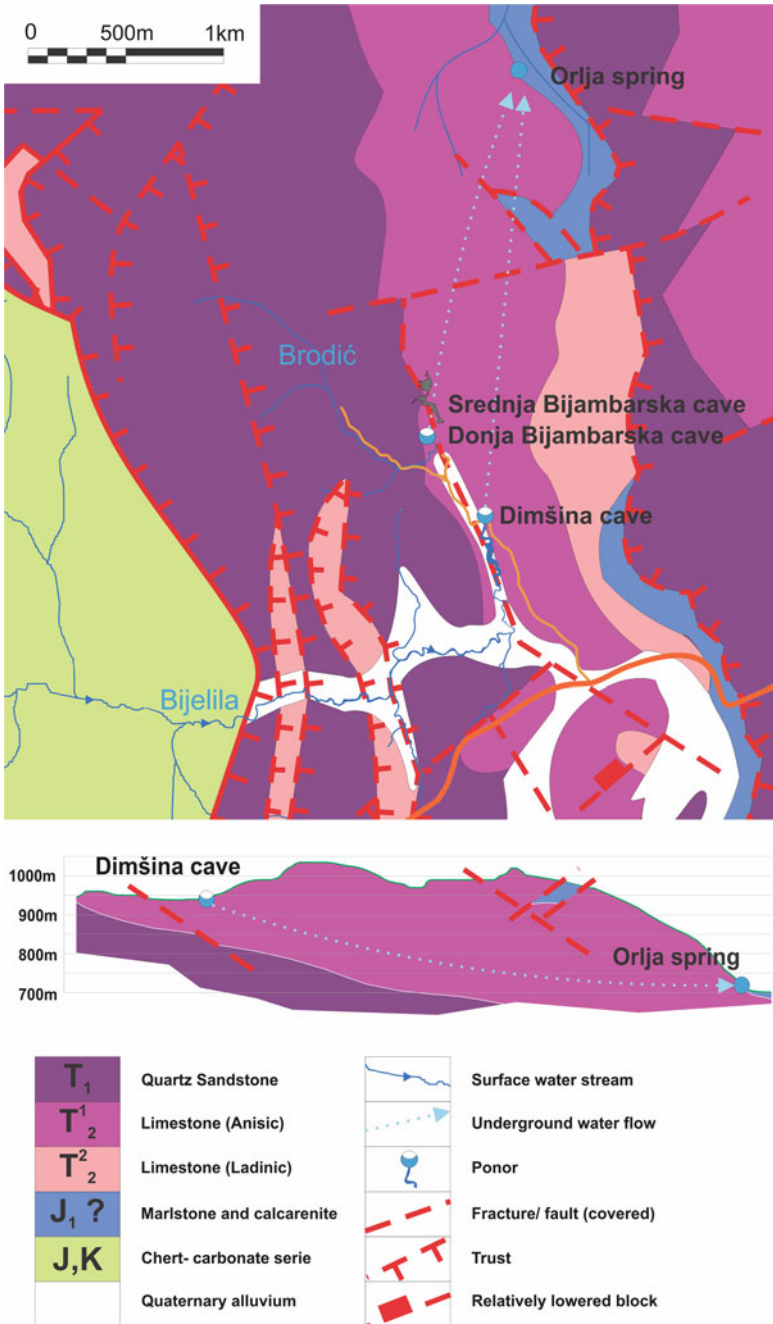


Fig. 2.4 Geological settings in the Bijambare region

Table 2.1 Analysis of a rock sample from Srednja Bijambarska pećina (Middle Bijambare cave).
Unpublished data

Element	Analysis result (%)
Humidity	0.09
Weight loss at 1100 °C	43.57
Calcium oxide (CaO)	52.74
Magnesium oxide (MgO)	1.63
Silicon dioxide (SiO ₂)	0.19
Phosphor oxide (P ₂ O ₅)	0.07
Iron (III) oxide (Fe ₂ O ₃)	0.15
Sulfates as SO ₃	0.09
Chlorides (Cl)	0.01
Total	98.54
CaCO ₃	94.40
MgCO ₃	3.40

An analysis of a rock samples from the Ledenjača cave shows a carbonate fraction over 99 %, where the remaining impurities were mainly clay (Milanolo et al. 2006). The same sample, under the microscope presented yellowish-reddish fractures probably due to the presence of iron.

Another rock sample taken from last chamber of the touristic cave was analyzed at HEIS laboratory in Sarajevo using standard gravimetric and volumetric methods. The results are presented in Table 2.1 (unpublished data).

Based on the geological map and rock analysis, it is evident that the main cave develops inside massive limestone with relatively low concentrations of magnesium and other impurities.

2.1.3 Hydrology

The hydrology of Bijambare area is dominated by two allogenic water streams: Bijelila and Brodić creeks, both originating from the adjacent area of impervious not carbonate rocks and sinking shortly after they reach a contact with limestone. Bijelila creek, whose watershed spans roughly 35 km² (COOR 2006) over the Nišići highlands, delivers the majority of the water contribution. Before sinking completely underground, it flows for around 500 m over carbonate rocks partially or completely covered by quaternary alluvial sediments and forming a temporary lake when the capacity of swallow hole is insufficient (e.g. heavy rain or snow melting periods).

A continuous record of water flow on this stream is not available and the only existing data (four measurements) report the range of flow rates between 26 and 191 L s⁻¹ (Đerković 1971; COOR 2006). In the tourist infrastructure reconstruction project report (COOR 2006), a correlation with the hydrological station on Stavnja

River (near Vareš) is presented (based on the three parallel measurements) and is used to estimate minimum and maximum flow of Bijelila creek.

The sinking area comprises several small ponors located over a wide area on the side of the temporary lake and a main sink connected with Dimšina cave. Furthermore, Ledenjača cave acts as ponor during extreme precipitation events.

Brodić creek with a catchment area of about 2.5 km² (COOR 2006) has approximately 10–15 times lower recharge than Bijelila creek. The three flow measurements range from 4 to 11 L s⁻¹.

The whole Brodić water stream sinks into Donja Bijambarska cave, located just below the touristic cave. Despite the lower water contribution, this sinking point is the largest (in the sense of portal dimensions) of the entire area, and in the past was equipped with a water mill just few meters before the cave entrance. Local people reported that during extreme precipitation events, water level may rise several meters flooding the entire cave. This is testified by several large wood pieces stacked to the cave roof and it points to a flow restriction in the underground channels.

Water sinking in the Bijambare protected area emerges at the surface at Orlja spring, around 2.5–3.0 km north and at 230 m lower elevation (Fig. 2.5). Connection has been verified by dye tracing Bijelila creek using 50 kg of natrium fluorescein. The tracer breakthrough time was 6 days, the peak concentration was recorded on the 7th day and maximal residence time of 20 days was detected (Đerković 1971). Fluorescein recovery was estimated to be around 81 %. Relatively long retention and dilution point to slow flow velocities, typical for small conduits and relatively large water storage volume. There are no data on other studies including autogenic water recharge from mountains and plateau located along the path from Bijambare to Orlja spring. During dye tracing test Đerković (1971) reported a flow of Bijelila creek of around 30 L s⁻¹ and a flow at spring of 100 L s⁻¹.

It should also be mentioned that, at the Orlja location, two springs are actually present and located only few ten of meters apart. One spring drains the water from Bijambare. The relatively cold water comes out from a siphon inside a short (4–5 m) cave. The second is mild thermal water used in a nearby swimming pool and spa which are nowadays abandoned. In Đerković (1971) there are no indications to assess if this source of thermal water was monitored during the dye tracing test and consequently if there is a cross-contamination between these two water sources.

2.1.4 Climatic Characteristics

Based on the general climate division of Bosnia and Herzegovina (Federalni Hidrometeorološki Zavod 2011), the Bijambare area belongs to the pre-mountain—mild continental zone. However, considering the relatively high elevation (around 1000 m a.s.l.), strong mountain-alpine type influence can also be expected. Based on the isotherms and isohyets from the vulnerability mapping of the territory of



Fig. 2.5 Orlja spring

Federation of Bosnia and Herzegovina (HEIS and IPSA 2008), an average temperature between 6 and 7 °C, and a yearly average precipitation between 1125 and 1375 mm can be expected (see Fig. 2.6).

Other sources of data can be derived directly from meteorological stations in Sarajevo (about 25 km South at the elevation of 630 m) or from Sokolac (30 km South-East at the elevation of 900 m). The station at Nišići only 3 km away has not been active since several decades.

During the project for the reconstruction of Bijambare vacation complex, a short analysis of climatic conditions was conducted (COOR 2006). The work is based on extrapolation of recorded temperatures from Sokolac meteorological station during the period 1962–1971, resulting in an average temperature of 6.2 °C, which is in agreement with the range provided by Fig. 2.6. The historical precipitation data recorded at Nišići meteorological station during years from 1970 to 1973 show an average yearly precipitation at Bijambare of 917 mm, which is significantly lower than the range provided by Fig. 2.6 and even lower than Sarajevo: 932 mm (Federalni Hidrometeorološki Zavod, bez datuma).

Temperature at Bijambare has been measured since late 2006 as a part of this study and the results are discussed in Chap. 5. Regarding precipitation, daily data have been retrieved from Sarajevo meteorological station since 2006 and presented in Fig. 2.7a. During the 5 years of this study a general increasing trend from 961 mm during 2006 to 1088 mm during 2010 can be noticed. Although the



Fig. 2.6 Average temperatures (white lines) and precipitations in the Bijambare region. Elaborated from data included in HEIS and IPSA (2008) (color figure online)

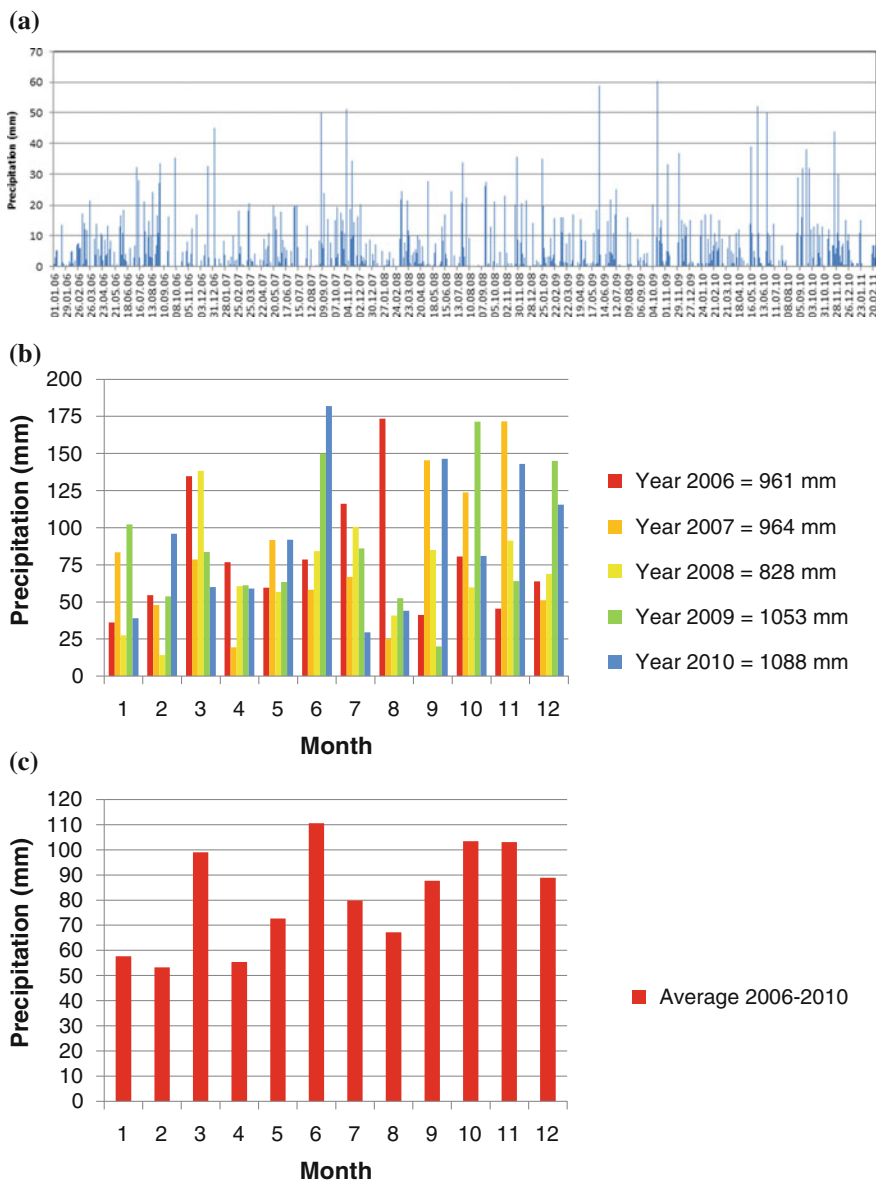


Fig. 2.7 a Daily precipitation at Sarajevo meteorological station for the period January 2006–February 2011; b Monthly precipitation for each single year; c Average monthly precipitation during the whole period

Bijambare reconstruction study (COOR 2006) estimated maximum amount of precipitation in July and minimum in December–January, at least from the period of this study data from the Sarajevo station cannot be fitted by any general seasonal

trend. From Fig. 2.7b it is evident how maximum precipitation occurred in August (2006), November (2007), March (2008), October (2009) and June (2010) while minimum precipitation occurred in: January (2006), April (2007), February (2008), September (2009) and July (2010). This does not exclude that a statistical analysis over a much longer period may show relevant seasonal trend. Average monthly precipitation values over the period 2006–2010 are presented in Fig. 2.7c.

Regardless of direct seasonality of precipitation, other phenomena, such as snow melting and evapotranspiration, surely introduce an important seasonal control on the water balance: the first, by accumulating water during the winter in the form of snow and then by releasing it during a relatively short period at spring while second by reducing the effective infiltration mainly during hot summer months.

2.2 Caves

2.2.1 *Speleological Explorations*

It is difficult to say when first speleological investigations of Bijambare caves commenced. The oldest signatures in the cave interior indicate the end of 19th century, when numerous foreign workers of Austro-Hungarian Monarchy came to Bosnia and Herzegovina and participated in exploitation of forest and mine resources, in construction of roads and railways. They are followed by members of first Bosnian and Herzegovinian hiking clubs, such as: “Prijatelji prirode” (Friends of nature), “Kosmos” (Cosmos) and HPD Bjelašnica, who left their signatures in Bijambare caves, as well as in many other caves in closer Sarajevo surroundings. Unfortunately, these first explorers did not leave any written documents, drawings or photographs.

The first popular texts about Bijambare area were written by famous Bosnian hikers Čurčić (1940) and Kumičić (1944) in the mountaineering periodical but during very unfortunate times—period of the World War II. The first more serious effort to evaluate the Bijambare area originates from the middle of 20th century, as part of the activities of the Republic Institute for Protection of Cultural Monuments and Natural Rarities of Bosnia and Herzegovina, especially in works of Rzehak (1958), Baucic and Rzehak (1959).

Within scientific circles, the Bijambare caves were of interest from the earliest 20th century. The coleopteran *Anthroherpon stenocephalum* from Srednja Bijambarska cave (Fig. 2.8a) was already described in the European scientific literature in 1901 (Apfelbeck 1901). Unfortunately, speleo-biological research almost ended there. Much later, continuing with the planned concept of expert evaluation of this area, Mirko Malez carried out significant pioneering speleological explorations of Gornja, Donja and Srednja caves, with excavations aimed at paleontological and archeological investigations (Malez 1968).

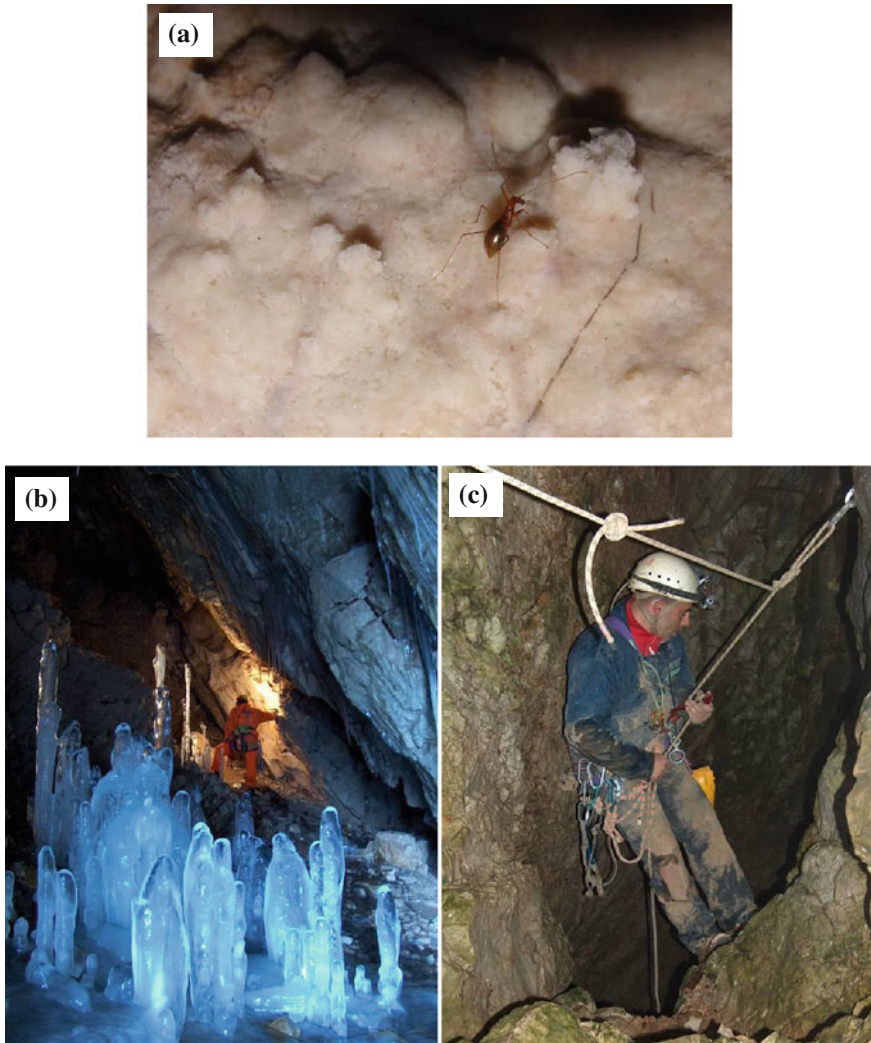


Fig. 2.8 a *Anthroherpon stenocephalum*; b Ice stalagmites in Donja Bijambarska cave; c Explorations in Dimšina cave

In the examined area, six caves were known and recorded before 2006 into the speleological cadaster (Mulaomerović et al. 2006). However, information for the Gornja and Srednja caves only were published in the scientific literature (mainly in the work of Malez 1968), while for all the other objects just the name and a few basic data were recorded.

In order to define an inventory of speleological objects in the area and to create valuable documentation for their protection and touristic evaluation, systematic

Table 2.2 Known speleological objects in the Bijambare protected area

Name	Cadaster N.	Length (m)	Depth (m)	Coordinates G.K.	Elevation (m)
Srednja (Glavna) Bijambarska ^a	1379	533	-24	6540707 E 4883506 N	959
Ledenjača	2200	323	-51	6540971 E 4882977 N	935
Donja Bijambarska	1377	148	+6/-11	6540660 E 4883422 N	930
Duricina	1634 ^b	142	-28	6541072 E 4882846 N	950
Gornja Bijambarska	1378	112	+10	6540759 E 4883460 N	980
Dimšina	3040 ^c	108	-30	6541028 E 4882845 N	935
Ledenica	2163	41	-18	6541083 E 4882784 N	940
Nova pećina	4037	28	-12	6541160 E 4882947 N	980

^aShow cave

^bThis cave is registered two times in cadaster: number 1554 with the name Djuricina pećina

^cInserted in cadaster as “Ponori Bijelila”

explorations have been carried out within the reconstruction project (Milanolo and Mulaomerović 2007, 2008).

Eight caves (see also Fig. 2.8b, c) have been identified; one of which was completely new to the literature. Basic data are summarized in Table 2.2.

2.2.2 *Srednja Bijambarska Pećina*

This cave is the longest speleological object in the area (533 m including branches) and it is currently used as show cave. A concrete path and illumination is provided along the majority of its length. Although it has been carefully explored in the past, the available survey (Malez 1968) covered only the main channel, without many details of the small lateral conduits. It should be noticed that, based on original protected area borders (as defined in 2003), more than half of the cave was outside the protected area borders, and thus its protection was not fully guaranteed. This situation has been fixed by extending protected area borders in 2009.

Srednja Bijambarska is morphologically simple (Fig. 2.9) and, based on previous published descriptions (Baucic and Rzehak 1959; Malez 1968), it comprises 5 sections: the entrance part and four connected halls.

In fact, the first three halls are part of a unique channel which extends to the north-west until it merges with another conduit entering from West. A narrow passage, which was partially enlarged by removing the floor sediments during the construction of the first tourist pathway, divides the main channel from the last chamber. This part (4th hall), due to its acoustics is named “Muzička Dvorana”

(Music Hall) and it was probably developed at the junction of several smaller channels (most of them with circular section) that are still partially visible as relicts on the hall ceiling.

The halls range in length from 30 to 80 m, and in width from 18 to 30 m. The height of the halls can reach over 12 m in the “Music Hall”. The whole cave is covered by a thick layer of fine cave sediment, over which different cave decorations, gours, stalagmites and calcite film have deposited.

Three lateral conduits should be mentioned:

- The first one, partially used for tourist visits, stretches to West before the narrow passage leading to the “Music Hall”. Its last part is characterized by small passages within rock blocks and it almost reaches the surface under a valley visible on the topographic map. Unfortunately, the surface above the cave is not accessible due to the presence of minefields. However, it is probable that this part of the cave acts as a temporary swallow hall during high precipitation events. During one visit in a heavy rainy period this channel contained a small water stream.
- The second lateral conduit is the natural continuation of the cave after the “Music Hall”. It ends in a breakdown and it probably reaches a point very close to the surface on the other side of the mountain. This idea is supported by the presence of troglophile insects typical of cave entrances. Since this channel is at higher elevation than the hall floor it is also the warmer place inside the cave with a temperature approaching 6–7 °C.
- The third conduit is a series of relict passages stretching above the “Music Hall”. The exploration of the area is still not complete but access is possible with climbing aids.

The cave is oriented along a fault, which is probably the main structural element guiding the cave genesis. The cave is a relict ponor which drained the wider Bijambare area in the past.

Morphologies due to turbulent water erosion-corrosion like scallops are completely hidden under the calcite deposition and traces are visible only on the walls before the narrow passage leading to the “Music Hall”. The orientation of the scallops indicates the direction of paleoflow towards the Music Hall.

Recently, the cave has no active streams. Allogenic waters sink into Donja cave about 30 m lower. Drip water drains in two depressions: one in the main channel (occasionally it becomes ponded) and the second in a narrow passage connecting the Music Hall with the main channel. Near this last sinking point there is a small (but permanent) water source located between rock wall and cave sediments.

Large halls, numerous dripstone decorations, immediate surroundings as well as good position on the road Sarajevo-Tuzla were the main motives for the Srednja Bijambarska Cave to be promoted as a tourist amenity. The works started at the end of 1960s and with interruptions they continue to this day with variable levels of intensity and quality.

References

- Apfelbeck V (1901) Drei neue Höhlenkäfer aus Bosnien. Verhandlungen der k. k. zoologisch-botanischen Gesellschaft LI:14–16
- Baucic I, Rzehak V (1959) Bijambarska pecina. Nase Starine Godisnjak Zemaljskog muzeja za zastitu spomenika kulture i prirodnih rijetkosti Narodne Republike Bosne i Hercegovine 6:219–230
- Čičić S (1998) Carbonate facies in geological constitution of the terrain of Bosnia and Herzegovina. Naš Krš 31:3–37
- COOR (2006) Hidrološke karakteristike prostora zaštićenog pejzaža Bijambara. Sarajevo, p 23
- Čurčić V (1940) Pećine u okolini Sarajeva. Hrvatski planinar 8–9:246–253
- Đerković BM (1971) Geološki i hidrogeološki odnosi područja srednje Bosne. Geološkog Glasnika, p 10
- Dudley N (ed) (2008) Guidelines for applying protected area management categories. IUCN, Gland
- Federalni Hidrometeorološki Zavod (2011) Klimatologija (Online). Available at <http://www.fhmzbih.gov.ba/latinica/klima.php>. Accessed 21 July 2011
- HEIS and IPSA (2008) Vulnerability study for FBiH, Sarajevo
- Kumičić E (1944) Krivajevičke špilje. Hrvatski planinar 4:67–70
- Malez M (1968) Bijambarske pecine kod Olova u srednjoj Bosni. Glasnik Zemaljskog muzeja Bosne i Hercegovine u Sarajevu, Prirodne nauke, Nova serija 7:154–191
- Milanolo S, Mulaomerović J (2007) Current status of speleological researches in the Bijambare. CESD/COOR, Sarajevo
- Milanolo S, Mulaomerović J (2008) Speleološka istraživanja na području zaštićenog pejzaža Bijambare. Naš Krš 40(41):3–24
- Milanolo S, Cella GD, Burek R (2006) Ledenjača. Labirinti 25:16–25
- Mulaomerović J, Zahirović D, Handžić E (2006) Katastar speleoloških objekata Bosne i Hercegovine. Speleološko društvo “Speleo dodo”, Sarajevo
- Rzehak V (1958) Manje poznate prirodne rijetkosti u Bosni i Hercegovini i potreba njihove zaštite. Nase starine 5:105–123

Chapter 3

Materials and Methods

Abstract Several parameters have been monitored at Srednja Bijambarska cave in the scope of this study. Temperature, relative humidity, pressure, air velocity, carbon dioxide and radon concentration have been measured in the cave atmosphere while physicochemical analyses have been conducted on the percolating water including determination of flow rate, calcium and magnesium concentration, alkalinity, pH, temperature and specific electric conductivity. Calcite deposition rates on glass plates left under three cave drip sites have been calculated by repeated measurements of plate weight. In this chapter characteristics of sensors and methods used on field and laboratory are presented, as well as the locations of measurements, and where available the estimated errors.

3.1 Introduction

The environmental monitoring of the show cave was done within the framework of different projects. As it often happens in such cases, at the beginning the goals are not clear, apart from observing environment and changes in it. In course of time, certain amount of interesting data was gathered, which served as a starting point for the developing of this thesis project.

During 2006, the show cave was equipped thanks to an EU commission—Canton Sarajevo project, with an underground atmospheric monitoring station aimed primary to establish the tourist impact on cave environment. Shortly after, the cave became part of the C6 monitoring network (Madonia 2008), introducing additional temperature sensors. Monitoring of drip water composition (made possible by the availability of chemical laboratory at HEIS institute) was intermittent during the thesis project due to the difficulty in maintaining a monthly sampling frequency and, at least in the early stage, a less than clear understanding of the utility of obtained results. Later on, the structure and objectives of this thesis became clear enough to allow a few additional experiments to be actively planned. In these last cases an important factor was the temporary availability of new instrumentation thanks to the cooperation with other researchers from Slovenia and Croatia.

At last, during the thesis topic presentation, comments from members of the commission and mentors stressed the necessity to cover few of the initial gaps and weakness advising on a final set of experiments and analyses. The result is that instruments and methods used in this work are a collection of different sensors and procedures with different origin and manufacturers, installed or implemented at different periods by different group of people and with different purposes. Inter-calibration of instruments and methods suffered because of these circumstances.

In the following paragraphs it is given a general overview of instrumentation and methods used in this thesis divided into the three main classes: air, water and calcite deposition.

3.2 Atmospheric Parameters

3.2.1 *Cave Monitoring System*

In October 2006, a monitoring system designed to assess the impact of cave visitors to the cave environment was installed. It consists of an infrared cell probe measuring the carbon dioxide concentration (C), two remote pT100 probes for the temperature (T_1 and T_3) and a forced ventilation wet and dry bulb system measuring the relative humidity (RH). The hygrometer also gives temperature data (T_2). All probes are connected to a central data logger (Elog Model) through compensated cables. The whole system (see Fig. 3.1) was manufactured by LSI-Lastem, Italy, factory-calibrated and installed at the site just before the beginning of the monitoring period (11 October 2006).

All instruments located inside the cave were continuously powered and had an acquisition rate of 1 min. However, the data logger recorded only the average and standard deviation of ten measurements (with the exception of a short period in January 2007 when the original data were retained in memory). The probes were positioned 1 m above ground and at least 1 m from the nearest wall as suggested by Cigna (2002).

From 23 May 2007 to 3 July 2007, data collection in the cave was suspended due to a malfunction of the electrical supply system. The system was repaired and data collection established again. However, after a second failure on 5 April 2008 the cave monitoring instrumentation was never restored. Description and main features of the monitoring system are summarized in Table 3.1.

3.2.2 *Gemini Tinytag Data Loggers*

Two Gemini tinytag data loggers have been installed as part of the project C6 in the Bijambare protected area. The first, mounting sensors for temperature (T_{out}) and relative humidity (RH_{out}), has been located outside, in an open field around 1.5 km

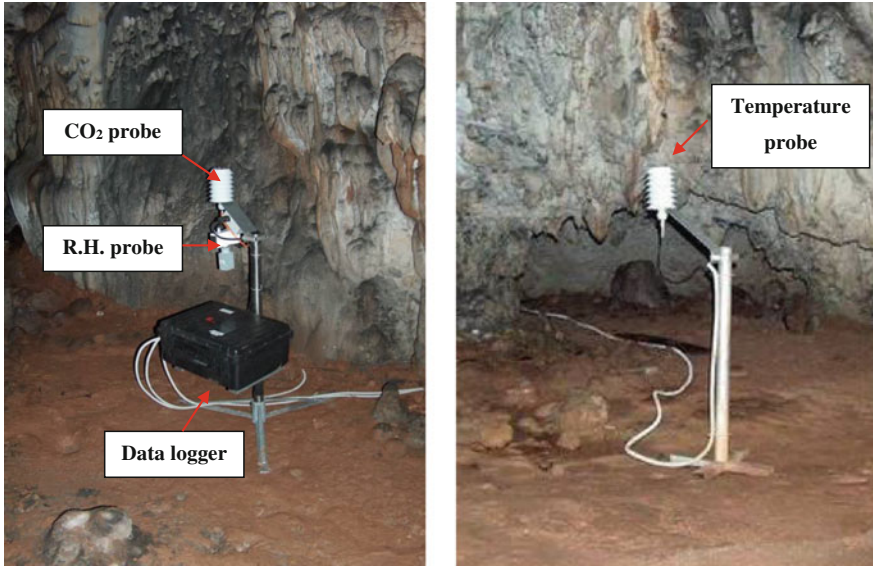


Fig. 3.1 Cave monitoring system including data logger carbon dioxide probe, relative humidity probe, and temperature probe

Table 3.1 Summary table of parameters measured by the cave monitoring system and the resolution and accuracy of sensors

	Abbreviation	Description	Characteristics
Temperature	T_1	Cave Pt100 probe	Res. 0.01 °C—Acc. ±0.08 °C
	T_2	Cave Pt100 probe	Res. 0.01 °C—Acc. ±0.16 °C
	T_3	Cave Pt100 probe	Res. 0.01 °C—Acc. ±0.08 °C
Carbon dioxide	C	Infrared CO ₂ probe	Res. 1 ppm—Acc. ±75 ppm
Relative humidity	RH	Wet and dry bulb with forced ventilation	Res. 0.1 %

from the cave entrance and at a 20–30 m lower elevation. The instrument is fixed to a wooden structure 1.8 m above the ground and shielded from solar radiation (see Fig. 3.2). The second data logger measuring temperature only (T_4) was installed inside the cave in a side channel, suspended around 20 cm from the passage ceiling. Both data loggers recorded data with a frequency of 1 h. The main instrument characteristics are illustrated in Table 3.2. In the case of temperature sensors, accuracy refers to original graphs provided by manufacturer in the data logger datasheet (reproduced in Fig. 3.3a, b).



Fig. 3.2 Mounting of the external temperature data logger. For location refer to Fig. 3.8

Table 3.2 Summary table of parameters measured by the Gemini tinytag data loggers and the resolution and accuracy of sensors

	Abbreviation	Description	Characteristics
Temperature	T_{out}	Gemini tinytag (outside cave)	Res. 0.01 °C
	T_4	Gemini tinytag	Res. 0.01 °C
Relative humidity	RH_{out}	Gemini tinytag (outside cave)—capacitive sensor	Res. 0.1 %RH—Acc. ±3.0 %RH

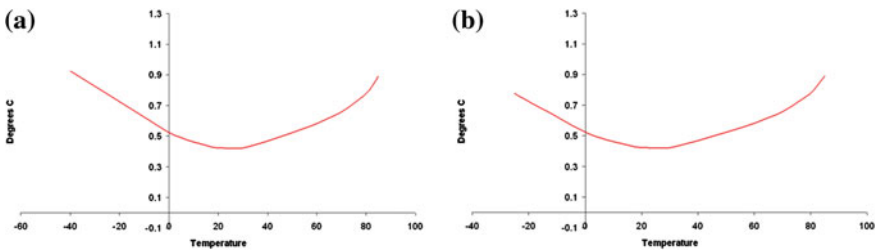


Fig. 3.3 **a** Accuracy for the outside installed data logger as a function of the measured value. **b** Accuracy for the data logger installed inside the cave as a function of the measured value

3.2.3 USB Stick Sensors

At the end of 2008, two data loggers CEM DT-171 (see Fig. 3.4) were used for a short experiment on the cave entrance gate. These instruments include temperature sensor plus a capacitive sensor for relative humidity. Accuracy and repeatability of relative humidity measurements in the cave environment are questionable, even more if the data are collected by capacitive sensors, and therefore they should be used carefully. Table 3.3 summarizes the main characteristics of these sensors. In order to test inter-calibration of the measured temperature and relative humidity the instruments have been left 6 days together under the same conditions. One hour frequency records have been statistically analyzed to evaluate possible differences. The results (Table 3.4) show a discrepancy between average temperatures of 0.35 °C (with T_{low} data logger giving high values). This disparity, based on a two sample paired t-test, is highly significant ($P \ll 0.01$). Based on correlation evidenced in Fig. 3.5 this difference is rather constant over the range of temperature tested. Using a similar approach for relative humidity data, there is an indication of a significant ($P = 0.03$) difference between the average relative humidity measured by the two instruments. However, this difference is of 0.03 % only, and is therefore negligible in the context of this study. It should also be highlighted that relative humidity inter-calibration was performed under environmental conditions far from almost saturated values typical of the cave atmosphere.



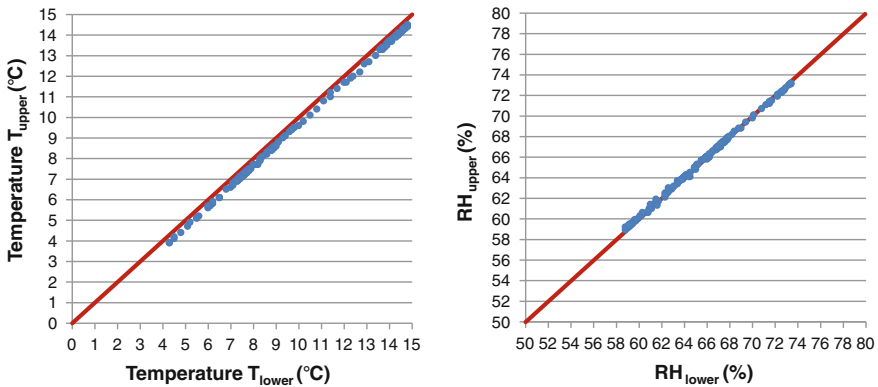
Fig. 3.4 USB stick model CEM DT-171

Table 3.3 Summary table of parameters measured by the USB stick data loggers and the resolution and accuracy of sensors

	Abbreviation	Description	Characteristics
Temperature	T_{up}	Upper gate data logger	Res. 0.1 °C—Rep. ± 0.2 °C—Acc. ± 1.0 °C
	T_{low}	Lower gate data logger	Res. 0.1 °C—Rep. ± 0.2 °C—Acc. ± 1.0 °C
Relative humidity	RH_{up}	Upper gate data logger	Res. 0.1 %RH—Rep. ± 0.2 %RH—Acc. ± 3.0 RH—Drift < 1 %RH/year
	RH_{low}	Lower gate data logger	Res. 0.1 %RH—Rep. ± 0.2 %RH—Acc. ± 3.0 RH—Drift < 1 %RH/year

Table 3.4 Descriptive statistics of data from retrieved both data loggers after a 6 day test (sampling frequency 1 h) under identical conditions

	T_{lower}	T_{upper}	RH_{lower}	RH_{upper}
Mean	9.73	9.38	64.85	64.88
Standard error	0.26	0.26	0.33	0.32
Median	8.7	8.4	64.70	64.65
Mode	7.6	13.7	59.1	66.0
Standard deviation	3.11	3.11	4.00	3.91
Sample variance	9.66	9.69	16.02	15.26
Kurtosis	-1.24	-1.24	-0.64	-0.68
Skewness	0.36	0.35	0.30	0.28
Range	10.5	10.6	14.6	14.3
Minimum	4.3	3.9	58.8	58.9
Maximum	14.8	14.5	73.4	73.2
Count	147	147	146	146
Confidence level (95.0 %)	0.51	0.51	0.65	0.64

**Fig. 3.5** Comparison between measured values by data loggers under identical conditions

3.2.4 Diver and Baro Sensors

During a 24 h experiment several Mini-Diver, Micro-Diver and Baro-Diver data logger (Schlumberger Water Services) were positioned along the cave path to monitor temperature and air pressure changes (T_{FR} , T_{SCup} , T_{SClow} , T_{MH} and P_{MH}). One additional Baro data logger has been installed outside the cave, around 20–30 m from the entrance gate (T_{OUT2} and P_{OUT}). All instruments are equipped with the same temperature sensor with 0.01 °C resolution and ± 0.1 °C typical accuracy. Barometric pressure is measured with a 0.2 cm of water resolution and a typical accuracy of ± 0.5 cm of water.

3.2.5 Air Velocity Sensor

A three-dimensional ultrasonic anemometer model “Windmaster” from Gill instruments (Fig. 3.6). This instrument was installed for a short (almost 24 h) experiment in the narrow passage between “Main channel” and “Music hall”. One of the instrument velocity vectors was aligned with the conduit direction with positive versus towards “Music hall”. The other two velocity vectors (vertical and lateral) therefore provided almost null results and were therefore discarded. The data logger records velocity with a 1 min frequency and a resolution of 0.01 ms^{-1} .

3.2.6 Handheld Carbon Dioxide Sensors

Three handheld carbon dioxide instruments were used in this work. The first (Telaire 7001) was used during two field visits in order to define the spatial variability of carbon dioxide concentration in the cave atmosphere. A Vaisala GM 70 instrument with GMP222 probe was used briefly to measure a vertical carbon dioxide profile in the “Music hall” and then was fixed in the “Music hall” for a 24 h experiment (C_{MH}). The last instrument was installed during the same 24 h experiment as the previous instrument, but located in the main channel just before the narrow passage leading to the “Music hall” (C_{MC}). Detailed characteristics of instruments are given in Table 3.5.

Fig. 3.6 3D ultrasonic anemometer



Table 3.5 Summary table of parameters measured by the handheld carbon dioxide meters and the resolution and accuracy of sensors

Abbreviation	Description	Characteristics	Use
None	Telaire 7001	Res. 1 ppm Acc. ± 50 ppm or ± 5 % of reading	Spatial carbon dioxide distribution
C_{MH}	Vaisala GM 70 with GMP222 probe	Res. 20 ppm Acc. ± 1.5 % of range and ± 2 % of reading	Fixed in the “Music hall” or used for vertical carbon dioxide profile
C_{MC} T_{MC}	Vaisala	Res. 1 ppm	Fixed before the narrow passage leading to the “Music hall”

3.2.7 Radon Detectors

Integrated measurements of radon and its short-lived progenies in the air were performed using a the passive track etching method with the LR-115 SSNT detector, type II (Kodak-Pathé, France) at 2 measuring sites in summer and winter period (July–August 2010, December–January 2011). The cylindrical detector cup (Fig. 3.7), with a diameter and length of 11 and 7 cm respectively, was either covered with a paper filter of 0.078 kg/m^2 surface density (diffusion detector), or was open. Radon concentration in the air was determined as a product of the sensitivity coefficient and track density of the diffusion detector. The measurement method with two detectors (diffusion and open one) enables determination of the equilibrium factor for radon and its progeny in the air (Planinić et al. 1997; Paar et al. 2008).

Fig. 3.7 Radon detector

The radon concentration and microclimate measurements and analysis in Srednja Bijambarska cave were performed in cooperation with dr. Vanja Radolić, Department of Physics, University of Osijek, Dr. Dalibor Paar, Department of Physics, Faculty of Science, University of Zagreb and Dr. Nenad Buzjak, Department of Geography, Faculty of Science, University of Zagreb.

3.2.8 *Air Sensors Location*

As described in the previous paragraphs, different instruments have been installed and used for the scope of this work (Table 3.6). Most of them were left in place only for short periods of several hours or days (e.g. USB stick sensor or diver and baro sensors) up to one month (i.e. radon detectors) while other (i.e. cave monitoring system and C6 instruments) were active for more than one year. Figure 3.8 provides diagrammatic summary of the location of all sensors that were used to monitor air parameters.

3.3 Water Analysis

3.3.1 *Sampling and Sample Handling*

Water samples were collected in the “Music hall” using two slightly different methods depending on the source of water:

- (a) **Dripping water**—Samples were collected into a 1 L plastic bottle equipped with a plastic funnel placed under the drip site (Fig. 3.9a). After a certain time (half an hour to 2 h), the collected water volume was measured in a graduate glass cylinder to estimate the discharge rate (see Sect. 3.3.2). Then the water was decanted into a half a litre plastic bottle and closed tightly without any headspace gas. Samples were transported to the laboratory and processed within 3–5 h. For the samples to be representative for the composition of drip water and to reduce post equilibration with the cave environment (further carbon dioxide degassing and deposition of calcite) the collection of water was done in the shortest time possible.
- (b) **Pool water**—Samples were collected using a glass syringe, into half litre plastic bottles and then processed together with samples of the dripping water. Due to the small volume of pools, the sampling process regularly emptied most of them. Nevertheless, the collected quantity of water was rarely enough to completely fill the half litre bottle, and therefore further degassing may have had occurred during transport to the laboratory.

Table 3.6 Overview of all measured air parameters

Abbreviation	Location	Type of instrument	Period of activity
Temperature			
T_{out}	External around 1 km from cave entrance	Gemini tinytag data loggers	From 13 November 2006 to 24 November 2010
T_{out2}	External around 30 m from cave entrance	Diver and baro sensors	9/10 October 2010 (24 h)
T_{up}	Entrance gate 1 m from the cave ceiling	USB stick	From 14 to 24 October 2008
T_{low}	Entrance gate 60 cm from the ground	USB stick	From 14 to 24 October 2008
T_{FR}	Located inside the cave just at the end of the initial slope	Diver and baro sensors	9/10 October 2010 (24 h)
T_{SClow}	Main channel at intersection with the side channel—low elevation	Diver and baro sensors	9/10 October 2010 (24 h)
T_{SCup}	Main channel at intersection with the side channel—high elevation	Diver and baro sensors	9/10 October 2010 (24 h)
T_1	Main channel before the narrow passage	Cave monitoring system	From 11 October 2006 to 5 April 2008
T_2	Beginning of “Music hall”	Cave monitoring system	From 11 October 2006 to 8 April 2007
T_3	About 15 m inside the “Music hall”	Cave monitoring system	From 11 October 2006 To 5 April 2008
T_4	End of side channel	Gemini tinytag data loggers	From 13 November 2006 to 16 May 2010
T_{MC}	Main channel before the narrow passage	Handheld CO ₂ sensor	9/10 October 2010 (24 h)
T_{BH}	10 cm deep borehole in the “narrow passage”	Air velocity sensor	9/10 October 2010 (24 h)
T_{NP}	“Narrow passage”	Air velocity sensor	9/10 October 2010 (24 h)
T_{MH}	Central part of the “Music hall”	Diver and baro sensors	9/10 October 2010 (24 h)
Relative humidity			
RH_{out}	Around 1 km from cave entrance	Gemini tinytag data loggers	From 13 November 2006 to 16 May 2010
RH_{up}	Entrance gate 1 m from the cave ceiling	USB stick sensors	From 14 to 24 October 2008

(continued)

Table 3.6 (continued)

Abbreviation	Location	Type of instrument	Period of activity
RH_{low}	Entrance gate 60 cm from the ground	USB stick sensors	From 14 to 24 October 2008
RH	Beginning of “Music hall”	Cave monitoring system	From 11 October 2006 to 5 April 2008
Barometric pressure			
P_{out}	External around 30 m from cave entrance	Diver and baro sensors	9/10 October 2010 (24 h)
P_{MH}	Central part of the “Music hall”	Diver and baro sensors	9/10 October 2010 (24 h)
Carbon dioxide concentration			
C_{MC}	Main channel before the narrow passage	Handheld CO ₂ sensor	9/10 October 2010 (24 h)
C	Beginning of “Music hall”	Cave monitoring system	From 11 October 2006 to 5 April 2008
C_{MH}	Central part of the “Music hall”	Handheld CO ₂ sensor	9/10 October 2010 (24 h)
Air velocity			
v_{air}	“Narrow passage”	Air velocity sensor	9/10 October 2010 (24 h)
Radon concentration			
R_{MC}	Main channel at intersection with the side channel	Radon detector	From 18/07/10 to 27/08/10 From 25/12/10 to 15/01/11
R_{MH}	“Music hall”	Radon detector	From 18/07/10 to 27/08/10 From 25/12/10 to 15/01/11

The equipment was cleaned with sulphuric acid and rinsed with distilled water after each sampling campaign to avoid presence of crystallization nuclei on the plastic/glass surface and thus reducing the chances that calcite deposition may have occurred during sampling and transport.

3.3.2 Discharge Rate

Discharge rate was estimated for each dripping site by measuring the collected water volume over a known time period.

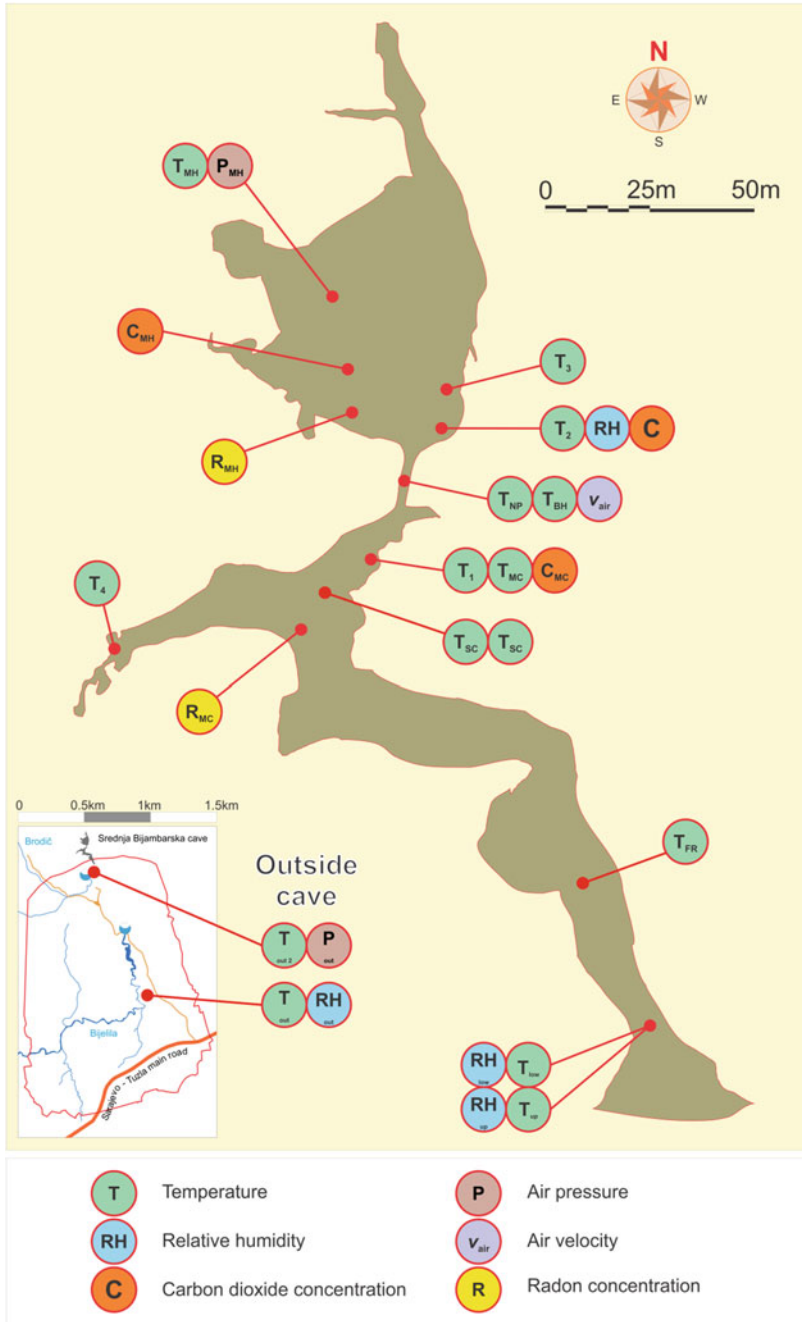


Fig. 3.8 Location of all air quality sensors

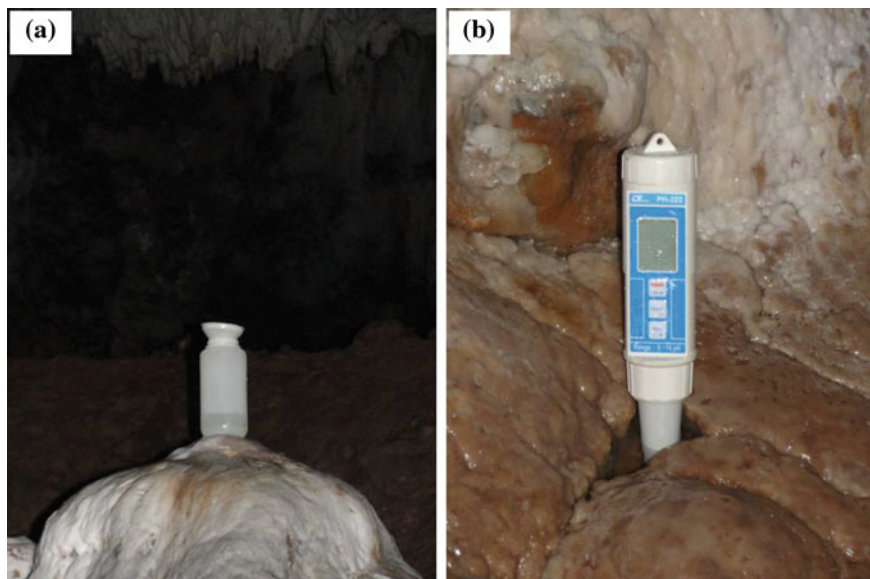


Fig. 3.9 a Collection of drip water. b Direct measurement of pH in pools

3.3.3 Chemical Analysis

The pH, defined as a negative logarithm of the activity of H^+ (or H_3O^+) ion, represents one of the key indicators of the state of equilibrium in $H_2O-CO_2-CaCO_3$ system. Equilibrium partial pressure of carbon dioxide and calcite saturation index show a high and almost linear correlation with pH, and therefore a precise determination of this parameter is crucial for defining the equilibrium status of cave water. For this reason, high attention was given to pH measurements, trying to avoid as much as possible errors, and improving the precision of the measurement. During the first four sampling campaigns in winter 2007–2008 the pH was measured at laboratory using an OAKTON 510 Series instrument (resolution 0.01 units) calibrated before each series of measurements.

On subsequent field campaign, the pH value was determined directly in the cave using an LT Lutron PH-222 handheld instrument (resolution 0.01 units). Calibration with buffer solutions was performed in the cave at each visit. Nevertheless, initially, pH was measured off-site (5–6 m from sampling points) in a small plastic beaker filled with sampled water. Very soon the method was changed to measuring the pH directly under the dripping water by hanging the instrument inside the sampling bottle. pH value was checked 3–4 times during at least 5 min until constant values was reached. For pool water, similar methods have been employed by leaving the instrument directly inside the pool until constant pH value has been reached (Fig. 3.9b). The same instrument measures water temperature for pH compensation (resolution 0.1 °C).

Specific Electrical Conductivity (SEC) was measured in the laboratory using a WTW LF196 instrument with a resolution of $1 \mu\text{S cm}^{-1}$. The instrument performs automatic adjustment for temperature ($20 \text{ }^\circ\text{C}$). The instrument has been calibrated using a 0.01 M KCl solution with a standard SEC of $1412 \mu\text{S cm}^{-1}$, recorded deviance were always lower than 1% .

Total hardness was measured in the laboratory by complexometric titration with 0.01 M EDTA solution using Erichrome-T as indicator while Ca^{2+} concentration was determined using a similar method, but using Murexide as indicator at high pH value. Considering a resolution of titration apparatus of 0.1 mL and a sample volume of 50 mL , the resolution of total hardness and Ca^{2+} concentration analysis can be estimated to be 0.8 mg L^{-1} .

Considering that the Ca^{2+} and Mg^{2+} represent majority of cations, the magnesium concentration can be estimated by difference between the total hardness and the calcium concentration. However it should be noticed that the errors of the two above mentioned methods needs to be at least summed and this, combined with the relatively low concentration of Mg^{2+} ions in Bijambare water, make the results for this ion questionable.

Carbonate alkalinity in cave waters is completely in the form of HCO_3^- (Appelo and Postma 2006, p. 94) and was measured in the laboratory by titration of a 50 mL sample with $0.02 \text{ N H}_2\text{SO}_4$ using metyl-orange as indicator. Resolution can be calculated to be around 2 mg L^{-1} .

Saturation Index with respect to calcite (SI_{Ca}) and the equilibrium pressure of carbon dioxide ($p_{\text{CO}_2,\text{eq}}$) was calculated using PHREEQC interactive software version 2.17.4799 (Parkhurst and Appelo 1999). Two runs were performed for each sample:

- First run using as input parameters: pH, temperature, calcium and magnesium concentrations. Inorganic carbon species concentration was calculated by the software to satisfy the electrical charge balance.
- A second run using as input parameters: pH, temperature, calcium and magnesium concentrations and alkalinity. In this case the electrical charge balance has been used to test the quality of the chemical analysis.

Only values of SI_{Ca} and carbon dioxide equilibrium partial pressure from the first run have been used for further processing. On a total population of 106 samples, the electrical charge balance error ranged between -3.22 and 10.25% with an average of 5.14% and a standard deviation of 2.85% (Table 3.7a and Fig. 3.10). All negative to slightly positive balances refer to samples collected in the winter 2006–2007 when pH values were measured at laboratory (Table 3.7b and Fig. 3.10). In fact, at this early stage, all chemical parameters were measured at laboratory and therefore the error did not include the carbon dioxide degassing from sampling point up to the moment of the analysis. On the other hand, when pH is measured directly on site, then further carbon dioxide degassing during following handling activities produces a decrease of alkalinity compensated by an increase of pH value. However, since alkalinity is measured in the laboratory, the overall effect is a deficit of anions in the solution and a positive electrical charge balance error.

Table 3.7 Descriptive statistics for the electrical balance error: (a) all samples; (b) only samples where pH has been measured in the cave

(a) Descriptive statics: all samples	
Mean	5.14
Standard error	0.28
Median	5.53
Mode	-0.06
Standard deviation	2.85
Sample variance	8.14
Kurtosis	0.41
Skewness	-0.75
Range	13.47
Minimum	-3.22
Maximum	10.25
Sum	544.65
Count	106
Confidence level (95.0 %)	0.55
(b) Descriptive statics: pH at site only	
Mean	5.68
Standard error	0.23
Median	5.98
Mode	6.29
Standard deviation	2.25
Sample variance	5.08
Kurtosis	-0.24
Skewness	-0.31
Range	11.6
Minimum	-0.91
Maximum	10.25
Mean	551.42
Standard error	97
Median	0.45

3.3.4 *The Location of Water Sampling Sites*

Four sites were selected for monitoring of drip water composition (named from 1 to 4). All sites are located in the “Music hall”. The first three of these never dries up, although discharge differs considerably between the sites and shows large temporal variations at all sites. Location number four is periodical and usually dries up few days after precipitation. This last site, different from the previous three, receives water flowing over a flowstone. The source of this water has never been explored.

Height differences between stalagmite and stalactite (drop free fall) for the sites 1–3 are 5, 5 and 4 m respectively.

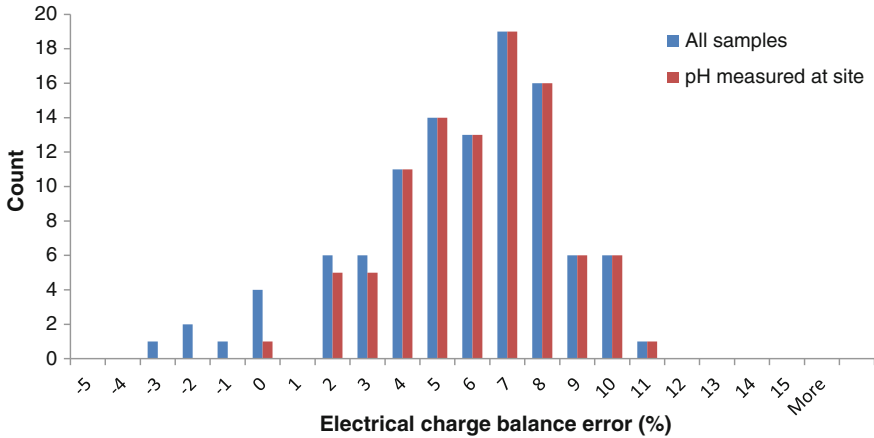


Fig. 3.10 Histogram of electrical balance error

In order to investigate the evolution of water composition further after the droplets have reached the stalagmite, samples from several pools were analyzed. The sampling points are located along two profiles on the opposite sides of drip site 2. Water is sampled from pools with approximate volume ranging from few milliliters to a couple of liters. During the summer months most of the pools were found to be dry. The main water source for all pools is dripping site 2, and only rare drops do not belong to the above mentioned drip site. Between pools, water flows over a flowstone surface. Location of sampling points is shown in Fig. 3.11.

3.4 Calcite Deposition

3.4.1 Determination of Calcite Deposition Rate

The process of limestone dissolution on the surface (denudation process) has been studied widely since at least 50 years. One of the most frequently employed method for determination of dissolution rates is based on precise measurements of weight difference of limestone tablets before and after exposure to the dissolution for a known interval of time. Similar methods have been used (but to a less extent) in cave environments to measure the intensity of speleogenetic processes (Prelovšek 2009). Even though the method can be conceptually easily extended to accomplish measurements of calcite deposition, there is modest amount of data available on this field. Banner et al. (2007) adapted the tablets method to measure calcite deposition under dripping site. The tablets were made of sandblasted glass, mounted horizontally using a plastic or clay supports and weighting was performed by electronic balance (using an ionizing system is reported to highly improve the reproducibility of weight measurements).

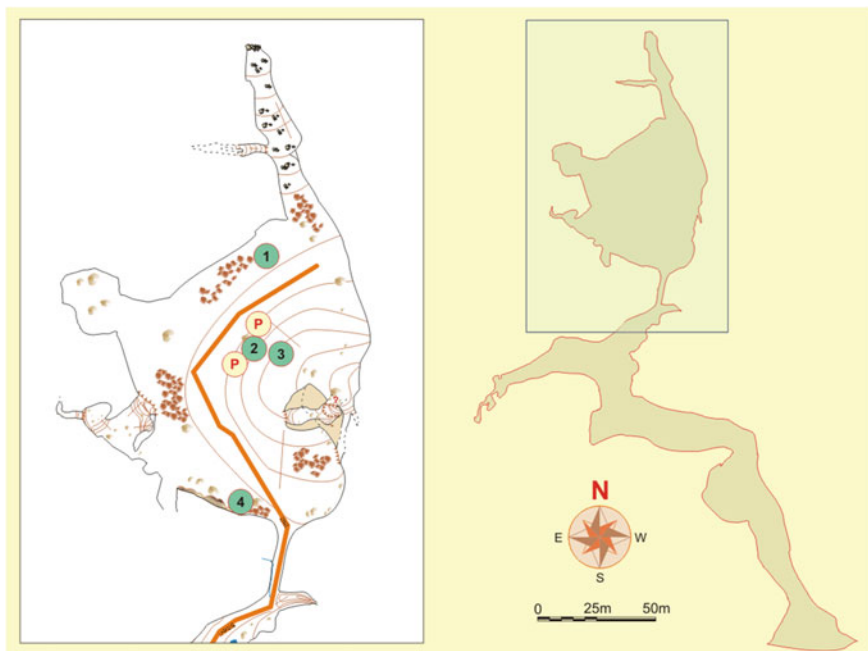


Fig. 3.11 Location of drip sites 1, 2, 3 and 4. Sampled pools are shown as “P” and they are located along two profiles on the opposite side of drip site 2

We applied a similar method to monitor calcite deposition rate under three dripping sites in Bijambare cave. Glass tablets were prepared from laboratory glassware dishes with diameter 8 cm and height of 1 cm. Glass was sand blasted on the top external surface (but not on the lateral surface) and washed with distilled water. The tablets were mounted horizontally under drip site (with drops falling to the center) and replaced regularly every 4–5 weeks (Fig. 3.12).

At arrival at laboratory, tablets were conditioned using a standard procedure comprising the following steps: a fast rinse with distilled water, drying at 105 °C (1 h) and cooling in a dessicator with silica gel (half hour). Weight determination was done using a digital balance (Sartorius TE214S) with a resolution of 0.0001 g. The balance calibration was checked monthly via an internal set of standard weight and every year by an authorized company. In all cases errors and drift were negligible (equal to the instrument resolution). The procedure from drying at 105 °C to weighting was repeated three times, the first obtained value (w_1) was usually disregarded and the subsequent two weight measurements for each tablet (w_2 and w_3), if reasonably equal, were averaged to get the final value.

To a first approximation, the difference between w_2 and w_3 can be used as an indication of the method error (Fig. 3.13). From the analysis of a population of 40 samples, it resulted an average difference of 0.00049 g almost comparable to the balance resolution. The fact that the average is not exactly null but slightly positive

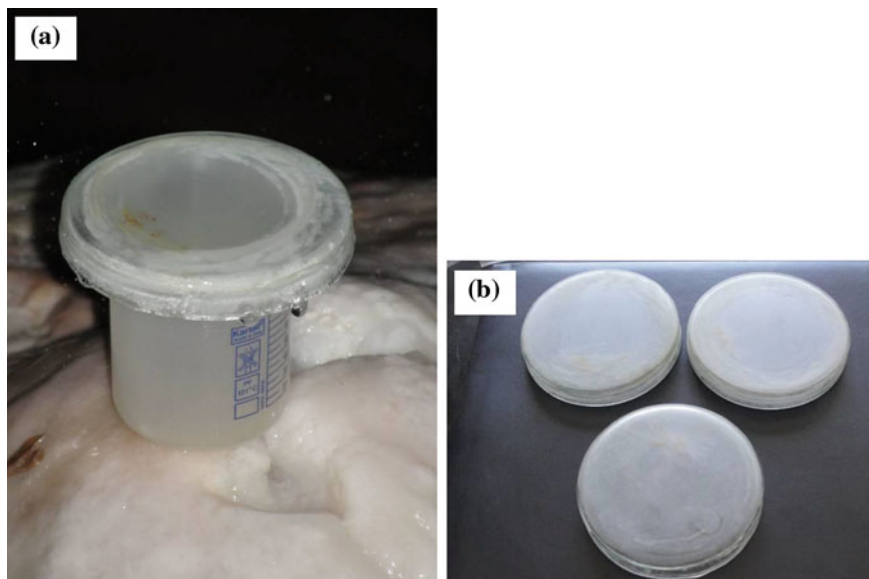


Fig. 3.12 a Glass plate mounted under drip site 2. b Set of three glass plates at laboratory

<i>Column1</i>	
Mean	0.00049
Standard Error	0.00015
Median	0.0004
Mode	-0.0001
Standard Deviation	0.00094
Sample Variance	8.85E-07
Kurtosis	0.08
Skewness	0.38
Range	0.0041
Minimum	-0.0013
Maximum	0.0028
Sum	0.0195
Count	40
Confidence Level (95.0%)	0.00030

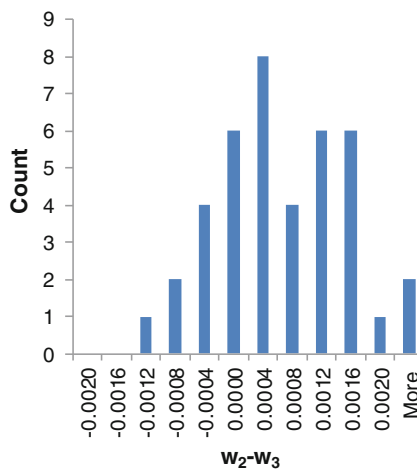


Fig. 3.13 Descriptive statistic and histogram for the difference of weight of tablet after second and third drying cycle

can be explained by the presence of a systematic error due to the drying-weighting routine methodology. In fact, under ideal conditions, the sample weight should, by repeating these steps, progressively lose moisture and therefore decrease its weight asymptotically to the value of the dry sample. Following this, the difference between two subsequently measured weights ($w_{n-1} - w_n$) is always a small but positive number. In addition to this systematic error it is necessary to add a random error which it is mostly caused by unpredictable fluctuations in the readings of the measurement apparatus. The standard deviation of $w_2 - w_3$ during the whole experiment period resulted to be 0.00094 g.

3.4.2 Location of Measurement Sites for Calcite Deposition

Since December 2009, three monitoring sites have been activated in Srednja Bijambarska cave to estimate calcite deposition rate. All of them are located in the “Music hall” and they have been chosen within the sites already monitored for drip water composition in order to have the most complete picture of factors potentially affecting the quantity of calcium carbonate precipitated. Only drip site 4 has not been used for calcite deposition measurement due to its temporary nature. The location of all monitored sites is shown in Fig. 3.14.

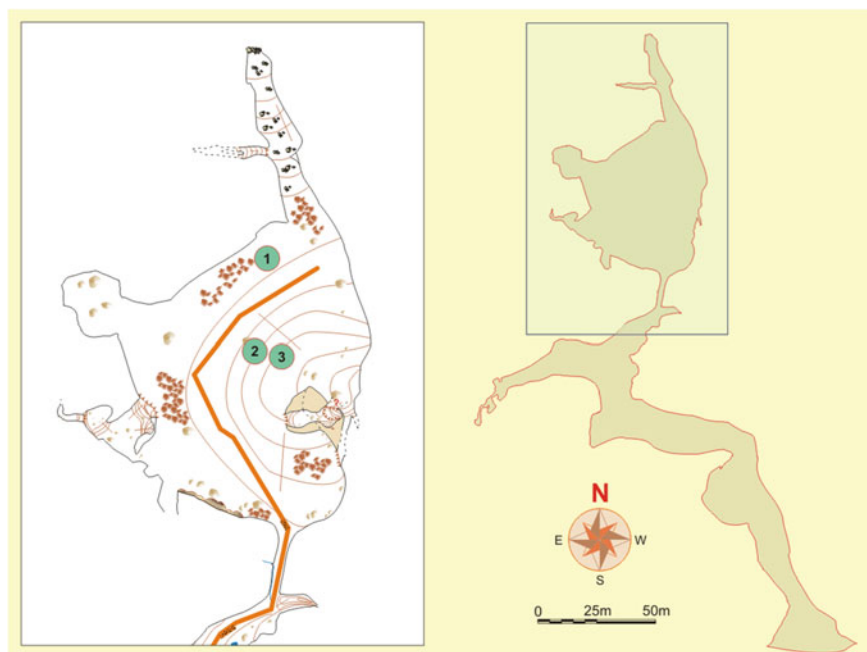


Fig. 3.14 Location of glass plates for calcite precipitation measurement

3.5 Isotopic Composition

The isotopic composition of air and water in terms of $\delta^{13}\text{C}$ and $\delta^{18}\text{O}$ has been investigated during two sampling campaigns in summer and winter 2010 respectively. Air and water samples were taken in proximity to drip sites 1, 2 and 3 (Fig. 3.11). Calcite collected during approximately one year over the plates used for calcium carbonate precipitation experiments (Sect. 3.4) has also been analysed for $\delta^{13}\text{C}$ and $\delta^{18}\text{O}$.

The stable isotope composition of dissolved inorganic carbon (DIC) in water was determined in 5 ml samples injected into He-flushed septum vials containing 100 % H_3PO_4 . The released CO_2 was then analysed using a continuous flow Europa 20–20 Stable Isotope Analyser with an ANCA TG separation module. The standard uncertainty of the analysis was 0.2 ‰. The same instrument was used for the analysis of the $\delta^{13}\text{C}$ of atmospheric CO_2 .

The results of the stable isotope analyses are reported in relative δ values in ‰, i.e. the difference in parts per mil of the isotopic ratios $^{18}\text{O}/^{16}\text{O}$ and $^{13}\text{C}/^{12}\text{C}$ from those of the reference materials VSMOW for O in water, and VPDB (defined by NBS19) for C and O in carbonate and dissolved inorganic C.

Isotope analysis have performed by Doc. Dr. Sonja Lojen at the Department of Environmental Sciences, Jožef Stefan Institute (Ljubljana–Slovenia).

References

- Appelo CAJ, Postma D (2006) *Geochemistry, groundwater and pollution*. AA Balkema Publishers, Leiden
- Banner JL, Guilfoyle A, James EW, Stern LA, Musgrove M (2007) Seasonal variations in modern speleothem calcite growth in Central Texas, U.S.A. *J Sediment Res* 77:615–622
- Cigna AA (2002) Monitoring of caves: conclusions and recommendations. *Acta Carsologica* 31:175–177
- Madonia P (2008) Monitoring climatic changes and carbon cycle in canyons and caves: the C6 project. In: 1st WSEAS international conference on environmental and geological science and engineering (EG'08), pp 135–142
- Paar D, Ujević M, Bakšić D, Lacković D, Čop A, Radolić V (2008) Physical and chemical research in Velebit pit (Croatia). *Acta Carsologica* 37:273–278
- Parkhurst DL, Appelo CAJ (1999) User's guide to PHREEQC (version 2)—a computer program for speciation, reaction-path, 1D-transport, and inverse geochemical calculations. US Geological Survey
- Planinić J, Radolić V, Faj Z, Šoveljak B (1997) Radon equilibrium factor and aerosols. *Nucl Instrum Methods Phys Res Sect A* 396:414–417
- Prelovšek M (2009) Present-day speleogenetic processes, factors and features in the epiphreatic zone, Nova Gorica

Chapter 4

A Conceptual Model of the Inorganic Carbon Transport Within a Karst Massif

Abstract The overall conceptual model of the inorganic carbon transport within a karst massif starts from decomposition of organic matter in the soil and epikarst which produces carbon dioxide. The biological activity gives rise to a gas phase in the porous soil with high CO₂ partial pressure, up to several tens of thousands ppm. Most of the carbon dioxide is released to the atmosphere, but a fraction is dissolved in the percolating water. When water enriched with soil CO₂ comes into contact with limestone in the soil (pebbles) or the epikarst, the calcium carbonate starts to be dissolved. In this process, carbon dioxide in water reacts with carbonate ions to form bicarbonate ions. Two end-members can be considered: (a) dissolution of carbonates occurs without presence of a gas phase (closed system); (b) dissolution process occurs in the presence of a carbon dioxide rich gas phase (open system). In this last case additional CO₂ is dissolved in the water enhancing the amount of calcium carbonate that can be kept into solution (and therefore the total amount of inorganic carbon). Water percolating through the vadose zone may reach the cave atmosphere with lower carbon dioxide content and therefore excess of CO₂ is released until a new equilibrium condition is achieved. The decrease of carbon dioxide content in the solution creates an oversaturation with respect to calcium carbonate, and consequently calcite precipitates. Direct diffusion from soil and epikarst voids and direct human release may be considered as supplementary sources of carbon dioxide in the cave atmosphere. Other potential sources such as decomposition of large quantity of organic matter in the cave and from deep seated sources have not been considered in this conceptual model. Carbon dioxide in cave air is transported between underground passages by advection and then released to the external atmosphere. Part of the inorganic carbon stays in the water and eventually reaches the phreatic zone, where it is stored until it ultimately exits at springs.

4.1 Karst and the Global Carbon Cycle

During the last few decades, quantification of the global carbon cycle has become an important scientific field of research, reflecting increasing interest in Earth climate change and its link with the rise of carbon dioxide concentration in the atmosphere due to anthropogenic sources.

Within the global cycle, carbonate rocks represent the largest carbon reservoir. In detail, all sedimentary rocks on Earth store around 61×10^6 PgC (Houghton and Woodwell 1989), and surface and near surface outcrops of carbonate rocks cover around 20 % of the ice-free land (Ford and Williams 2007, p. 5).

In karst areas, carbon is transported by percolating water and sinking streams in the form of inorganic carbonate-bicarbonate compounds (Dissolved Inorganic Carbon, DIC) and organic matter (Organic Carbon, OC).

During the path from soil to spring, seeping water exchanges DIC with two important carbon reservoirs: in the form of carbon dioxide with the gas compartment (dissolving or outgassing) and with limestone in the form of carbonate (weathering/deposition).

OC is composed by residual of soil matter, wood and leave fines and products of their partial degradation, and it represents an important input in the underground ecosystem food chain. It can be divided into Dissolved Organic Carbon (DOC) and Particulate Organic Carbon (POC). A conceptual model for the flow and distribution of OC is presented by Simon et al. (2007) in the attempt to define energy levels in the cave environment.

It should be noted that once underground, transported organic matter is partially biodegraded into carbon dioxide and this flux may represent an additional important source of inorganic carbon into the system. In fact, extremely high concentrations of carbon dioxide have been found recently in boreholes in a karst region (Benavente et al. 2010), and they have been explained as deep biological degradation of OC in a poorly ventilated unsaturated zone.

The relevance of the contribution of karst areas with their peculiar processes to the global carbon cycle is still under debate. As will be detailed later in this chapter, carbonate rocks weathering process strongly enhance DIC concentration in water. The uptake of carbon, from the atmosphere and from carbonate rocks, proceeds with a stoichiometric ratio of 1:1. However it is generally accepted that, in steady conditions, once runoff waters reach ocean, 50 % of the carbon returns in the form of carbonate sediment and the remaining is released again to the atmosphere. Although the global DIC flow in the world due to carbonate rock weathering is estimated around $0.4 \text{ PgC year}^{-1}$, the net carbon sink of the whole process at global scale is consequently null (Farquhar et al. 2001). However, Liu and coauthors (Liu and Zhao 2000; Liu et al. 2010), partially question this conclusion. In detail, they suggest that, by introducing photosynthetic uptake of DIC in the aquatic environment, only a fraction of the theoretical carbon dioxide quantity is returned to the atmosphere. By their estimation the overall process of carbonate rock weathering represent globally a net atmospheric carbon dioxide sink of around $0.7 \text{ PgC year}^{-1}$.

Yet, regardless of the importance at global scale, the carbonate rocks weathering processes may have a relevant importance on a local ecosystem scale or on a short, seasonal, time scale (Serrano-Ortiz et al. 2010).

A large uncertainty in the global carbon cycle is related to the measurements of the carbon dioxide exchange between terrestrial ecosystems and atmosphere. This flux (overall around 120 PgC year⁻¹) is measured by extrapolating data from several pilot locations encompassing different ecosystems and global land cover maps (Farquhar et al. 2001) or more precisely by calculating it from the more accurate ocean and atmospheric data (Denman et al. 2007). Flux tower measurements (eddy covariance or other micrometeorological techniques) of carbon dioxide exchange with atmosphere in ecosystems developed on karst terrains can be affected by the transport and storage of carbon dioxide in the underlying networks of connected voids (caves) (Kowalski et al. 2008). In fact, caves drain carbon dioxide from the soil layer and return it to the atmosphere through surface openings. Ventilation of caves is a dynamic process (Baldini et al. 2006; Faimon et al. 2006; Kowalczk and Froelich 2010; Milanolo and Gabrovšek 2009; Frisia et al. 2011) following rather complex regimes that are uncoupled with other biological processes and may explain recorded “anomalous” carbon dioxide fluxes recorded at surface (Kowalski et al. 2008; Serrano-Ortiz et al. 2010).

It is known that to close the carbon balance between oceans, atmosphere and the known terrestrial carbon flux due to land use changes it is necessary to include an additional undefined carbon sink named “residual land sink” (formerly the “missing sink”) (Denman et al. 2007). Study of carbon cycle in karst terrains may potentially provide clues to appreciate the nature of this unseen sink.

A better understanding of the carbon cycle in karst terrains requires knowledge of the limestone weathering/precipitation processes and the carbon storage and transport dynamics in the karst regions. The aim of the following paragraphs is therefore to:

- introduce the basic mechanisms controlling limestone weathering and precipitation processes and the inorganic carbon storage and transfer within gas, liquid and solid phases;
- discuss the occurrence and relative weight of these processes in different functional ideal sections of a karst massif and their link with the water cycle.
- draft a conceptual model for the inorganic carbon sources and transport in the unsaturated zone of karst.

4.2 The Equilibria of the H₂O–CO₂–CaCO₃ System

The chemistry of water in contact with carbonate rocks and atmosphere is controlled by a series of chemical equilibria that determine the dominant ionic species activities in water with solid and gas phases. These mechanisms represent the core

of karstification process. From one side the carbonate mineral solubility (in this case calcite) can be expressed by the equilibrium:



that is defined by the solubility product:

$$K_c = (\text{Ca}_1^{2+})(\text{CO}_3^{2-}) \quad (4.2)$$

On the other side, at the liquid-gas interface, the solubility of carbon dioxide in water can be summarized by:



that further reacts with water to give the carbonic acid:



Although this last equilibrium is mostly oriented towards the left side of the reaction it is usual (Appelo and Postma 2006), in order to simplified further calculation, to introduce the notation H_2CO_3^* to summarize in one unique term both $\text{CO}_{2(\text{aq})}$ and H_2CO_3 forms. The global equilibrium is controlled by the Henry's law:

$$K_H = \frac{\text{H}_2\text{CO}_3^*}{p\text{CO}_{2(\text{g})}} \quad (4.5)$$

These two interfaces (solid-liquid and liquid-gas) are linked together by the two steps dissociation equilibriums of the carbonic acid:



that are controlled by the respective temperature dependent dissociation constants:

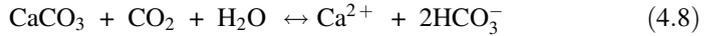
$$K_1 = \frac{(\text{HCO}_3^-)(\text{H}^+)}{(\text{H}_2\text{CO}_3^*)} \quad (4.7a)$$

$$K_2 = \frac{(\text{CO}_3^{2-})(\text{H}^+)}{(\text{HCO}_3^-)} \quad (4.7b)$$

Hence, by combining all these equilibria plus the water dissociation equilibrium and charge balance constraints, it is possible to define exactly the equilibrium concentration of all single species in water solution (H_2CO_3^* , HCO_3^- , CO_3^{2-} , OH^- , H^+ and Ca^{2+}). It should be noticed that the global

equilibrium depends on partial pressure of carbon dioxide ($p_{\text{CO}_2(\text{g})}$) in the gas phase and by temperature influencing all equilibrium constants.

Although calcite dissociates in pure water, its solubility product is relatively low. The addition of carbon dioxide to the solution (i.e. dissolving from a carbon dioxide rich gas phase) strongly enhances calcite solubility. In fact, the overall reaction can be simplified as:



It is evident that by this mechanism one mole of carbon dioxide is required in order to dissolve one mole of limestone rock.

4.3 Open and Closed Systems

In the previous paragraph, has been considered the general case of a solid phase composed by pure calcite in equilibrium with a water solution containing additional amount of dissolved inorganic carbon provided by the equilibrium with a carbon dioxide rich gas phase. This situation, where all three phases are simultaneously in equilibrium, is the so called open system (Hendy 1971) and it represents one of the two end members of the range of conditions that can be found on the field (see Fig. 4.1). The other equally important end member arise when the equilibrium between the three phases does not occur simultaneously but as series of two biphasic steps (first water and gas phase and then calcite and water solution). This has a paramount effect on the dissolution equilibria in karst systems.

While in an open system carbon dioxide consumed to dissolve calcite can be continuously restored from the gas phase reservoir, in the closed system this cannot happen because when calcite dissolution occurs the solution is isolated from the gas phase. In other words, during the dissolution process, in an open system there is an excess of carbon dioxide available in the gas phase while in a closed system there is no carbon dioxide available in the gas phase.

The effect on water solution composition caused by these two different approaching paths to equilibrium is substantial.

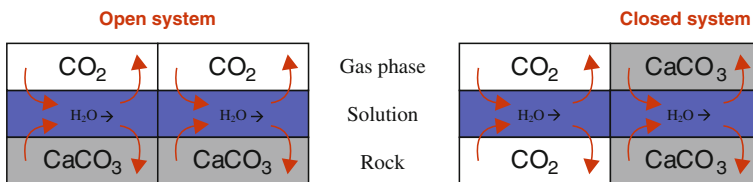


Fig. 4.1 Schematic representation of open and closed conditions

If we consider the same partial pressure of carbon dioxide in the gas phase, the open system will achieve a significant higher quantity of dissolved limestone. Moving to the opposite stand point, and looking to a water solution this could be originated either by an open system or closed system, but the required partial pressure of carbon dioxide in the gas phase for the closed system would be substantially higher.

In natural systems conditions are usually somewhere between these two extremes, introducing a new degree of freedom to consider in addition to gas phase composition and temperature to define the final solution composition.

4.4 The Calcium Carbonate Dissolution and Precipitation

Up to now, the composition of a solution in equilibrium with calcite and a carbon dioxide rich phase in both the cases when this happened simultaneously or as series of two bi-phase equilibria, has been discussed. To realize these equilibria, a certain amount of time governed by reaction kinetics and mass transport phenomena is required.

During transient periods between the two different conditions, the solution is in disequilibrium with the other two phases, and therefore it actively dissolves or outgases carbon dioxide at the interface with the gas phase, or dissolves or deposits calcium carbonate in order to balance its chemical composition. In a certain instant, the “distance” from equilibrium conditions for a pure calcite system is given by two parameters: the saturation index (SI_C) and the partial pressure of carbon dioxide in equilibrium with the solution. The first is defined as the logarithm of the ratio between the product of actual activities of dissociated ions and the solubility product:

$$SI_C = \log\left(\frac{(Ca^{2+})(CO_3^{2-})}{K_c}\right) \xrightarrow{\text{Eq.4.7b}} SI_C = \log\left(\frac{(Ca^{2+})(HCO_3^-)K_2}{(H^+)K_c}\right) \quad (4.9)$$

The values of SI_C spans from negative infinity to positive infinity, with negative numbers indicating solution undersaturation (and therefore with potential for additional calcite dissolution) while positive values are associated with solutions oversaturated (and therefore with potential for deposition of calcite crystals). An exact null value of the saturation index denotes perfect equilibrium. It should be noted that at equilibrium, dissolution and precipitation of calcium carbonated are not null but they compensate each other. In the real case there is an important exception where a positive saturation index does not correspond directly to a net deposition of calcite. This happen when oversaturated solution is not in contact with a calcite solid phase but the first crystal nuclei have to be generated. In fact, under these conditions the first very small agglomerates of solid phase crystal have a very

high surface to volume ratio and therefore a high surface energy. The additional energy stored in the interface between solid phase and solution makes these nuclei unstable and their dissolution velocity at equilibrium is higher than the deposition rate. In order to compensate this additional energy is therefore necessary a certain amount of oversaturation in order to induce precipitation.

The partial pressure of carbon dioxide in equilibrium with the solution is very often also expressed in logarithmic form starting from Eq. 4.5:

$$\log(p\text{CO}_2) = \log \frac{\text{H}_2\text{CO}_3^*}{K_H} \xrightarrow{\text{Eq. 4.7a}} \log(p\text{CO}_2) = \log \left(\frac{(\text{H}^+)(\text{HCO}_3^-)}{K_1 K_H} \right) \quad (4.10)$$

The kinetics of limestone dissolution and precipitation are governed by three rate limiting processes:

- The dissolution/precipitation kinetics at the calcite/solution interface. This is usually described by a rate model (widely known as the PWP equation) developed from experimental data by Plummer and et al. (1978):

$$F = k_1(\text{H}^+) + k_2(\text{H}_2\text{CO}_3^*) + k_3 + k_4(\text{HCO}_3^-)(\text{Ca}^{2+}) \quad (4.11)$$

F is the rate; k_1 , k_2 and k_3 are kinetic constants depending on temperature while k_4 is also a kinetic constant dependent on temperature and equilibrium partial pressure of carbon dioxide.

- The conversion kinetics of CO_2 to HCO_3^- . This is a slow process requiring at pH values between 6 and 8 up to 1 min to reach equilibrium (Dreybrodt et al. 1997). For conditions where high solid/solution interface per unit of solution volume occurs, this process represents the limiting factor.
- The transport of ionic species between the mineral surface and the solution bulk. This process is governed by molecular diffusion velocities into the whole solution in case of stagnant or laminar flow, or through the laminar boundary layer for turbulent motion.

By combining the above processes, deposition rates have been estimated for laminar flow (Buhmann and Dreybrodt 1985a, b) and turbulent flow (Dreybrodt and Buhmann 1991) at different solution film thicknesses, temperatures and calcium concentrations. Similarly dissolution rates at different solution film thicknesses, temperatures and calcium concentrations have been calculated and presented in the works of Kaufmann and Dreybrodt (2007).

It should also be noted that the PWP rate equation is valid for pure mineral surfaces. At real conditions, while approaching the equilibrium, the dissolution rate of natural calcite drops from a linear to a nonlinear rate law because of the presence of impurities. This usually happens from 70 to 90 % of calcium carbonate saturation concentration (Dreybrodt and Gabrovšek 2002). This phenomenon has a tremendous impact on early speleogenetic processes: by decreasing the velocity at which the solution and rock reach the equilibrium, it allows some residual water

aggressiveness to propagate deeply into the limestone fracture network, slowly enlarging the rock fissures and preparing the path for the fast dissolution rates that will follow after the moment (breakthrough) when the water will be able to pass all the way through the karst massif retaining most of its aggressiveness (Palmer 2002).

4.5 Water and Inorganic Carbon in a Karst Massif

4.5.1 *The Soil*

The soil is the first barrier that rain water encounters (eventually after partial interception by vegetation). Precipitated water infiltrates into the soil cover, increasing its moisture content. When the soil water storage capacity is surpassed, the excess water runs on the surface. Roots absorb soil moisture for the vegetation's biological needs and this water evaporates again in the atmosphere. The evapo-transpiration effect depends on the temperature and on the soil moisture content. If the soil moisture concentration decreases below some level, the root's capacity to extract water from the ground is impaired. This effect achieves the results that even after long dry periods the soil will still contain some water. The soil is perched on the epikarst layer. The water is retained in the soil until gravity forces are stronger than capillary forces. At this point water is transmitted down to the epikarst layer and it is considered as effective infiltration.

It is generally accepted that underground CO₂ found in cave atmosphere originates mainly from biological activity (i.e. plant root respiration, degradation of organic material by bacteria) in the soil layer (Ford and Williams 2007, pp. 49–50). The organic origin has been confirmed also by the recent studies of isotopic composition ($\delta^{13}\text{C}$) (Batiot-Guilhe et al. 2007; Kowalczk and Froelich 2010). Hence, most of the carbon dioxide from the soil is released directly to the atmosphere and does not penetrate deeper into the underground (soil efflux).

The concentration of carbon dioxide in the soil layer is highly variable in time and space and depends on many environmental factors. The numerical model developed by Jassal et al. (2004) shows that in addition to parameters that are site specific (soil texture, composition and vegetation cover), the concentration follows an in depth profile that depends to a large extent on the soil temperature and to a minor extent, with soil moisture. The model predicts that carbon dioxide transported downward by water drainage it was always less than 1 % of the total CO₂ production. Nevertheless, it should be noticed that the model was developed for acidic soils and thus it neglects the effect of an open system with calcium carbonate dissolution that enhances on the positive side the quantity of carbon dioxide that is dissolved in the water. The numerical model by Jassal et al. (2004) solve the hydrochemistry system of carbon dioxide and carbonate and hydrocarbonated ions in the water in terms of species equilibrium under the assumption that the water residence time in the soil is higher enough that reaction kinetics can be neglected.

Baldini et al. (2008) studied an Arrhenius-type model, function of the external temperature, to describe soil biological activity as a source of biogenetic carbon dioxide in a cave environment.

4.5.2 *The Epikarst and Vadose Zone*

Epikarst as the uppermost fissured and weathered section of bedrock (Klimchouk 2004; Williams 2008) often exhibits a very complex hydraulic behavior. In fact, its porosity is very high at its contact with the soil, but decreases strongly with depth, causing a bottleneck effect for the vertical transport of water. Hydraulic conductivity in epikarst may be up to three orders of magnitude higher than in the remaining unsaturated zone (Klimchouk 2004). This situation forces water to:

- (a) To be stored in the epikarst when input flow exceeds the amount that can be transmitted in the lower vadose zone.
- (b) To move horizontally even for tens of meter to zones with higher permeability (main fissures, fractures ...).
- (c) To give rise already at this level to a fast transferred water components through major fissures and a slow fraction moving much slower and that can be retained even during dry period by capillary forces.

This early differentiation in epikarst has to be considered in the determination of the karst aquifer recharge-discharge function (Petrič 2002, p. 87). Bottrell and Atkinson (1992) identified three components of flow for the vadose zone, ranging from a rapid through-flow with residence time of approximately three days, a short term storage and residence time of 30-70 days and a long term storage with a characteristic time of 160 days or more. Correlating internal cave CO₂ partial pressure with carbon dioxide production in the soil predicted by an Arrhenius type model dependent on the external temperature Baldini et al. (2008) found that introducing a 39 day lag greatly improved the match between modeled and measured results. This delay has been attributed by the authors to the soil to cave transfer time. Tooth and Fairchild (2003) give a conceptual model of possible hydraulic conditions from the soil to the vadose zone which may control water hydrochemistry evolution.

If the soil is the main source of carbon dioxide, and therefore the place where the rain water gains much of its aggressiveness against the limestone bedrock, around 70 % of autogenic water aggressiveness is usually spent in the uppermost 10 m of the rock layer (Ford and Williams 2007, p. 93).

The first important control on water hydrochemistry occurs on the interface between soil and the limestone. Dissolution can occur in open, closed or any intermediate system. The open system achieves the highest level of limestone dissolution. The existence of three flow velocities (fast, medium and slow/storage) and thus residence times across the epikarst and the vadose zone allows different saturation levels to be reached. This phenomenon is of paramount importance for

trace and slowly soluble elements like Mg and Sr. The variability of residence time in the fissures results in another important degree of variability in drip water composition since the same dripping water point can be fed by a mix of different path ways, each one with different characteristic response time. Of course slow velocity pathways became controlling during dry period, while fast flow fissures and shafts are responsible for most of the flow during wet periods. The last but not least important control on water chemistry is at the boundary with the air filled voids in the lower vadose zone. At this point the water enters in contact with a gas phase (for example the cave atmosphere) with a generally lower partial pressure of carbon dioxide, dependent on the balance between the input (degassing from water) and output (ventilation with external atmosphere) fluxes.

Carbon dioxide degassing from the water leads to oversaturation with respect to CaCO_3 and consequently deposition of calcite. It should be noted that these last phenomena bring about changes in the C isotopic composition also (degassing of lighter isotopes), and concentration of trace elements like Mg and Sr in the solution. Explanations of trace elements and isotopic changes in drip water chemistry are provided in Fairchild and McMillan (2007), together with a simplified conceptual model of the epikarst control on drip water chemistry.

4.5.3 *The Phreatic Zone*

The phreatic zone is the lowest part in karst cross-section where all voids, ranging from rock porosity to large conduits, are water filled. Once water is collected in this region, it flows towards the spring, with a predominantly horizontal component, in contrast with the vadose zone where vertical percolation prevails. The interface between the phreatic and vadose zones is termed water table, and it represents a surface with relative minimum elevation located at spring points. The elevation of each point of this surface is a result of boundary conditions, geometry of the aquifer, and hydraulic conductivity, which is highly inhomogeneous and anisotropic in karst. The water table is also the only place where water stored in the phreatic network is in contact with a gas phase. Phreatic zone can be almost absent or limited in free draining springs (Ford and Williams 2007, p. 120).

The water table is a dynamic surface, with variations over at least two different time scales:

- over several tens of thousands of years governed by speleogenetical and geological processes and
- over hourly to yearly scale governed by hydrological conditions

The first variations are associated with karst massif evolution and increased extension and efficiency of the conduit network due to progressive limestone dissolution. This evolution continuously increases the hydraulic transmissivity of an aquifer. As a consequence, the water table is lowering within the karst massif. Other geological events occurring on the same time scale may also produce changes in

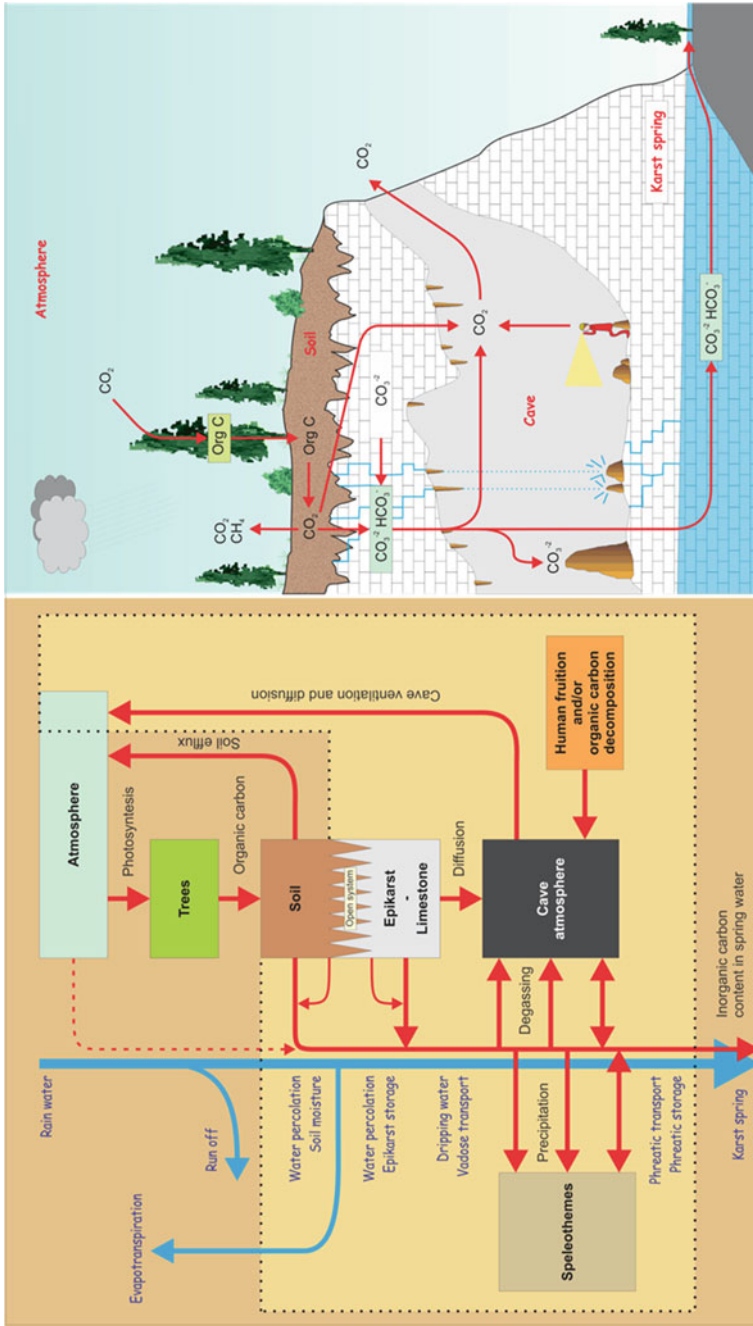


Fig. 4.2 Inorganic carbon sources and transport in the vadose zone of karst, a conceptual model

water table level. As an example, lowering of spring level due to the erosion of valleys will produce a lowering of the water table, but on the other hand, filling of valley bottom with sediments may produce dammed aquifers with a water table level higher than the original.

On shorter time scales, hydrological conditions are the predominant factor controlling the water level in the karst aquifer. Water level in karst aquifers can fluctuate for more than hundred meters depending on hydrological conditions. Region of water table fluctuation is called the epiphreatic zone.

4.6 Conclusions

An overall conceptual model of the inorganic carbon transport within a karst massif is presented in Fig. 4.2. Decomposition of organic matter produces carbon dioxide. This activity is located mainly in the soil layer, although evidence supports also an important, and in some cases a possibly predominant, component generated by decomposition of organic carbon which has been transported deep within the vadose zone. Consequently the biological activity gives rise to a gas phase in the soil porosity with high CO_2 partial pressure up to several tens of thousands ppm. The majority of this carbon dioxide is released back to atmosphere, but a fraction is dissolved in the downward percolating water. When this solution arrives in contact with limestone in the soil or epikarst, the calcium carbonate starts to be dissolved. In this process, carbon dioxide in water enhanced rock solubility by transforming carbonate ions into hydrocarbonate ions. Two end-members can be considered: (a) when the solution enters in contact with the carbonate rock and there is no longer any contact with a gas phase (closed system); (b) when the rock dissolution process occurs in the presence of a carbon dioxide rich gas phase (open system). In this last case additional CO_2 is dissolved during dissolution enhancing the amount of calcium carbonate that can be kept into solution (and therefore the total amount of inorganic carbon). The real conditions found in nature are usually intermediate between these end members. Another consequence of an open or partially open condition is that even when chemical equilibrium is reached and net flux is null still exchange of carbon dioxide between phases occurs. Hence part of carbon atoms introduced in solutions by the carbonate rock dissolution are released into the gas phase and substituted by an equivalent flux from gas phase to the solution. From a chemically stand point this phenomenon is irrelevant since the net flux is null. However, because carbon atoms from rock and gas phase have different isotopic composition the extent of the above mentioned exchange is reflected in a specific isotopic signature of the resulting percolating solution.

Water percolating across the vadose zone may reach a cave. Generally the cave atmosphere has a lower carbon dioxide content than the original gas phase in the soil or epikarst, and therefore excess CO_2 is released until a new equilibrium is achieved. The decrease of carbon dioxide content in the solution creates an over-saturation with respect to calcium carbonate and consequently calcite precipitation

occurs. Therefore part of the inorganic carbon originally present in the percolating solution is released as carbon dioxide to the cave atmosphere and as calcium carbonate in the form of speleothems.

In addition to degassing from dripping water, another source of inorganic carbon into the cave atmosphere is direct diffusion from soil and epikarst voids. This mechanism could occur only if there is an open connection between these two gas phases and is prevented if fractures and cracks in the epikarst are filled with water.

In some shallow caves, plant roots can protrude into the cave ceiling, pumping in CO₂ by root respiration.

Cave atmosphere may also receive an anthropogenic carbon dioxide input from human breathing while other potential sources such as decomposition of large quantity of organic matter in the cave and hypogenic source have not been considered in this study.

Carbon dioxide is stored in cave air, transported between underground passages and then release to external atmosphere by advection and diffusion. Inorganic carbon which is not degassed or precipitated from the drip water eventually reaches the phreatic zone where it is stored until it ultimately exits at springs.

Potentially some of carbon dioxide may be transported to depth or directly diffused to sea via the continental shelf in coastal settings. Both these phenomena have not been considered relevant for the study area.

References

- Appelo CAJ, Postma D (2006) *Geochemistry, groundwater and pollution*. AA Balkema Publishers, Leiden
- Baldini JUL, Baldini LM, McDermott F, Clipson N (2006) Carbon dioxide sources, sinks, and spatial variability in shallow temperate zone caves: evidence from Ballynamindra cave, Ireland. *J Cave Karst Stud* 68:4–11
- Baldini JUL, McDermott F, Hoffmann DL, Richards DA, Clipson N (2008) Very high-frequency and seasonal cave atmosphere PCO₂ variability: Implications for stalagmite growth and oxygen isotope-based paleoclimate records. *Earth Planet Sci Lett* 272:118–129
- Batiot-Guilhe C, Seidel J-L, Jourde H, Hébrard O, Bailly-Comte V (2007) Seasonal variations of CO₂ and ²²²Rn in a mediterranean sinkhole—spring (Causse d’Aumelas, SE France). *Int J Speleol* 36:51–56
- Benavente J, Vadillo I, Carrasco F, Soler A, Liñán C, Moral F (2010) Air carbon dioxide contents in the vadose zone of a Mediterranean Karst. *Vadose Zone J* 9:1–11
- Bottrell SH, Atkinson TC (1992) Tracer study of flow and storage in the unsaturated zone of a karstic limestone aquifer. In: Hotzl H, Werner A (eds) *Tracer hydrology*. Balkema, Rotterdam, pp 207–211
- Buhmann D, Dreybrodt W (1985a) The kinetics of calcite dissolution and precipitation in geologically relevant situations of karst areas: 1. Open system. *Chem Geol* 48:189–211
- Buhmann D, Dreybrodt W (1985b) The kinetics of calcite dissolution and precipitation in geologically relevant situations of karst areas: 2. Closed system. *Chem Geol* 53:109–124
- Denman KL, Brasseur G, Chidthaisong A, Ciais P, Cox PM, Dickinson RE, Hauglustaine D, Heinze C, Holland E, Jacob D, Lohmann U, Ramachandran S, da Silva Dias PL, Wofsy SC, Zhang X (2007) Couplings between changes in the climate system and biogeochemistry. In: Solomon S, Qin D, Manning M, Chen Z, Marquis M, Averyt KB, Tignor M, Miller HL

- (eds) *Climate change 2007: the physical science basis. contribution of working group I to the fourth assessment report of the intergovernmental panel on climate change*. Cambridge University Press, Cambridge, p. 996
- Dreybrodt W, Buhmann D (1991) A mass transfer model for dissolution and precipitation of calcite from solutions in turbulent motion. *Chem Geol* 90:107–122
- Dreybrodt W, Gabrovšek F (2002) Basic processes and mechanisms governing the evolution of karst. In: Gabrovšek F (ed) *Evolution of karst: from prekarst to cessation*. Karst research Institute ZRC SAZU, Postojna-Ljubljana, pp 115–154
- Dreybrodt W, Eisenlohr L, Madry B, Ringer S (1997) Precipitation kinetics of calcite in the system $\text{CaCO}_3\text{-H}_2\text{O-CO}_2$: The conversion to CO_2 by the slow process $\text{H}^{++}\text{HCO}_3 \rightarrow \text{CO}_2 + \text{H}_2\text{O}$ as a rate limiting step. *Geochim Cosmochim Acta* 61:3897–3904
- Faimon J, Stelcl J, Sas D (2006) Anthropogenic CO_2 -flux into cave atmosphere and its environmental impact: a case study in the Cisaraska Cave (Moravian Karst, Czech Republic). *Sci Total Environ* 369:231–245
- Fairchild I, McMillan E (2007) Speleothems as indicators of wet and dry periods. *Int J Speleol* 36:69–74
- Farquhar GD, Fasham MJR, Goulden ML, Heimann M, Jaramillo VJ, Khesghi HS, Le Quéré C, Scholes RJ, Wallace DWR (2001) The carbon cycle and atmospheric carbon dioxide. In: Houghton JD, Ding Y, Griggs DJ, Noguer M, van der Linden PJ, Dai X, Maskell K, Johnson CA (eds) *Climate change 2001: the scientific basis. contribution of working group I to the third assessment report of the intergovernmental panel on climate change*. Cambridge University Press, Cambridge, p 881
- Ford DC, Williams PW (2007) *Karst hydrology and geomorphology*. John Wiley and Sons Ltd
- Frisia S, Fairchild IJ, Fohlmeister J, Miorandi R, Spötl C, Borsato A (2011) Carbon mass-balance modelling and carbon isotope exchange processes in dynamic caves. *Geochim Cosmochim Acta* 75:380–400
- Hendy CH (1971) The isotopic geochemistry of speleothems—I. The calculation of the effects of different modes of formation on the isotopic composition of speleothems and their applicability as palaeoclimatic indicators. *Geochim Cosmochim Acta* 35:801–824
- Houghton RA, Woodwell GM (1989) Global climate change. *Sci Am* 260:18–26
- Jassal RS, Black TA, Drewitt GB, Novak MD, Gaumont-Guay D, Nesic Z (2004) A model of the production and transport of CO_2 in soil: predicting soil CO_2 concentrations and CO_2 efflux from a forest floor. *Agric For Meteorol* 124:219–236
- Kaufmann G, Dreybrodt W (2007) Calcite dissolution kinetics in the system $\text{CaCO}_3\text{-H}_2\text{O-CO}_2$ at high undersaturation. *Geochim Cosmochim Acta* 71:1398–1410
- Klimchouk A (2004) Towards defining, delimiting and classifying epikarst: its origin, process and variants of geomorphic evolution. *Speleogenesis Evol Karst Aquifers* 2:23–35
- Kowalczyk AJ, Froelich PN (2010) Cave air ventilation and CO_2 outgassing by radon-222 modeling: how fast do caves breathe? *Earth Planet Sci Lett* 289:209–219
- Kowalski AS, Serrano-Ortiz P, Janssens IA, Sánchez-Moral S, Cuezva S, Domingo F, Were A, Alados-Arboledas L (2008) Can flux tower research neglect geochemical CO_2 exchange? *Agric For Meteorol* 148:1045–1054
- Liu Z, Zhao J (2000) Contribution of carbonate rock weathering to the atmospheric CO_2 sink. *Environ Geol* 39:1053–1058
- Liu Z, Dreybrodt W, Wang H (2010) A new direction in effective accounting for the atmospheric CO_2 budget: considering the combined action of carbonate dissolution, the global water cycle and photosynthetic uptake of DIC by aquatic organisms. *Earth Sci Rev* 99:162–172
- Milanolo S, Gabrovšek F (2009) Analysis of carbon dioxide variations in the atmosphere of Srednja Bijambarska Cave, Bosnia and Herzegovina. *Bound-Layer Meteorol* 131:479–493
- Palmer AN (2002) Speleogenesis in carbonate rocks. In: Gabrovšek F (ed) *Evolution of karst: from prekarst to cessation*. Institut za raziskovanje krasa, Ljubljana, Slovenia, pp 43–59
- Petrič M (2002) Characteristics of recharge-discharge relations in karst aquifer. Karst research Institute ZRC SAZU, Postojna-Ljubljana

- Plummer LN, Wigley TML, Parkhurst DL (1978) The kinetics of calcite dissolution in CO₂-water systems at 5 degrees to 60 degrees C and 0.0 to 1.0 atm CO₂. *Am J Sci* 278:179–216
- Serrano-Ortiz P, Roland M, Sanchez-Moral S, Janssens IA, Domingo F, Godd ris Y, Kowalski AS (2010) Hidden, abiotic CO₂ flows and gaseous reservoirs in the terrestrial carbon cycle: review and perspectives. *Agric For Meteorol* 150:321–329
- Simon KS, Pipan T, Culver DC (2007) A conceptual model of the flow and distribution of organic carbon in caves. *J Cave Karst Stud* 69:279–284
- Tooth AF, Fairchild IJ (2003) Soil and karst aquifer hydrological controls on the geochemical evolution of speleothem-forming drip waters, Crag Cave, southwest Ireland. *J Hydrol* 273:51–68
- Williams P (2008) The role of the epikarst in karst and cave hydrogeology: a review. *Int J Speleol* 37:1–10

Chapter 5

Cave Climate

Abstract The overall climate of Srednja Bijambarska cave appears to be characterized by two distinct seasons or climatic regimes. The switch between these two regimes is triggered by the difference between external and internal temperatures. When the outside temperature is lower than the underground temperature, the cave is highly ventilated. The CO₂ concentration is low, slightly lower than averages are also relative humidity and temperature. All these parameters exhibit high fluctuations in response to external changes. Conversely, when the outside temperature is higher than the underground temperature, ventilation is inhibited, and therefore carbon dioxide accumulates, relative humidity increases as well as temperature. During this period, all these parameters show weaker relationship with external temperature changes.

5.1 Introduction

Monitoring of cave temperature and observations of wind speed and direction in underground channels has a long tradition. However, since the first single measurements of temperature using mercury thermometers, technological advances today provide a wide range of sensors and data loggers for measuring several different parameters. To the original temperature and relative humidity instruments have been added pressure, air velocity and carbon dioxide concentration measuring instruments and, more recently, radon detectors and isotopic analysis of the cave atmosphere.

Most studies on cave climate and cave atmosphere have been focused on the anthropogenic impact in show caves (Dragovich and Grose 1990; Cigna 1996, 2002; Song et al. 2000; Calaforra et al. 2003; Faimon et al. 2006; Fernandez-Cortes et al. 2006).

Nevertheless, with the expanding interest in speleothems as archives of past climatic conditions, the role of natural cave atmospheric processes governing carbon

dioxide dynamics (Milanolo and Gabrovšek 2009) and consequently influencing speleothem growth and drip water composition have received renewed consideration (Spötl et al. 2005; Baldini et al. 2008).

The theory of cave climate is summarized by Badino in several works (Badino 1995, 2010) and expanded in detail for phenomena like clouds and mist formation in underground passages (Badino 2004a) and the response of a karst massif to the external climate changes (Badino 2004b). The complexity of the study of underground meteorological phenomena is often underestimated due to the fact that changes in the cave environment are very small and therefore justifying the widely accepted but false idea that the cave climate is absolutely stable. To experimentally measure the details of most cave meteorological processes, high resolution and high stability sensors need to be developed (Badino and Chiri 2005; Badino 2010). On the other hand, data loggers including cave temperature sensors with resolution up to one hundredth of degree and acceptable accuracy are nowadays largely available on the market and they allow identifying at least basic cave climatic behavior and its dependency with external factors. Unfortunately, data of cave atmosphere monitoring are provided in the literature only with general descriptive statistics and basic explanations, while efforts to investigate the correlations of observed changes with other parameters are scarce. Going towards this last direction are, among the other, the works of Gamble et al. (2000) (relationship between external and internal temperatures), Bourges et al. (2006) (relationship between pressure and temperature), Baldini et al. (2008) (relationship between carbon dioxide concentration and external temperature) and for more long term changes the work of Stoeva and Stoev (2005) (relationship between cave temperature and solar and geomagnetic activities). In this work we try to link a basic conceptual climatic model with variations of different parameters and to provide a statistical analysis of internal–external temperature relationship to further support this model.

5.2 Results and Discussion

5.2.1 *Historical Data*

The first basic microclimatic data from Srednja Bijambarska cave were collected by Baučić and Ržehak (1959), Pašić (1962) and Malez (1968). All authors stressed the necessity to perform more detailed and continuous researches in prospective of tourist adaptation or to improve the comprehension of karst microclimatic characteristics.

Based on a series of measurements included in the previous cited works, the cave temperature was shown to rise from 3.6 °C (10 m after the entrance) to 6 °C (in the “Music Hall”) with an outside temperature of 17 °C. The final cave chamber shows the most stable temperature pattern. Relative humidity rises from 80 % at 10 m from the entrance to values up to 95 % in the most distant channels.

Baučić and Ržehak (1959) and Malez (1968) report a weak air circulation which was sensed only in the narrow passage between the main channel and final chamber (“Music hall”).

The observations provided by Baučić and Ržehak (1959) may suggest that the flow direction was towards the final chamber. In winter, ice stalagmites are observed up to a couple of hundred meters from the cave entrance.

5.2.2 Temperature

Three years and five months of external and internal (T_4) temperatures presented in Fig. 5.1, showing the direct relationship between cave and outside climates. The external temperature (T_{out} —Fig. 3.8) fluctuates seasonally and daily within the range -32 to 37 °C. The recorded average external temperature is 6.4 °C (from 24th November 2006 to 23rd November 2010) and it is slightly higher than historical data (6.2 °C). The T_4 cave average temperature, measured in a partly isolated gallery to the east of the main cave axis (Fig. 3.8) is lower than external (5.4 vs. 6.4 °C). Fluctuations at T_4 are reduced to the range 4.7 – 6.2 °C. Cave temperature data are available from other three locations (T_1 , T_2 and T_3) but for a limited period of only one year and four months (Fig. 5.1). These last time series show similar behaviour compared to T_4 with reduced fluctuation amplitude proceeding northward towards the internal part of the cave (“Music Hall”—Fig. 3.8).

Both external temperature and T_4 have been interpolated by a linear plus trigonometric function with 365 days period in the form:

$$T = a + b \cdot t + c \cdot \sin\left(\frac{2\pi}{365} \cdot (t + d)\right) \quad (5.1)$$

The coefficients a , b , c , and d , estimated by least square regression are shown in Table 5.1.

While the external temperature signal is fitting uniformly with the sinusoidal interpolation of Eq. 5.1, the T_4 time series presents evident anomalies during the autumn-winter season. During seasonal cave warming, the temperature rise rather constantly without high amplitude fluctuation over the short period (days) and the cave acts efficiently as low-pass filter with regards to daily external temperature changes. The situation radically changes when the outside temperature drops below the cave temperature (i.e. winter season). During these cold periods T_4 sensor records high fluctuations of temperature in accordance with the external temperature behaviour showing a stronger connection with the external environment.

It appears that while external temperature shows a decreasing trend of -7.8×10^{-4} °C day $^{-1}$ the internal temperature increase as average of 7.9×10^{-4} °C day $^{-1}$ (parameter b in Table 5.1). However, these values should not be considered statistically relevant since they refer to only three/four years and even more important, the instrument drift is unknown and no cross calibration was performed. On the

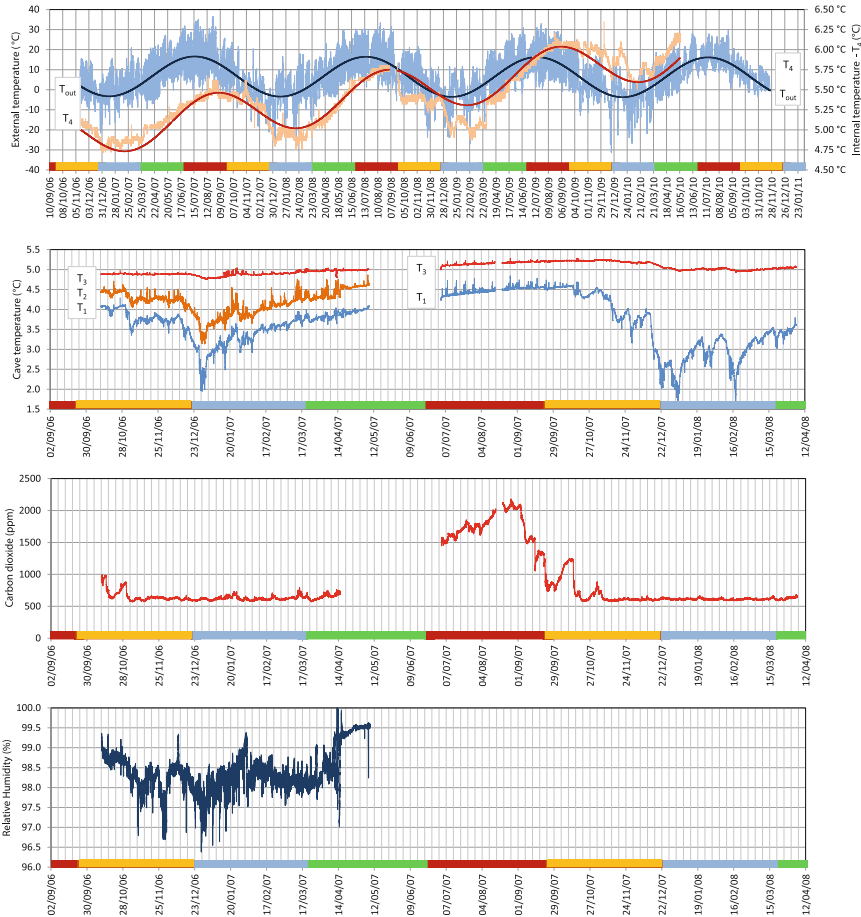


Fig. 5.1 Long term records of several parameters: external temperature (T_{out}) and internal temperature (T_4); internal temperature T_1 , T_2 and T_3 ; carbon dioxide concentration in the “Music hall”; relative humidity in the “Music hall”. Note that upper graph has a different time scale than remaining charts. *Colored bars* at the bottom of each graph represent seasons (*green* spring; *red* summer; *brown* autumn; *blue* winter). Locations of sensors are shown in Fig. 3.8 (color figure online)

Table 5.1 Coefficients from interpolation of Eq. 5.1

	a (°C)	b (°C/day)	c (°C)	d (days)
T_{out}	6.89	-7.8×10^{-4}	-9.95	30.3
T_4	4.94	7.9×10^{-4}	-0.29	-13.0

other hand, it is interesting to notice that the two interpolated sine functions for T_{out} and T_4 have a mutual delay of 43.3 days. Similar delay is obtained by cross correlation analysis (maximum correlation coefficient at 51 days of delay).

This delay of the internal temperature time series is often interpreted as time necessary for the signal to travel from outside to the measuring point. It is caused by the thermal inertia of the cave system. This term has been formally defined by Badino (2004b) as “*the ratio between the thermal energy absorbed by the mountain through the cave and the corresponding temperature increase of the whole system*”. The presence of this term introduces (in analogy to an inductance element in an electric circuit) a phase delay between the two temperature signals. The thermal inertia of the system and consequently the phase delay depends, among other factors, on the frequency of the signal. Very fast changes in cave temperature impact only on the cave atmosphere while low frequency signals penetrate deeper into the rock surrounding the cave and as a result generating a higher thermal inertia. In particular, for changes of external temperature of period higher than few minutes it can be demonstrated that the thermal inertia of a cave is dominated by the thermal capacity of the surrounding layer of rock up to depth of few meters (Badino 2004b).

5.2.3 Climatic Regimes

In order to attempt an explanation for the dual behaviour of the cave environment and the lower internal temperature with respect the external average, a “cold trap” conceptual model has been considered.

The “cold trap” model is common for many caves characterized by only one entrance localized at an upper level of the underground system (Bourges et al. 2001, 2006; Piasecki et al. 2005) and it consists of two climatic conditions:

Regime 1—When outside is colder than the cave environment, the external air descends into the cave displacing an equal volume of warmer cave air which flows backward to the entrance moving under the ceiling of underground passages due to its relatively higher temperature and consequently lower density. During this regime the cave is highly ventilated and the internal temperature is influenced by short period changes of external temperature.

Regime 2—When the external temperature rises above the cave temperature, the internal cold and dense air is trapped and stable thermal stratification occurs. During this regime there is no or limited air circulation and the convective exchange of heat with the external atmosphere is inhibited.

It should be noticed that in the definition of the climate model it has been implicitly assumed that air density at a given pressure is controlled only by air temperature. Therefore it has been assumed that air density differences can be explained in terms of temperature differences alone. This simplification is generally valid for most cases. However, air composition in terms of humidity and carbon dioxide concentration should be considered in detail calculation. This problem is usually simplified by defining a virtual temperature for the cave environment equal to temperature necessary for an air composed of only nitrogen, oxygen and argon to

attain identical density as the real cave atmosphere (Badino 1995, p. 17; Kowalski and Sánchez-Cañete 2010). By applying equation developed by Kowalski and Sánchez-Cañete (2010) to the conditions recorded at the site investigated in this study (relative humidity 100 % and carbon dioxide concentration between 1000 and 2000 ppm), the difference between virtual temperature and real cave temperature is within 0.5 °C and, even if higher than measurement error, this correction has been neglected further on in the study.

To confirm the existence of two distinct climatic regimes, two data loggers were fixed at different elevations on the entrance gate of the cave, for a period of 10 days.

The lower instrument (T_{low}) was located at 60 cm from ground, while the upper one (T_{up}) was tied at around 1 m from the cave ceiling. The results presented in Fig. 5.2 clearly depict the switch between the two climatic regimes. During the first two days the external temperature was lower than cave temperature (regime 1). During the following three days the external temperature rises above the cave

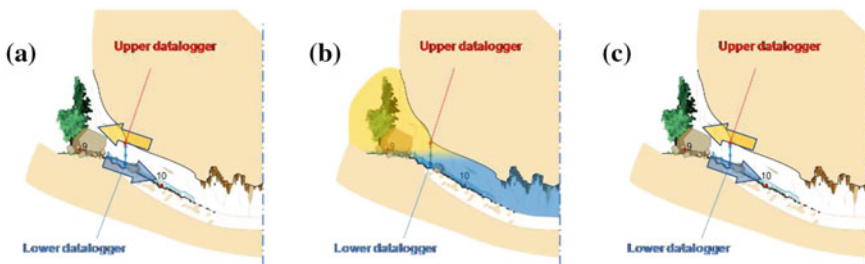
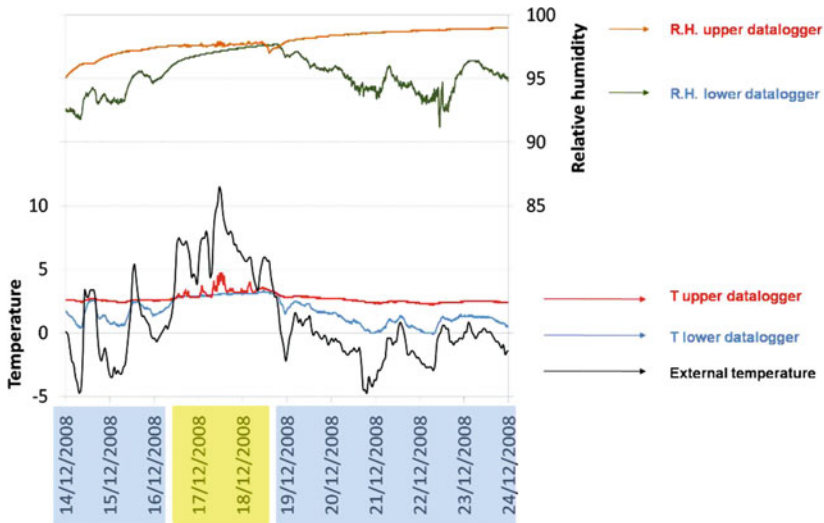


Fig. 5.2 Switching between climatic regimes recorded by data loggers installed at the cave entrance gate

temperature and immediately the cave climate switch to regime 2. During this period the T_{low} becomes almost constant, at a value close to the cave main channel temperature due to the inhibition of air circulation (Fig. 5.2b) while T_{up} located at an elevation somewhat higher than the entrance ground level slightly responds to the external variations of temperature. When the outside temperature again falls below the underground temperature, the regime 1 is resumed (Fig. 5.2c) and cave ventilation is re-established.

5.2.4 *Developing an Internal–External Temperature Semi Empiric Relationship*

The internal temperature is clearly influenced by the external temperature. A simple method to assess this relationship is a direct linear regression between these two temperatures. This approach has been used for example by Gamble et al. (2000) to relate different internal temperature time-series with the external temperature in tropical flank margin caves. A linear regression applied to Bijambare T_1 measures (the only available time series with enough measurements and significant signal amplitude) would give a value of R^2 of 0.331 and 0.167 for regime 1 and 2 respectively. However, this approach ignores the physical background and, for example, it cannot explain the phase delay between the two signals. The dependency is highly complex and it is not the scope of this work to develop a rigorous theoretical approach to this problem, but instead to find a general form for a regression equation. A highly simplified transient heat balance considering only convective heat transfer between external and internal atmosphere due to an air flow Q should have a general form of:

$$\frac{dT}{dt} = AQ(T_{out} - T) \quad (5.2)$$

As mentioned before, in this equation, at least few important factors such as the enthalpy contributions from water, condensation phenomena, geothermal flux and heat exchange with rock have been neglected. The arbitrary factor A includes among other physical terms, the cave thermal inertia which depends on many features like cave geometry, rock characteristics and frequency of the signal (low frequency signals have longer penetration length into the surrounding rock layer of the cave passage and thus the thermal inertia of the cave system is higher).

In Milanolo and Gabrovšek (2009) it has been found that average air flow in Bijambarska cave, following the analysis of one year monitoring data, was around $3450 \text{ m}^3 \text{ h}^{-1}$. Which, for a cross section of 40 m^2 (half of the main channel typical section), gives an average velocity of 2.40 cm s^{-1} . The critical velocity for the laminar to turbulent transition can be calculated by the approximate equation (Badino 1995):

$$v_c \approx \frac{150}{r} \quad (5.3)$$

where v_c is the critical velocity in cm s^{-1} and r is the conduit radius in cm. The main channel half cross section can be approximated by a pipe of 350 cm of radius leading to a critical velocity of roughly 0.4 cm s^{-1} . This critical velocity is much lower than the estimated average velocity and for this reason we can assume that for most of the time the air moves following a turbulent regime. Laminar flow should be limited to situations when driving force is very low and thus in a narrow range of external-internal temperature difference close to zero.

Heat transport by air advection depends on air flow rate and on the difference between external and internal temperatures. In a turbulent flow, the pressure drops increase with the square of fluid velocity, and therefore with the square of the flowrate. Moreover, in a steady state motion the pressure drops are equal to the driving force. Reversing, we can assume that the flow rate depends on the root of driving forces and if we consider as driving force only the difference of densities caused by difference of temperature between inside and outside atmospheres (neglecting for example other driving forces such as differences of barometric pressure) then:

$$Q = A' \cdot (T_{out} - T)^{0.5} \quad (5.4)$$

Combining Eqs. 5.2 and 5.4 we obtain:

$$\frac{dT}{dt} = A'' \cdot (T_{out} - T)^{1.5} \quad (5.5)$$

Another factor has been added to this equation in order to account for the heat transferred due to the disequilibrium between cave temperature and rock bulk temperature (approximated as average external temperature $T_{ave} = 6.2 \text{ }^\circ\text{C}$). This term is surely very complex, but for the purpose of this work has been assumed to depend linearly on the difference of temperatures. The final equation used to fit a regression model is:

$$\frac{dT}{dt} = A'' \cdot (T_{out} - T)^{1.5} + B''(T_{ave} - T) + C'' \quad (5.6)$$

5.2.5 Linear Regression Results

Figure 5.3a shows the time derivative of signal T_1 (sampled from the original time series every hour), versus the difference of temperature between outside (T_{out}) and internal temperature (T_1). Figure 5.3b illustrates the same data, but plotted against the difference between average temperature (T_{ave}) and internal temperature (T_1).

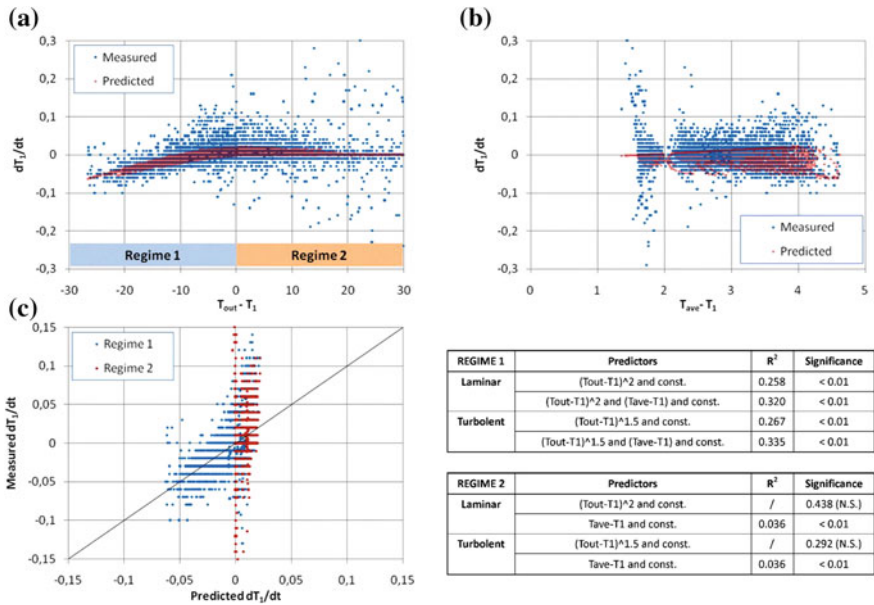


Fig. 5.3 Measured and predicted values obtained by best fitting of Eq. 5.6. For description refer to text

Other signals maybe treated similarly but, due to the small changes in temperature, the potential relationship is hidden behind the background noise and for this reason they are not presented.

In the same figure are presented the result of a statistical analysis using a linear regression method where the dependent variable is the time derivate of the T_1 signal and as predictors are the terms included in Eq. 5.6. The regression analysis has been performed separately for each climate regime. The results show that for Regime 1, the term including the outside temperature is the main factor responsible to the total variability predicted by the model ($R^2 = 0.267$) and that its contribution is highly statistically significant. The second term, including T_{ave} , only slightly improves the prediction capacity of the model (total $R^2 = 0.335$) however, also this contribution is statistically significant. The situation changes completely when the cave climate is in regime 2. As described previously, when the outside temperature rises above the internal temperature, exchange between the inside and outside is inhibited, and the term including the outside temperature loses statistical power to predict the temporal changes of T_1 . The remaining factor (difference of T_{ave} and T_1) is still statistically significant, but the prediction capacity is very low ($R^2 = 0.036$).

The results of the model (Eq. 5.6) are shown in Fig. 5.3a and b, while the equation coefficients and their confidence interval are reported in Table 5.2.

Figure 5.3c details the predicted values against the measured value of the time derivate of T_1 . If a model described the experimental data exactly, then the points should lie on a line passing from the origin and a slope of 1. As mentioned before,

Table 5.2 Linear regression coefficients and their confidence interval for Eq. 5.6

Regime 1	Coefficient	95 % confidence interval	
		Lower	Upper
A''	-0.00063	-0.00066	-0.00061
B''	0.00957	0.00884	0.01030
C''	-0.01799	-0.01989	-0.01610
Regime 2			
A''	/	/	/
B''	0.00940	0.00794	0.01085
C''	-0.01574	-0.01898	-0.01240

the model is able to estimate 33.5 % of measured variability during regime 1 but only 3.6 % during Regime 2. Although 33.5 % may seem a relatively low prediction capacity, the presence of noise in the original temperature signal is amplified during the time derivate operation, and it may explain large part of the missing variability. Another important factor neglected in the model are the pressure fluctuations which may provide for an unaccounted barometric cave breathing and thus heat exchange by advection with the external atmosphere or, as analysed by Bourges et al. (2006), by heat released/adsorbed due to the gas compression/expansion. The coefficients provided in Fig. 5.2 in the reality include terms that are dependent on signal period (i.e. the cave thermal inertia) and thus a more correct approach also mentioned in Bourges et al. (2006) should be to perform the regression analysis on signals filtered around important periods (i.e. 365 days and/or 24 h).

Working with temperature derivate of the internal temperature signal has the advantage that gives explanation for the existence of the phase delay between the two signals. The cave temperature achieves its maximum when its time derivate is null. This happens when the right side of Eq. 5 is null and not when the outside temperature is maximum.

5.2.6 Relative Humidity

Measurement of relative humidity with the commonly employed transducer in a range close to saturation (as in a cave atmosphere) is often problematic. The data collected in Fig. 5.2, based on capacitive sensors, suffer greatly from such extreme humidity conditions. Relative humidity values shown in Fig. 5.1d are instead measured by a dry and wet bulbs instrument with forced ventilation and, even if also this instrument loses precision at values close to saturation, it can be considered more trustworthy than capacitive sensors. Although relative humidity values, for the above mentioned reasons, should not be considered reliable, a tentative discussion of the results is given hereafter.

Cave relative humidity data (Fig. 5.1d) measured in the “Music hall” are available for only 7 months (from October to April). During this period the

instrument recorded values in the range from 96.5 to 99.5 % with the lowest values acquired during cold spells (Regime 1) due to the access in the cave of external colder and drier air.

Furthermore, the results of the experiment performed at the cave gate with two data loggers located at different elevation (Fig. 5.2) can be interpreted as well as function of the switch between the two cave climatic regimes. In detail, during the first two and last four cold days (regime 1), the relative humidity recorded by the lower data logger had high fluctuations featuring approximately the external air humidity entering into the cave (during the whole experiment the external relative humidity stayed always in the interval 75–100 %—data not shown) while the upper data logger measures were approaching asymptotically the equilibrium with the more humid air from the underground conduits. During the three days between December 16th and 18th 2008 the cave climate switches to Regime 2 and thus the cave ventilation was inhibited. During this period there is no longer a flow of cave air moving under the ceiling of the cave passages towards the exit, and the upper instrument stops to measure a rising of relative humidity showing a more constant flat trend. Similarly, the lower instrument is not influenced anymore by the external atmosphere and the recorded values rise slowly to approach the measurements of the upper instrument. Both instruments seem to be dipped into a stable atmosphere volume with little exchange and influence from internal and external atmospheres. Because of lack of reliable measurements, other phenomena related to mixing of air volumes with different characteristics have been neglected in this interpretation. These events may generate locally over saturations responsible for clouds and mist formation and vapour condensation (Badino 2004a) and they have an important role to explain relative humidity variations in the cave atmosphere.

5.2.7 Carbon Dioxide

Carbon dioxide variations in space and time were in detail investigated in Milanolo and Gabrovšek (2009) in order to estimate the CO₂ input and output fluxes in the cave atmosphere (see Chap. 6). The result of spatial survey of concentrations along the cave during the Regime 1 and Regime 2 given in the above mentioned work clearly depicted the presence of two extreme situations. During Regime 1, carbon dioxide concentration slowly increased along the main channel, and achieved a maximum value around 600 ppm in the “Music hall” chamber. These low concentrations are caused by the high ventilation rate affecting the cave atmosphere during the outside cold season. Conversely, during Regime 2, the carbon dioxide accumulates in the cave due to the very low ventilation with the external atmosphere. During this regime, the carbon dioxide concentration spatial profile rapidly achieves the maximum concentration level in few meters from the cave entrance. The data of time variability of carbon dioxide concentration in the “Music hall” chamber reported in Fig. 5.1c and drive to similar conclusions: The carbon dioxide level drops rapidly when outside temperature decreases under cave temperature

triggering the beginning of the cave high ventilation season (Regime 1). The concentration reaches a more or less constant minimum (around 550–600 ppm) level during whole winter season and slowly rising when the outside temperature achieves again values above cave temperature inhibiting the exchange with external atmosphere. The maximum level (around 2200 ppm) is reached at the end of summer at conclusion of the warm season (Regime 2).

5.2.8 Radon Concentration

Radon is a naturally occurring radioactive gas that is produced by the decay of uranium and other elements included in the rocks. Radon gas moves through rocks voids and the soil by diffusion and advection and, when entering poorly ventilated underground areas such as caves, it may reach potentially dangerous concentrations for human health. This is recognized as one important issue to monitor in show caves not usually associated to tourist risk but mostly to people spending long time underground as the tour guides.

Radon concentration measurements were performed at two locations in Srednja Bijambarska cave in two periods (July–August 2010, December–January 2011). The results are given in Table 5.3. Recorded concentrations are low comparing to mean radon concentrations worldwide, that are from 0.1 to 20 kBq/m³ (Hakl et al. 1997). New measurements in Croatia showed that there are possible radon concentrations in Dinarides up to 22 kBq/m³ (Paar et al. 2009).

Even though carbon dioxide and Radon have different origins and input modality into the cave environment, accumulation and advection dynamics are similar and largely related to the local ventilation rate. Hence, in most of cases, it is possible to establish a similar correlation between variations of concentrations of these two parameters to the ventilation rate (Faimon et al. 2006; Kowalczk and Froelich 2010). This similar behavior is confirmed in Bijambare cave where high concentrations of carbon dioxide and Radon are both recorded during summer

Table 5.3 Measurements of radon concentration c and equilibrium constant F at two locations in Srednja Bijambarska cave in two periods (July–August 2010, December–January 2011)

Location	Detector nr.	Start of meas.	End of meas.	Radon concentration (Bq m ⁻³)	Equilibrium constant F
R_{MC} (main channel)	S-189	18.07.2010. 12:15	27.08.2010. 13:30	867 ± 66	0.48 ± 0.05
R_{MH} (Music hall)	S-188	18.07.2010. 11:30	27.08.2010. 13:15	885 ± 68	0.28 ± 0.04
R_{MC} (main channel)	S-251	25.12.2010. 11:00	15.01.2011. 12:00	199 ± 20	0.77 ± 0.11
R_{MH} (Music hall)	S-252	25.12.2010. 11:00	15.01.2011. 12:00	157 ± 17	0.33 ± 0.09

when cave ventilation is at minimum (Regime 2) and minimum concentrations (4.4 times lower) in winter (Regime 1).

There is a small inversion between values at location R_{MC} and R_{MH} during the two investigated periods. Main channel (R_{MC}) is between Music hall and the cave entrance and, when the ventilation is small (summer period), it has the lowest radon concentration is in Music hall (R_{MH}). In winter period, when the ventilation is much bigger, the radon concentration in Music hall is the lowest. However the differences between the two locations are relatively low and close to the expected error of the measurement.

5.3 Conclusions

The overall climate of Srednja Bijambarska cave is characterized by two distinct seasons or climate regimes. The switch between these two regimes is triggered by the difference between external and internal temperatures though pressure oscillations may represent another important cofactor. When outside temperature is lower than underground temperature the cave environment is highly ventilated, with low concentration of carbon dioxide and radon, slightly lower than average values of relative humidity and temperature featuring high fluctuation in response to external changes.

Conversely, when outside temperature is higher than underground temperature ventilation is inhibited and therefore carbon dioxide and radon accumulate, relative humidity increases as well as temperature. During this period, all these parameters show weaker relationship with external temperature changes. A multi parameter linear regression confirm how the relationship between time derivate of internal temperature and the external temperature loses statistical significance when external temperature rise above cave temperature.

References

- Badino G (1995) Fisica del Clima Sotterraneo. Memorie dell'Istituto Italiano di Speleologia, Serie II, vol 7, Bologna
- Badino G (2004a) Clouds in caves. Speleogenesis and evolution of karst aquifers 2:1–8
- Badino G (2004b) Cave temperatures and global climatic change. Int J Speleol 33:103–114
- Badino G (2010) Underground meteorology—What's the weather underground? Acta Carsologica 39:427–428
- Badino G, Chiri M (2005) First data from the underground meteorological station of Rio Martino, Italy. In: Proceedings of the 14th international congress of speleology 2005, Athens, Greece
- Baldini JUL, McDermott F, Hoffmann DL, Richards DA, Clipson N (2008) Very high-frequency and seasonal cave atmosphere PCO_2 variability: implications for stalagmite growth and oxygen isotope-based paleoclimate records. Earth Planet Sci Lett 272:118–129

- Baučić I, Ržehak V (1959) Bijambarska pecina. Nase Starine Godisnjak Zemaljskog muzeja za zastitu spomenika kulture i prirodnih rijetkosti Narodne Republike Bosne i Hercegovine 6:219–230
- Bourges F, Mangin A, d'Hulst D (2001) Le gaz carbonique dans la dynamique de l'atmosphère des cavités karstiques : l'exemple de l'Aven d'Orgnac (Ardèche). *Comptes Rendus de l'Académie des Sciences—Series IIA—Earth and Planetary Science* 333:685–692
- Bourges F, Genthon P, Mangin A, D'Hulst D (2006) Microclimates of l'Aven d'Orgnac and other French limestone caves (Chauvet, Esparros, Marsoulas). *Int J Climatol* 26:1651–1670
- Calaforra JM, Fernández-Cortés A, Sánchez-Martos F, Gisbert J, Pulido-Bosch A (2003) Environmental control for determining human impact and permanent visitor capacity in a potential show cave before tourist use. *Environ Conserv* 30:160–167
- Cigna AA (1996) Risultati di una prima campagna di misure ambientali nelle grotte di Toirano. In: *Proceedings international symposium show caves and environmental monitoring*, Cuneo, Italy, pp 87–98
- Cigna AA (2002) Monitoring of caves: conclusions and recommendations. *Acta Carsologica* 31:175–177
- Dragovich D, Grose J (1990) Impact of tourists on carbon dioxide levels at Jenolan Caves, Australia: an examination of microclimatic constraints on tourist cave management. *Geoforum* 21:111–120
- Faimon J, Stelcl J, Sas D (2006) Anthropogenic CO₂-flux into cave atmosphere and its environmental impact: a case study in the Císarska cave (Moravian Karst, Czech Republic). *Sci Total Environ* 369:231–245
- Fernandez-Cortés A, Calaforra JM, Jimenez-Espinosa R, Sanchez-Martos F (2006) Geostatistical spatiotemporal analysis of air temperature as an aid to delineating thermal stability zones in a potential show cave: implications for environmental management. *J Environ Manage* 81:371–383
- Gamble DW, Dogwiler JT, Mylroie J (2000) Field assessment of the microclimatology of tropical flank margin caves. *Clim Res* 16:37–50
- Hakl J, Hunyadi I, Csige I, Géczy G, Lénárt L, Várhegyi A (1997) Radon transport phenomena studied in Karst caves-international experiences on radon levels and exposures. *Radiat Meas* 28:675–684
- Kowalczyk AJ, Froelich PN (2010) Cave air ventilation and CO₂ outgassing by radon-222 modeling: how fast do caves breathe? *Earth Planet Sci Lett* 289:209–219
- Kowalski AS, Sánchez-Cañete EP (2010) A new definition of the virtual temperature, valid for the atmosphere and the CO₂-rich air of the vadose zone. *J Appl Meteorol Climatol* 49:1692–1695
- Malez M (1968) Bijambarske pećine kod Olova u sredisnjoj Bosni. *Glasnik Zemaljskog muzeja Bosne i Hercegovine u Sarajevu, Prirodne nauke, Nova serija* 7:154–191
- Milanolo S, Gabrovšek F (2009) Analysis of carbon dioxide variations in the atmosphere of Srednja Bijambarska cave, Bosnia and Herzegovina. *Bound-Layer Meteorol* 131:479–493
- Paar D, Radolić V, Lacković D, Buzjak N, Čop A, Bakšić D (2009) Radon concentration measurements on Mt. Velebit and Mt. Žumberak (Croatia). In: Gabrovšek F, Mihevc A (eds) *17th International Karstological School "Classical Karst"*. IZRK ZRC SAZU, Postojna, p 78
- Pašić H (1962) Neki meteorološki podaci o pećini Biambara. *Proceeding of Treći Jugoslavenski speleološki kongres—Sarajevo* (1962)
- Piasecki J, Sawinski T, Zelinka J (2005) Spatial differentiation of the air temperature in the entrance collapse of Dobsinska ice cave as contribution to the recognition of the problem of air exchange between cave and the surface. *Acta Carsologica Slovaca XLIII*:81–96
- Song L, Wei X, Liang F (2000) The influences of cave tourism on CO₂ and temperature in Baiyun cave, Hebei, China. *Int J Speleol* 29:77–87
- Spötl C, Fairchild IJ, Tooth AF (2005) Cave air control on dripwater geochemistry, Obir caves (Austria): implications for speleothem deposition in dynamically ventilated caves. *Geochim Cosmochim Acta* 69:2451–2468
- Stoeva P, Stoev A (2005) Cave air temperature response to climate and solar and geomagnetic activity. *Mem Soc Astron Ital* 76:1042–1047

Chapter 6

Carbon Dioxide Sources, Storage and Transport in the Cave Atmosphere

Abstract The results of carbon dioxide (CO₂) monitoring in Srednja Bijambarska Cave (Bosnia and Herzegovina) are presented and discussed. Temporal variations of the concentration are controlled by the switching between two ventilation regimes driven by outside temperature changes. A regression model with a simple perfectly mixed volume applied to a cave sector (“Music hall”) resulted in an estimate of ventilation rates between 0.02 and 0.54 h⁻¹. Carbon dioxide input per plan surface unit is estimated by the model at around 50 × 10⁻⁶ m h⁻¹ during the winter season, to more than 1000 × 10⁻⁶ m h⁻¹ during the first temperature falls at the end of summer (0.62 and 12.40 μmol m⁻² s⁻¹ at normal conditions respectively). These values have been found to be related to the cave ventilation rate and dependent on the availability of CO₂ in the surrounding environment. For airflow close to zero the values of CO₂ input per plan surface are in the order of few 10⁻⁶ m h⁻¹. The anthropogenic contribution from cave visitors has been calculated, based on two experiments, at between 0.35 and 0.45 L_{CO₂} min⁻¹ person⁻¹.

6.1 Introduction

Carbon dioxide (CO₂) plays a key role in limestone dissolution and deposition of speleothems. Changes in partial pressure of CO₂ in the cave environment can enhance limestone precipitation, turn the equilibrium toward aggressive solutions or augment the effect of corrosion by condensation. Therefore the control of the additional CO₂ input originating from tourist visits has been recognized as a potential issue for the conservation of caves. The concentration of CO₂ has been included by Cigna (2002) in the list of important parameters for monitoring systems

Material from this chapter has been originally published in Milanolo S, Gabrovšek F (2009) Analysis of Carbon Dioxide Variations in the Atmosphere of Srednja Bijambarska Cave, Bosnia and Herzegovina. *Boundary-Layer Meteorology* 131(3):479–493. doi:[10.1007/s10546-009-9375-5](https://doi.org/10.1007/s10546-009-9375-5).

in show caves. With the growth of studies that use speleothems as a proxy for paleoclimate there is an increase in interest in understanding how cave climate and thus the variability of carbon dioxide in the underground atmosphere influences speleothem growth and composition (Spötl et al. 2005; Fairchild and McMillan 2007; Baldini et al. 2008).

The concentration of carbon dioxide in caves has been recorded extensively (Dragovich and Grose 1990; Cigna 1996) to assess the tourist impact on the cave environment. Nevertheless, there is still a lack of data that enable quantitative treatment of spatial and temporal variations of CO₂. Recently, high resolution CO₂ maps were presented to identify the sources and sinks in a cave (Baldini et al. 2006a). Faimon et al. (2006) used a perfectly mixed reactor model to interpret the temporal variation of CO₂ concentration in Císařská Cave (Czech Republic). The scope of the present chapter is to link together a conceptual model of the cave climate and carbon dioxide temporal and spatial distributions while also considering possible anthropogenic contributions to this variability.

6.2 Carbon Dioxide Concentration Variability in the Cave Atmosphere

6.2.1 Seasonal and Diurnal Variability

A conceptual model of the cave climate has been proposed and discussed in Chap. 4. Hereafter only final conclusions potentially affecting the carbon dioxide concentration in the cave atmosphere are briefly summarized.

An overview of the general cave microclimate, with data recorded by the monitoring system, is given in Fig. 6.1. Periods when the outside temperature was higher than the inside temperature, are shown in the upper graph as darker areas.

The cave, due to its morphology, acts as a “cold trap” allowing stable thermal stratification during warm periods. Two regimes can be visualized:

Regime 1—When the outside temperature T_{out} is lower than the cave temperature (e.g. during December), external cold and dense air descends by gravity into the cave displacing the relatively warmer cave air. The warm air flows backward to the entrance passing under the cave ceiling (Fig. 6.2a). The temperatures T_1 , T_2 and T_3 follow the outside fluctuations with amplitude decreasing with distance from the entrance. During this period CO₂ concentration reaches minimum values, around 580–590 ppm due to the high cave ventilation.

Regime 2—During warm periods when T_{out} is greater than the cave temperature (e.g. from 20 to 30 October 2006), the cold internal air is denser than the outside and is thus trapped inside the cave and circulation with the external atmosphere is inhibited (Fig. 6.2b). However a local circulation between “Music hall” and the main channel may persist for a while due to the differences in temperature in these two parts of the cave.

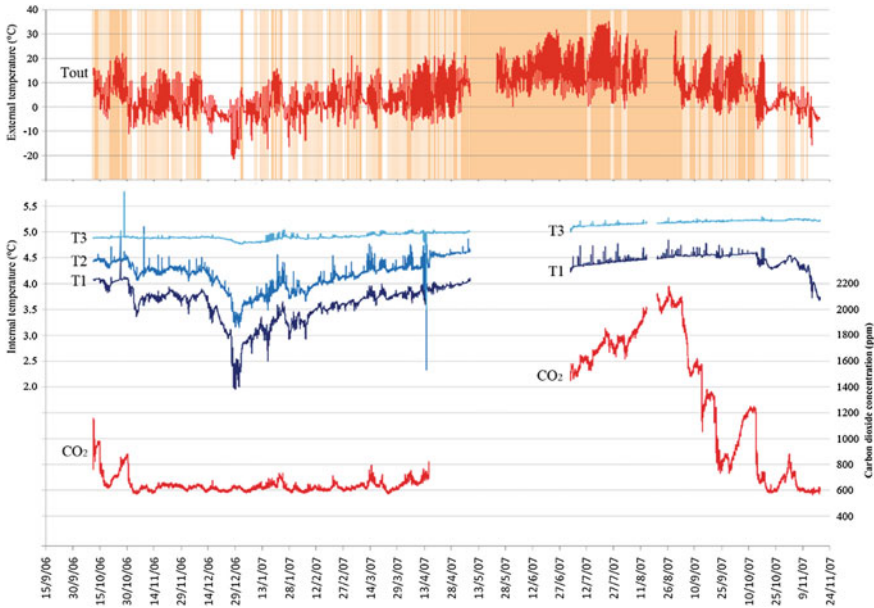


Fig. 6.1 Variation of some measured parameters during the monitored period. Darker areas in the upper graphs represent periods when the outside temperature is higher than the cave temperature

The temperatures T_1 , T_2 and T_3 slowly increase and do not respond to the outside daily temperature fluctuations. In the same warm periods CO_2 accumulates inside the cave, reaching values of almost 2200 ppm (August–September).

During days when cave temperature lies between the daily maximum and minimum external temperatures, a transition between the two regimes occurs during the 24-h period. The changes in ventilation rate produce typical carbon dioxide transient relaxation/accumulation curves.

6.2.2 Spatial Variability

A first detailed profile of CO_2 concentration made on April 1, 2007 is shown in Fig. 6.3a. In this period of the year, the winter season, with a predominant “regime 1” condition, was ending. Entrance concentration is higher than the typical value for the atmosphere (447 vs. 380 ppm) because of the location and abundance of vegetation.

Clearly two different regions with diverse carbon dioxide levels are present. The main channel has very low concentration, close to 500 ppm with change in concentration versus distance from the entrance of 0.2 ppm m^{-1} . CO_2 abruptly increases after the narrow passage leading to the “Music hall”, where the

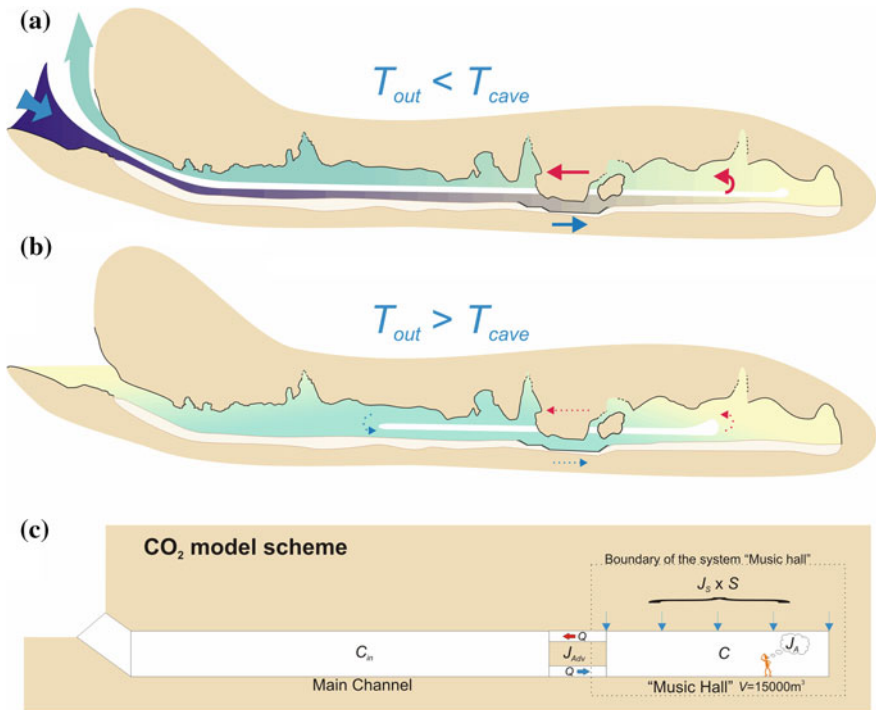


Fig. 6.2 Conceptual model of cave climate: **a** “regime 1”; **b** “regime 2”; **c** schematic representation for modelling purposes

concentration is around 700 ppm but a slope one order of magnitude higher (2.2 ppm m^{-1}) is found in the environment following the narrow passage. Similarly, Baldini et al. (2006a) indicate that, in the Ballynamindra Cave in Ireland, major spatial changes in CO_2 concentration generally occur after tight passages. A low slope in the concentration versus distance relationship can be indicative of a well-mixed environment. In Baldini et al. (2006a) and in Ek and Gewelt (1985) values of the slope of 34.29 ppm m^{-1} (cave with numerous constrictions) and 5.3 ppm m^{-1} (cave with large and wide passages) were reported.

Analysis of the carbon dioxide spatial variability showed the presence of roughly two units that coincide with the two morphological sectors of the cave: the “Music hall” and the main channel. The narrow passage between them controls the exchanges of mass and energy.

For the opposite pattern, the profile recorded on September 17, 2007 (Fig. 6.3b) represents the cave’s atmospheric situation after the summer season and thus after a period with a predominance of “regime 2”. Carbon dioxide composition is rather uniform along the whole length of the cave (slope of 0.2 ppm m^{-1}) while the transition from the external composition (around 380 ppm) to the internal composition (around 1200 ppm) occurred almost completely in the first 20 m of cave.

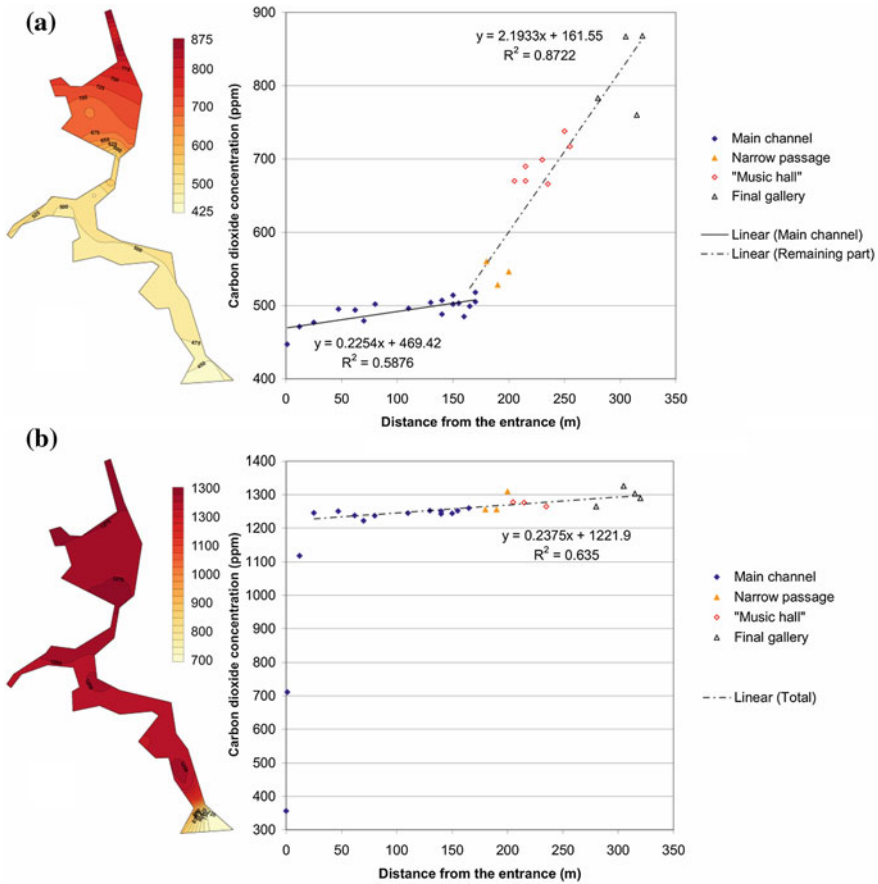


Fig. 6.3 Spatial variability of carbon dioxide concentration: **a** recorded on April 1, 2007; **b** recorded on September 17, 2007

This situation clearly depicts the effect of stable thermal stratification of the internal atmosphere and the inhibition of air exchange with the outside environment.

6.2.3 Vertical Distribution

Carbon dioxide distribution along a vertical profile located on the touristic path, 9 m inside the “Music hall”, has been measured during a site visit on October 10, 2010. Outside temperature was reasonably above internal temperature (9 vs. 5 °C) so that cave could be considered to be in climatic regime 2 conditions with low ventilation rate. However airflow velocity measurements done on the same day showed that a local circulation between “Music hall” and the main channel was still in place due

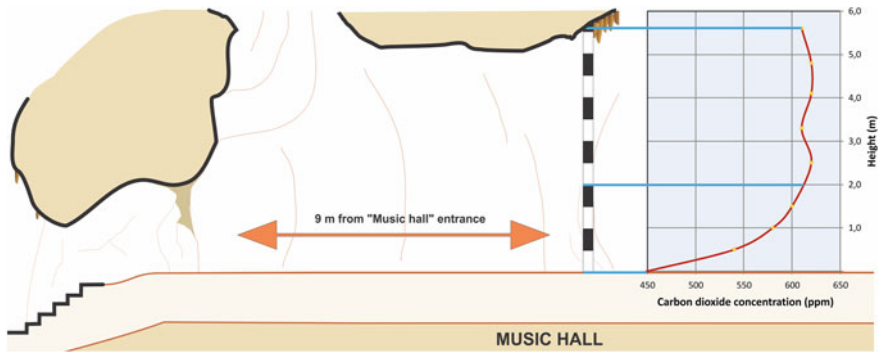


Fig. 6.4 Carbon dioxide vertical profile

to the differences in temperature in these two parts of the cave (around 0.1 m/s measured in the narrow passage between the parts of the cave). The results (Fig. 6.4) illustrate a relatively expressed gradient with a maximum difference of concentrations of 170 ppm over 5.6 m height. Most of CO_2 increase (150 ppm) happens within the first 1.5 m of elevation where the detected concentrations are most probably controlled by mixing with the air plume entering from the main channel and composed by fresh air with low carbon dioxide levels (450–490 ppm). The absence of a CO_2 gradient above the above mentioned first 1.5 m is confirmation of a good mixing capacity. In a ceiling pocket located nearby measured profile has been detected the maximum concentration of 700 ppm.

6.3 Modelling

6.3.1 Model Description

We propose a simple model for the temporal variability of carbon dioxide in the “Music hall”. Following Faimon et al. (2006) we consider three flows of CO_2 exchange (Fig. 6.2c):

- CO_2 from soil (J_S): J_S is the natural input of carbon dioxide per unit of cave plan surface originating from biological activity in the soil or epikarst layer and entering the cave environment by degassing from percolating water and diffusion through rock fractures. Although this flux is dependent on the partial pressure of CO_2 (p_c) in the cave atmosphere (Spotl et al. 2005; Baldini et al. 2006b), this dependency is not included in the model. The simplification is acceptable if the equilibrium partial pressure in the epikarst is always much higher than in the cave.

- CO₂ from anthropogenic activities (J_A): J_A is the production of CO₂ due to human respiration in the cave volume under consideration.
- CO₂ advection (J_{Adv}): this term is the net flow of CO₂ generated by convective movements of the air between two cave volumes.

Other processes, such as the diffusion between cave volumes, biological decomposition within the cave, and hypogenic flows are not included because they are not deemed relevant for the investigated site.

The advection term is given by:

$$J_{Adv} = |Q|(C_{in} - C) \quad (6.1)$$

where C and C_{in} are the concentration of carbon dioxide in the “Music hall” and inlet stream respectively while Q is the convective airflow rate.

Based on the above definitions, the “Music hall” system can be described by the following mass balance:

$$V \frac{dC}{dt} = S J_S + J_A + J_{Adv} = S J_S + J_A + |Q|(C_{in} - C) \quad (6.2)$$

where S is the plan surface of the “Music hall” (around 2500 m²) and V its volume (around 15,000 m³).

Under the assumption that J_S , J_A , Q and C_{in} are constant during a single carbon dioxide variation event, Expression 6.2 can be integrated to obtain:

$$\frac{C - \frac{S J_S + J_A + |Q| C_{in}}{|Q|}}{C_0 - \frac{S J_S + J_A + |Q| C_{in}}{|Q|}} = \exp(-|Q|t/V) \quad (6.3)$$

for $|Q| \neq 0$, where C_0 is the initial carbon dioxide concentration.

If there is no air current through the passage, integration of Eq. 6.2 gives:

$$C - C_0 = \frac{S J_S + J_A}{V} (t - t_0) \quad (6.4)$$

Equations 6.3 and 6.4 are applicable only if $C \ll C_{epikarst}$. If this condition is not satisfied then the assumption of constant J_S becomes invalid and its dependency on C and $C_{epikarst}$ should be introduced. For other reasons, if C rises above values where a sensible effect on human physiology occurs, then the assumption of constant J_A may be incorrect.

6.3.2 Model Regression

The model has been applied under three different conditions in order to split the contribution of natural (J_S), anthropogenic fluxes (J_A) of carbon dioxide and to validate the results:

- *Case 1*: natural CO₂ fluctuations with no tourists inside the cave ($J_A = 0$);
- *Case 2*: short tourist visits where the contribution of natural carbon dioxide input can be considered negligible;
- *Case 3*: Artificial input of carbon dioxide;

Case 1: Natural CO₂ Fluctuations

A total of 92 relaxation curves and 62 accumulation curves, clearly emerging from the background signal, were identified in the monitoring data. These data have been used to calibrate Eq. 6.3, written in the form:

$$C = A_1 + (A_2 - A_1) \exp(-A_3 t) \quad (6.5)$$

Least-squares regression using an iterative nonlinear algorithm gives values of three optimized parameters, namely:

$$A_1 = \frac{S J_S + J_A + |Q| C_{in}}{|Q|}, \quad (6.6a)$$

$$A_2 = C_0, \quad (6.6b)$$

$$A_3 = \frac{Q}{V} \quad (6.6c)$$

From A_2 and A_3 we obtain directly C_0 and Q . Parameter A_1 contains four physical parameters: J_S , Q , C_{in} and J_A . J_A is taken = 0 since we deal with periods with no people inside. Q is known from A_3 , which leaves two independent parameters, J_S and C_{in} to be determined.

A simple steady state mass balance for the whole cave has been constructed under the assumptions that Q and J_S are constants within the cave:

$$C_{in-s.s.} = (S_{m.c.} + S) \frac{J_S}{Q} + C_{am} \quad (6.7)$$

where $S_{m.c.}$ is the surface of the main channel (3300 m²), C_{am} is the external atmospheric concentration of CO₂ (380 ppm) and $C_{in-s.s.}$ is the concentration in the main channel during steady state conditions. Though obtained under steady state conditions, the value of $C_{in-s.s.}$ was used as a first approximation to C_{in} . The Eqs. 6.6a and 6.7 (with $C_{in-s.s.} = C_{in}$) were solved together to obtain J_S and C_{in} respectively. Figure 6.5 shows the relaxation data and best fit for October 14, 2006.

The optimized values of Q/V (“Music hall” ventilation rate), J_S , and estimated values of C_{in} for all the curves are presented in Figs. 6.6, 6.7 and 6.8 respectively.

Case 2: Anthropogenic Change of CO₂ Concentration

On 26 October 2006, 100 children visited the cave, staying in the “Music hall” for an estimated 20 min. During 21 January 2007 another experiment was organized and 65 people stayed in the final room of the cave for 30 min. In both cases the rise of CO₂ concentration is clearly visible in Fig. 6.9. Carbon dioxide increased rapidly during

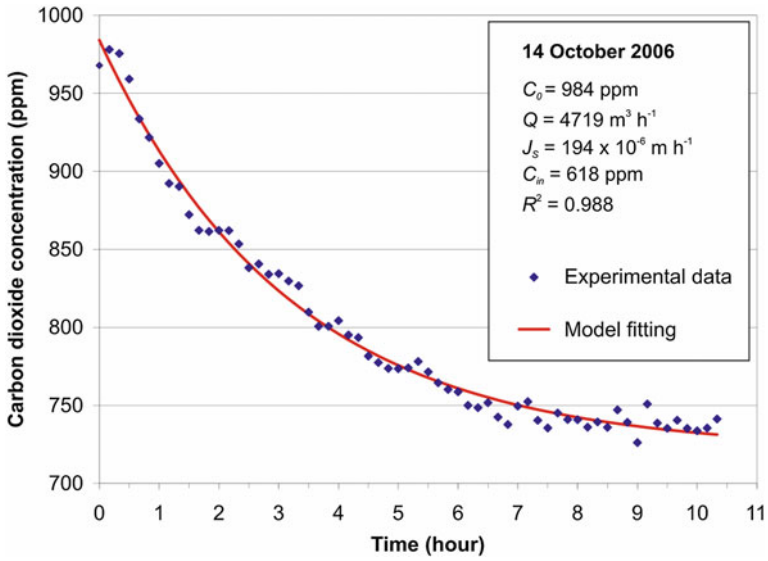


Fig. 6.5 Example of model regression

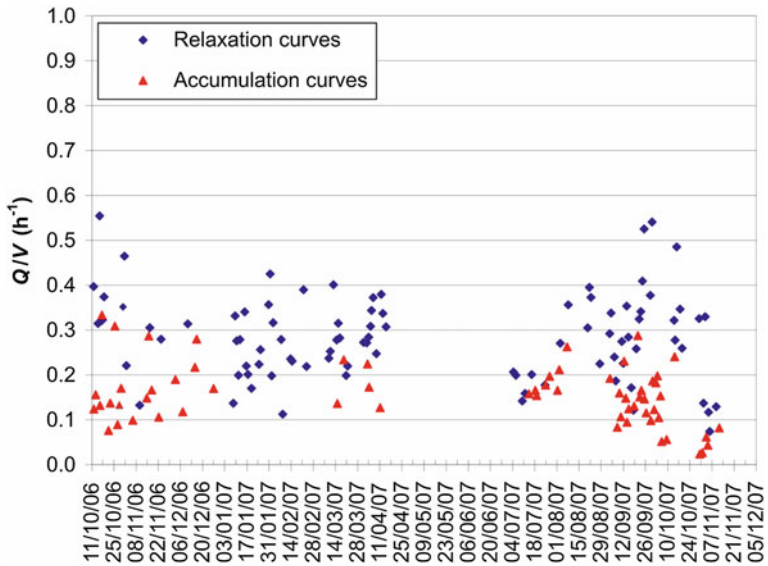


Fig. 6.6 Estimated ventilation rates

the first few minutes of each visit and at the end the CO₂ is practically confined within the room. J_A has been calculated based on the difference of the carbon dioxide concentration before and after the visits and Eq. 6.4. Both exchange with the main

channel and natural carbon dioxide input have been considered negligible due to the short duration of the visit. The term J_A can be calculated as $2700 \times 10^{-3} \text{ m}^3 \text{ h}^{-1}$ (26 October 2006) and $1350 \times 10^{-3} \text{ m}^3 \text{ h}^{-1}$ (21 January 2007) respectively.

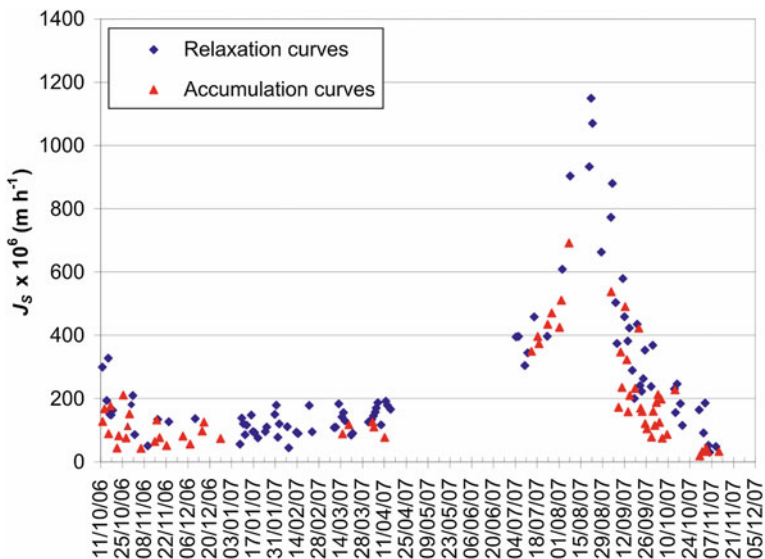


Fig. 6.7 Estimated natural input from soil (J_S)

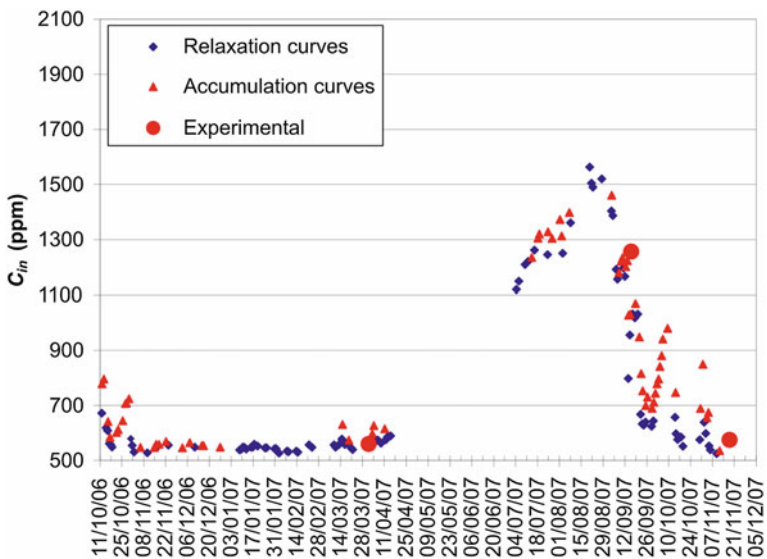


Fig. 6.8 Estimated concentrations in the inlet stream (C_{in})

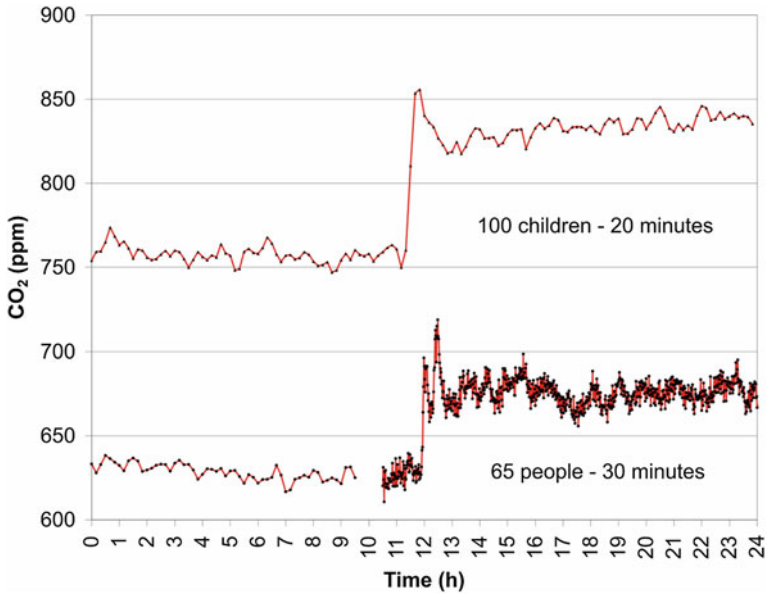


Fig. 6.9 Carbon dioxide concentration rise due to anthropogenic contribution

6.4 Discussion

6.4.1 Ventilation Rate

The calculated values lie in a range from 0.02 to 0.54 h^{-1} (average = 0.23 h^{-1} , standard deviation = 0.11 h^{-1}). Although it probably varies greatly from cave to cave, depending strongly on morphology and cave climate, Faimon et al. (2006) found values of the same magnitude for a cave in the Czech Republic (from 0.03 to 0.16 h^{-1}). The air flow rate estimated for the Srednja Bijambarska Cave ($300\text{--}8100 \text{ m}^3 \text{ h}^{-1}$) has not been directly verified. The corresponding wind speeds in the narrowest passage (cross section of around 2 m^2) are in the range $0.05\text{--}1.10 \text{ m s}^{-1}$. Although no measurements were performed, during two field visits, wind speeds up to $0.1\text{--}0.2 \text{ m s}^{-1}$ were noted.

In addition, Fig. 6.6 shows that ventilation rates associated with accumulation events are, on average, lower than those calculated from relaxation events. This result was of course expected. It should be noticed that even lower ventilation rates could be present in the examined period but the resulting CO_2 concentration transient curves did not emerge clearly from the background noise and thus were not identified.

6.4.2 Natural Input

The natural input of carbon dioxide begins at around $300 \times 10^{-6} \text{ m h}^{-1}$ during the first monitored days in autumn, decreases to an average minimum of roughly $100 \times 10^{-6} \text{ m h}^{-1}$ in winter and then slowly recovers reaching its maximum value around $1000 \times 10^{-6} \text{ m h}^{-1}$ in late August. During September, with the first sustained cold spell, the flux rapidly decreases towards winter values of about $50 \times 10^{-6} \text{ m h}^{-1}$.

In the Cisařská cave, values of $20 \times 10^{-6} \text{ m h}^{-1}$ in March and $40 \times 10^{-6} \text{ m h}^{-1}$ in September (corrected for a plan surface of 390 m^2) have been found (Faimon et al. 2006). The data are in fair agreement but values in Srednja Bijambarska Cave show a higher annual variability.

A much higher value of J_S ($14,400 \times 10^{-6} \text{ m h}^{-1}$) has been estimated by Bourges et al. (2001), based on a productive rock surface, a value that is around 12 times greater than the highest values found in Srednja Bijambarska Cave. However, it should be noted that the two results cannot be directly compared since they may refer to different surface definitions (productive rock surface vs. plan surface).

Kowalczk and Froelich (2010) derived cave ventilation rates from ^{222}Rn dynamics modeling and use the results for estimates carbon dioxide fluxes in Hollow Ridge cave (U.S.A.). The net amount of carbon dioxide reaching the cave environment from the epikarst has been found variable among the seasons with higher values ($0.83 \mu\text{mol m}^{-2} \text{ s}^{-1}$ or $67 \times 10^{-6} \text{ m h}^{-1}$) during summer and minimum in winter ($0.14 \mu\text{mol m}^{-2} \text{ s}^{-1}$ or $11 \times 10^{-6} \text{ m h}^{-1}$). Even if exist a large diversity in site conditions (average external temperature of $6.2 \text{ }^\circ\text{C}$, average precipitation 917 mm and elevation of 960 m a.s.l. in Bijambare versus $20 \text{ }^\circ\text{C}$, 1480 mm and 30 m a.s.l. respectively in Hollow Ridge cave) which may have large impact in biological activity and thus carbon dioxide production, the estimated carbon dioxide fluxes for the two caves are similar.

High seasonal fluctuations of carbon dioxide concentration in the soil atmosphere have been reported in the literature (Buyanovsky and Wagner 1983; Amundson and Davidson 1990) and they are often considered directly responsible for cave atmospheric composition changes. However, few authors reported that, if the dripping water derives from a well-mixed epikarst system, its equilibrium p_c can be assumed rather constant (Fairchild et al. 2000; Spötl et al. 2005).

The seasonal penetration of low p_c cave air into a biphasic air-water compartment upflow from the point where dripping occurs (causing enhanced carbon dioxide degassing) has been proposed to explain part of the chemical and isotopic variability found in speleothems and dripping water, (Fairchild and McMilan 2007).

The calculated values of J_S show a positive relationship with the ventilation rate (Fig. 6.10), probably related to imperfectly mixed conditions in the ‘‘Music hall’’ (situation improved at higher ventilation rates) and/or by the expansion of the area of influence of cave air into the surrounding environment with the possible contribution of CO_2 enhanced degassing. The figure also depicts two different limit situations:

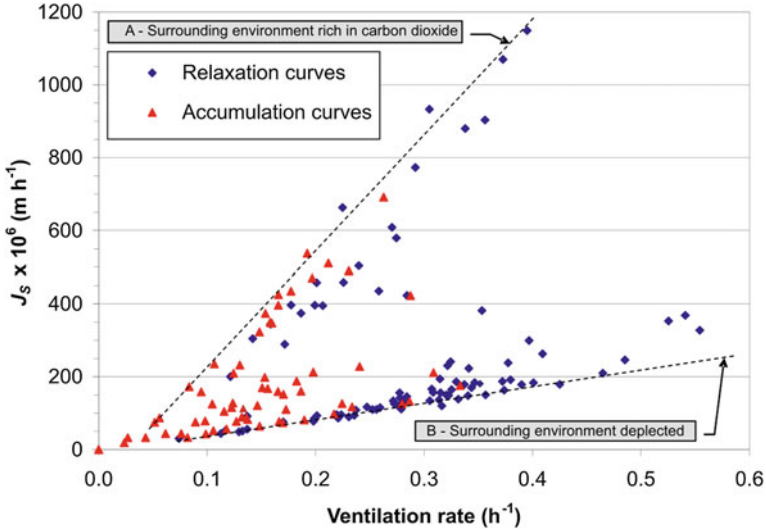


Fig. 6.10 Relationship between the natural input from the soil (J_S) and the ventilation rate

- A. During periods when “regime 2” is predominant, the relationship between J_S and the ventilation rate lies at higher values of J_S . This indicates that the surrounding environment is rich in CO_2 , and can quickly provide high amounts of carbon dioxide during the first fall in concentration in the cave atmosphere.
- B. During periods when “regime 1” is predominant, the surrounding area is already depleted and thus an increase of ventilation is reflected in a lower increase of J_S .

Unfortunately the model output in terms of ventilation rate could not be verified in the field and this uncertainty affects the trustworthiness of values of predicted J_S at different Q . On the other hand the dependency itself shows that spot measurements of carbon dioxide effluxes from a cave maybe misleading if interpreted as background values of CO_2 input to the underground environment.

Both limit situations A and B seems to converge for Q close to zero to values of J_S of a few 10^{-6} m h^{-1} . A partial confirmation of this order of magnitude for the background input of carbon dioxide in the cave arrives from the analysis of the rise of concentration during a long summer period using Eq. 6.4 (under the approximation that $Q = 0$ for the whole period and J_A is negligible). From 5 July to 26 August the CO_2 concentration increases from 1500 to 2100 ppm giving an average value of J_S of $2.9 \times 10^{-6} \text{ m h}^{-1}$.

6.4.3 Concentration in the Inlet Stream

The values of C_{in} , as expected mimic the behaviour of carbon dioxide concentration in the “Music hall” but at lower concentrations closer to the outside air composition.

The values predicted by Eq. 6.5 are compared with three experimental concentrations obtained during the year (Fig. 6.8) and are found to match quite satisfactorily.

6.4.4 Anthropogenic Input

Based on J_A values obtained by the two “Case 2” experiments, values of 0.45 and 0.35 $\text{L}_{\text{CO}_2} \text{min}^{-1} \text{person}^{-1}$ have been calculated as individual production rates. It should be noted that, while children walked along the normal visitors path, during the second experiment people stood for the entire time at the same place in the centre of the “Music hall”. The dissimilarity of physical activity during the two experiments could explain the difference in the results obtained. A wide range of CO_2 exhalation rate (from 0.2 to 2 $\text{L}_{\text{CO}_2} \text{min}^{-1} \text{person}^{-1}$) has previously been documented (Dragovich and Grose 1990; Cigna 1996) depending on age and rate of physical activity. Faimon et al. (2006) found similar values ($0.39 \pm 0.11 \text{L}_{\text{CO}_2} \text{min}^{-1} \text{person}^{-1}$) for children.

6.4.5 Model Sensibility to Data Selection

The preliminary selection of relaxation and accumulation curves from the monitoring data was made following the criteria that the absolute difference between initial and final CO_2 concentration is at least double than the background carbon dioxide concentration oscillations (signal noise). Usually only events with concentration changes higher than 20 ppm have been selected. Curves with a high difference between the initial and final concentrations give the best fitting results with R^2 close to 1 (e.g. on 14 October 2007: $R^2 > 0.99$). On the other hand, curves with a concentration difference close to the background noise level produce poor fitting results. Only curves with $R^2 \geq 0.6$ were retained for further elaboration.

The fact that curves with low slope may stay hidden behind the background noise gives a bias toward high ventilation rates.

The selection of the initial and final point of each curve has also been done manually. The procedure becomes problematic for curves close to the background noise. The choice of the end point influences the length of the final steady state tail. If too many points belong to the final relaxation stage their relative importance compared to the points on the steep part will be overestimated during the regression.

These activities introduced some subjectivity in the analysis. However due to the relatively high number of curves processed this problem should be at least statistically unimportant. Estimates of cave geometry (volume, surface) also have a direct influence on the final output.

6.5 Conclusions

Temporal variations of carbon dioxide concentration in Srednja Bijambarska Cave are controlled by the switching between two ventilation regimes driven by outside temperature changes that may even be diurnal. In agreement with recent studies, the CO₂ spatial profile shows a clear dependence on cave morphology with major increases after narrow passages. However this distribution also depends on the ventilation regime since spatial distribution and time evolution cannot be completely decoupled. The regression of a simple perfectly mixed volume model applied to a cave sector (“Music hall”) enabled estimation of ventilation rates between 0.02 and 0.54 h⁻¹ (average = 0.23 h⁻¹, standard deviation = 0.11 h⁻¹). The natural input of CO₂ is estimated by the model at around $50 \times 10^{-6} \text{ m h}^{-1}$ during the winter season and up to more than $1000 \times 10^{-6} \text{ m h}^{-1}$ during the first temperature falls at the end of summer (0.62 and 12.40 $\mu\text{mol m}^{-2} \text{ s}^{-1}$ at normal conditions respectively). These values have been found to be related to the cave ventilation rate and dependant on the availability of CO₂ in the surrounding environment. For airflow close to zero the values of J_S seem to converge to a few 10^{-6} m h^{-1} .

The anthropogenic contribution has been calculated from two experiments, giving values of 0.45 and 0.35 LCO₂ min⁻¹ person⁻¹.

References

- Amundson RG, Davidson EA (1990) Carbon dioxide and nitrogenous gases in the soil atmosphere. *J Geochem Explor* 38:13–41
- Baldini JUL, Baldini LM, McDermott F, Clipson N (2006a) Carbon dioxide sources, sinks, and spatial variability in shallow temperate zone caves: evidence from Ballynamindra cave, Ireland. *J Cave Karst Stud* 68:4–11
- Baldini JUL, McDermott F, Clipson N (2006b) Effects of high-frequency cave atmosphere variability on stalagmite climate proxy records. *Geochimica et Cosmochimica Acta* 70:A30
- Baldini JUL, McDermott F, Hoffmann DL, Richards DA, Clipson N (2008) Very high-frequency and seasonal cave atmosphere PCO₂ variability: implications for stalagmite growth and oxygen isotope-based paleoclimate records. *Earth Planet Sci Lett* 272:118–129
- Bourges F, Mangin A, d’Hulst D (2001) Le gaz carbonique dans la dynamique de l’atmosphère des cavités karstiques: l’exemple de l’Aven d’Orgnac (Ardèche). *Comptes Rendus de l’Académie des Sciences—Series IIA—Earth and Planetary Science* 333:685–692
- Buyanovsky GA, Wagner GH (1983) Annual cycles of carbon dioxide level in soil air. *Soil Sci Soc Am J* 47:1139–1145
- Cigna AA (1996) Risultati di una prima campagna di misure ambientali nelle grotte di Toirano. In: *Proceedings international symposium show caves and environmental monitoring*, Cuneo, Italy, pp 87–98
- Cigna AA (2002) Monitoring of caves: conclusions and recommendations. *Acta Carsologica* 31:175–177
- Dragovich D, Grose J (1990) Impact of tourists on carbon dioxide levels at Jenolan caves, Australia: an examination of microclimatic constraints on tourist cave management. *Geoforum* 21:111–120

- Ek C, Gewalt M (1985) Carbon dioxide in cave atmospheres. New results in Belgium and comparison with some other countries. *Earth Surf Proc Land* 10:173–187
- Faimon J, Stelcl J, Sas D (2006) Anthropogenic CO₂-flux into cave atmosphere and its environmental impact: a case study in the Cisarska cave (Moravian Karst, Czech Republic). *Sci Total Environ* 369:231–245
- Fairchild I, McMillan E (2007) Speleothems as indicators of wet and dry periods. *Int J Speleol* 36:69–74
- Fairchild IJ, Borsato A, Tooth AF, Frisia S, Hawkesworth CJ, Huang Y, McDermott F, Spiro B (2000) Controls on trace element (Sr–Mg) compositions of carbonate cave waters: implications for speleothem climatic records. *Chem Geol* 166:255–269
- Kowalczyk AJ, Froelich PN (2010) Cave air ventilation and CO₂ outgassing by radon-222 modeling: How fast do caves breathe? *Earth Planet Sci Lett* 289:209–219
- Milanolo S, Gabrovšek F (2009) Analysis of carbon dioxide variations in the atmosphere of Srednja Bijambarska cave, Bosnia and Herzegovina. *Bound-Layer Meteorol* 131:479–493
- Spötl C, Fairchild IJ, Tooth AF (2005) Cave air control on dripwater geochemistry, Obir caves (Austria): implications for speleothem deposition in dynamically ventilated caves. *Geochim Cosmochim Acta* 69:2451–2468

Chapter 7

Cave Atmosphere Response to Artificial Input of Carbon Dioxide

Abstract Ten kilogram of carbon dioxide was released into the cave environment during a short experiment with detailed monitored conditions. Several assumptions, hypothesis and results obtained from modeling of natural carbon dioxide concentrations have been tested. Based on carbon dioxide concentration increase, following the CO₂ release, it has been confirmed that “Music hall” can be considered to a good approximation as a perfectly mixed volume. The volume estimated by data regression is 22,800 m³, broadly similar to the 15,000 m³ estimated by cave survey. The mixing and transport processes between and inside cave sections appear to be related to advective processes while diffusion playing a lesser role. The model provides results comparable with experimental measured data (i.e. air velocity).

7.1 Introduction

Karst terrain is characterized by a very peculiar interaction with the global carbon cycle, different from any other landscape. Abiotic processes such as carbonate rock dissolution represent a local sink for atmospheric carbon dioxide (Liu and Zhao 2000; Liu et al. 2010). The exchange of CO₂ between soil and atmosphere can be influenced by presence of carbonate rocks (Kowalski et al. 2008; Serrano-Ortiz et al. 2010). Vadose zone in limestone massifs can host high concentration of carbon dioxide (Benavente et al. 2010) while cave systems intersecting the unsaturated bedrock act as an important reservoir and/or an efficient drainage networks venting significant quantities of CO₂ back to the atmosphere (Kowalski et al. 2008; Kowalczk and Froelich 2010; Sanchez-Moral et al. 2010). Concentration of carbon dioxide in a cave volume is highly variable in time and space as result of a simple not stationary mass balance between input from soil or other cave compartments and output towards other cave sections or to the external atmosphere. Diffusion or advection mechanisms govern the transport of carbon dioxide and are responsible for the formation of concentration gradients between sources and sinks. High concentration of carbon dioxide at the bottom of several vertical profiles as found in

several caves is due to the presence of a CO_2 source and not as results of gravity stratification due to the carbon dioxide higher density (Badino 2009).

Despite large number of observations of carbon dioxide concentration in cave atmosphere and the fact that transport mechanisms are known in theory, only few works attempted to elaborate theory into models that can be tested in the field. The main difficulties reside in the complex geometry of underground voids and large number and variability of factors influencing carbon dioxide production, storage and transport.

A simple model describing dynamics of carbon dioxide concentration in terms of a perfectly mixed volume with a constant carbon dioxide input and an advection output have been proposed in Chap. 6. However, the outcome of the model could be only partially verified because important model parameters have not been monitored by the instrumentation normally installed in the cave. The scope of this chapter is to provide additional validation to the model and to test some of the assumptions introduced. In order to accomplish this task, an experiment involving release of a known quantity of carbon dioxide in the cave atmosphere has been made to reduce the degrees of freedom of the system and therefore to provide for a short period of time a more controlled environment.

7.2 The Experimental Set-Up

On 9 October 2010 at 14:45, 10 kg of carbon dioxide was released from a pressurized cylinder to the cave atmosphere approximately at the centre of the “Music hall” (5 m north of location of carbon dioxide probe C_{MH} in Fig. 3.8). The gas plume was directed toward north (opposite of the “Music hall” entrance). For safety reasons the cave was immediately evacuated after valve opening and therefore the whole gas release process was unattended.

Just before the beginning of the experiment the cave was equipped with several instruments (for details description and location refer to Sect. 3.2) which are summarized in Fig. 7.1.

Carbon dioxide concentration was measured hourly at two places: “Music hall” (C_{MH}) and in the main channel just before the narrow passage (C_{MC}). Temperature was monitored at 8 profiles: in “Music hall” (T_{MH}), in the narrow passage (T_{NP}), in an approximately 10 cm deep borehole located also in the narrow passage (T_{BH}), in the main channel at the entrance of the narrow passage (T_{MC}), at two elevation at the crossroad between main channel and side channel (T_{SClow} , T_{SCup}), at the cave first room just after the initial descent from entrance (T_{FR}) and outside the cave (T_{out2}).

Additionally, pressure signals were recorded at the “Music hall” (P_{MH}) and outside the cave (P_{out}). Air velocity in the narrow passage was measured by a 3D anemometer (v_{air}) as outlined previously in Chap. 3. Cross section of the passage was calculated by scaling photography of the section with main dimensions measured in the field and resulted in 2.7 m^2 . All parameters were retrieved with hourly frequency during the 20 h period following the gas release. Results are given in Fig. 7.2.

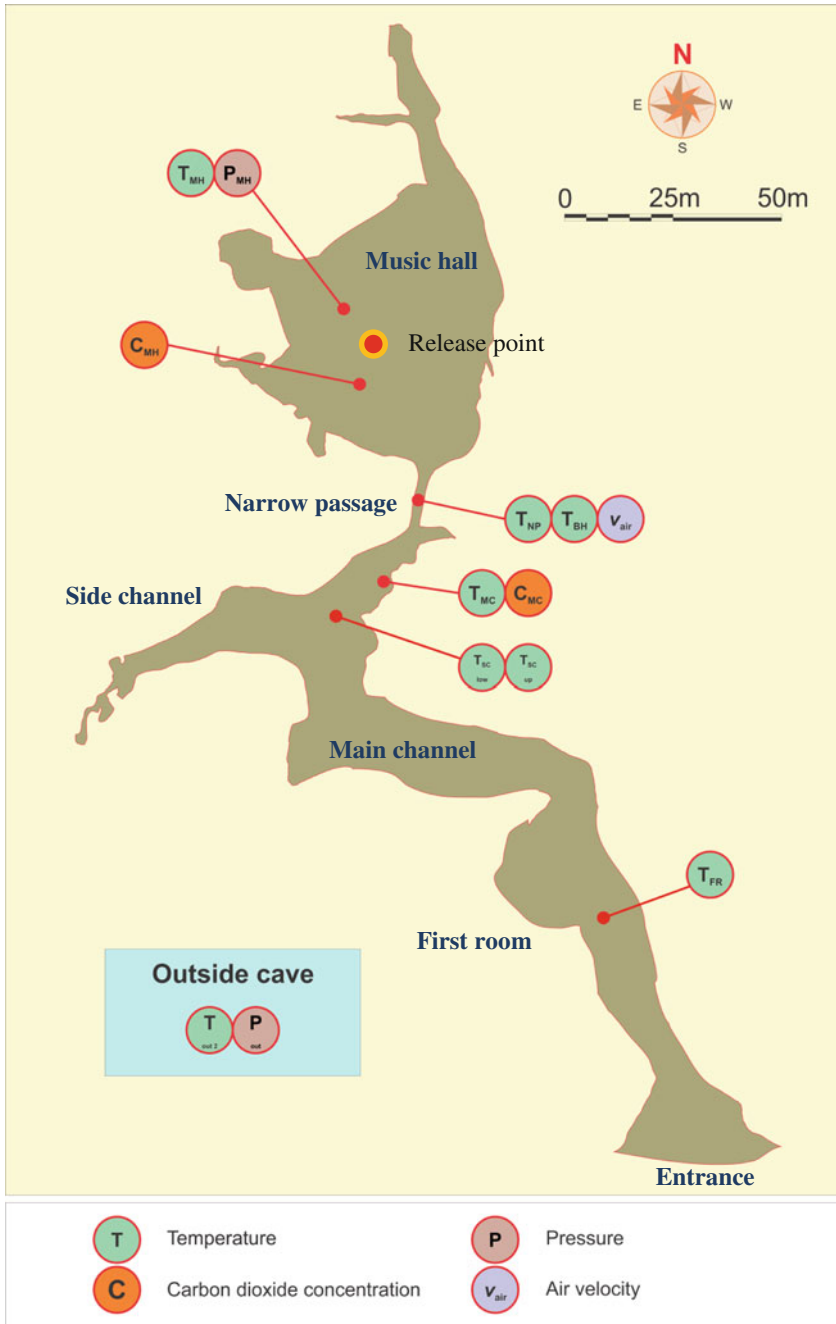


Fig. 7.1 Summary of instrumentation location and symbol used during the experiment of carbon dioxide release

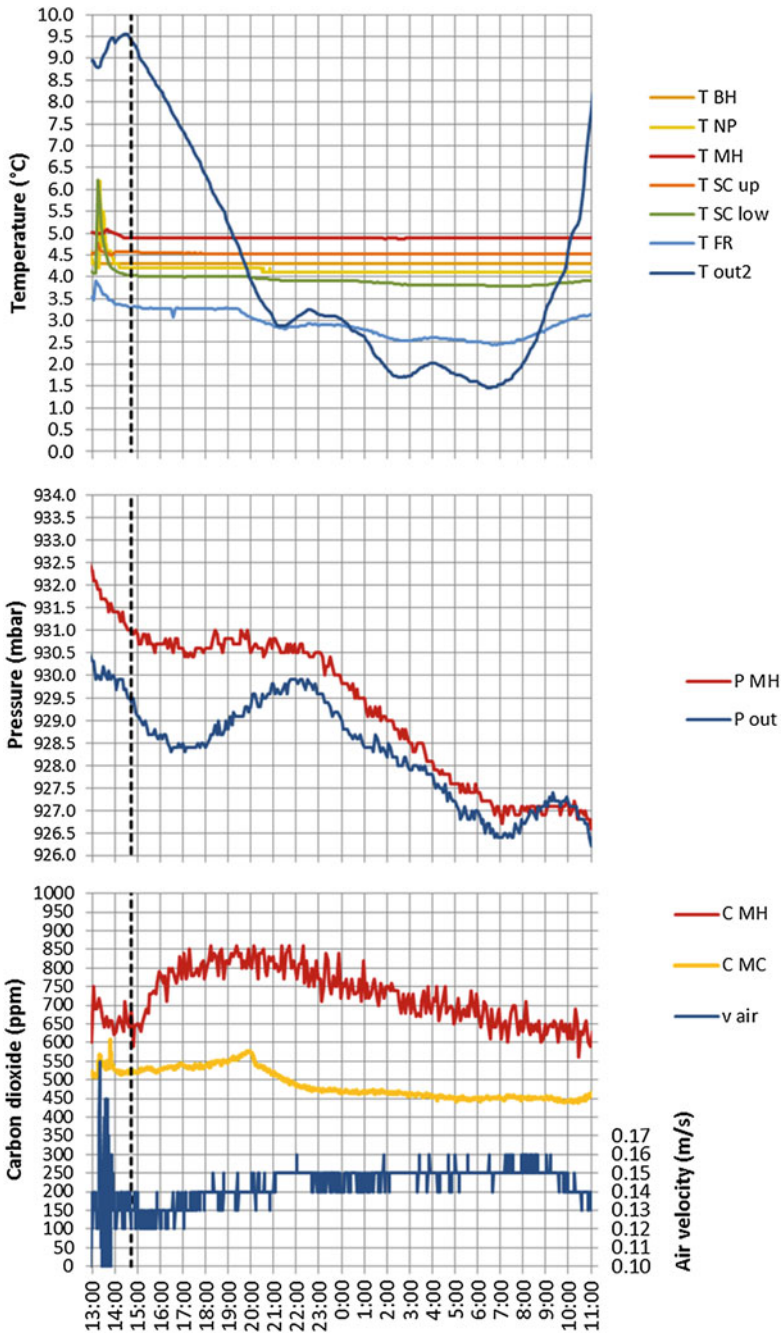


Fig. 7.2 Graph of selected atmospheric parameters during the artificial release of carbon dioxide. Air velocity is positive towards the “Music hall”

7.3 Results

7.3.1 Temperature Records

The external temperature (T_{out2}) started from around 9.0 °C at 13:00 rising to the maximum value of 9.5 °C at 15:00 and then decreased almost linearly at a rate of 1.0 °C h⁻¹ until 21:00. During night, the temperature fluctuates, reaching a minimum value of 1.46 °C at dawn (6:30), then raising fast again with last recorded value of 8.5 °C at 11:00 when the data loggers were stopped.

Cave temperature measured in the “Music hall” (T_{MH}), from a borehole in the narrow passage and by the upper data logger located at the intersection of the “Main channel” with the side channel just before the narrow passage leading to the “Music hall” (T_{SCup}) show almost no variations during the whole duration of the experiment (with the exclusion of first two hours due disturbance caused by installation of instrumentation). The recorded values at these three locations range between 4.87 and 4.90 °C for T_{MH} , 4.3 °C (no changes) for T_{BH} and 4.51–4.57 °C for T_{SCup} . Conversely, the other measured temperature signals show variations that can be explained by the climatic regimes proposed in Chaps. 5 and 6. The temperature signal from data logger located under the initial slope (T_{FR}) exhibits the highest amplitude. Initially it stays constant from 15:00 to 19:30 with a range of 3.25–3.30 °C then decreases with two large oscillations recalling external temperature behavior and reaches the minimum value of 2.43 °C at 6:40 in the morning. For the end of the experiment (11:00) T_{FR} reached almost the same initial value (3.14 °C). The other signals (T_{SCLow} and T_{NP}) show a similar evolution, but with lower amplitudes in the inner parts of the cave so that the changes of T_{NP} are almost undetectable. In addition to changes of amplitude the signals present a time shift of the switching between the flat part and the decreasing sections (T_{FR} at 19:30, T_{SCLow} at 20:00 and T_{NP} at 20:24).

7.3.2 Pressure Records

External pressure decreases from 930.5 to 928.5 mbar at between 13:00 and 17:00, and rises to a maximum at 930 mbar at 22:00, before decreasing to 926.5 mbar at 7:00. After 7:00, another local maximum occurs at 927.5 mbar at 10:30. The external pressure at the end of recorded period (11:00) decreases almost to 926 mbar. Internal pressure signal mimics oscillating behavior of external pressure time series. However, at the beginning of the recorded period (13:00), there is pressure difference between “Music hall” and external atmosphere: underground pressure (P_{MH}) is around 2 mbar higher than pressure (P_{out}) measured outside the cave (932.5 vs. 930.5 mbar). This pressure difference approximately correspond to the change of barometric pressure (2.5 mbar) caused by difference in elevation of

the sensors (sensor located outside is around 20 m higher than the one installed in the “Music hall”).

The recorded 22 h pressure signal is modulated over pressure variations due to seasonal and climatic changes. Nevertheless, the day hours when maxima and minima occur correspond satisfactory with typical day times expected for atmospheric tides. Bussani (2007), found a good fit between the filtered pressure signal in the cave “Abisso di Trebiciano” and a 12 h periodic function with pressures maximum at 10:30 and 22:30.

7.3.3 Air Velocity

During the duration of the experiment, a weak wind blew into the narrow passage bringing air to the “Music hall”. The anemometer (v_{air}) measured air speed starting between 0.12 and 0.13 m s⁻¹ and then progressively increasing during the night reaching a maximum between 0.14 and 0.16 m s⁻¹ between 7:00 and 9:00 in the morning. At the end of the experiment (11:00), the air velocity already dropped to values close to the initial situation (0.13–0.14 m s⁻¹). Considering a cross section of the narrow passage of 2.7 m² the resulting flow rate are ranging between 0.32 and 0.43 m³ s⁻¹ equivalent to ventilation rate for the “Music hall” of about 0.08–0.10 h⁻¹.

7.3.4 Carbon Dioxide Concentration Records

Concentration of carbon dioxide in the “music hall” (C_{MH}) at the beginning of the experiment is elevated by the presence of persons installing the necessary instrumentation. At the instant when the cylinder is opened and the gas released (14:45), the surrounding concentration was around 590–600 ppm. The CO₂ in the Music hall initially showed rapid increase due to the artificial input reaching the maximum of slightly more than 850 ppm somewhere between 19:00 and 21:00 and then slowly decreasing during the night to values between 600 and 650 ppm. At the same time, the concentration in the main channel (C_{MC}) slowly increases from 520 ppm at the beginning of the experiment to 576 ppm at 19:53. After this peak value there is a rapid decrease of CO₂ that finish to stabilize to values around 450 ppm.

7.3.5 Results Interpretation by Cave Climatic Regimes

Before quantitative analysis of the recorded data, we present a qualitative discussion of the behavior of measured parameters compared to cave climatic regimes.

In general we follow the line of arguments already presented in Chap. 5 and further developed in Chap. 6. The cave, acting as a cold trap, is characterized by two opposite climatic conditions or regimes. However, although one regime is predominant during cold season and the other during the warm season, during intermediate conditions diurnal switches between these two states may also happen. The experiment of artificial release of carbon dioxide in the cave atmosphere began (at 14:45) with an outside temperature around 9.5 °C, at least 4.5 °C higher than the maximum temperature recorded underground (around 5 °C in the “Music hall”). During the following 4 and half hours the external temperature had decreased until it reached the same values as in the “music hall” (at around 19:15). When the outside temperature is above the cave temperature, colder and denser cave atmosphere is trapped inside and the exchange of mass and energy with the warmer and lighter external air is inhibited (Regime 2). This situation is evident in the data collected by the temperature sensor located just few tens of meters from cave entrance (T_{FR}) which records showed no correlation with the external temperature variations. At the same time during this period, the air flow recorded at the narrow passage is at minimum. The fact that wind velocity is not null may be explained by the persisting difference of temperature between the cold main channel (T_{SCup} or T_{SClow}) and the warm “Music hall” (T_{MH}). This difference creates a local convective cell with consequent air circulation.

Badino (1995, p. 126) give an empirical criterion when temperature difference between inside and outside temperature play an important role for air circulation:

$$|T_{out} - T_{cave}| > 3 + 6\Delta z \quad (7.1)$$

Δz is the altitude difference between two entrances of the cave system (the height of the air column expressed in km).

For differences lower than this limit, local air circulation, winds and other external and internal factors other than temperature may be predominant.

In Bijambare, despite that the system may have only one entrance, we can estimate that driving force is created by an air column of only few tens of meter (10–20 m most probably) and therefore a difference of temperature of 3.1 °C should be acceptable.

After the external temperature fell below temperature in the “Music hall” (switch to Regime 1) a “cold wave” propagated into the cave as recorded in sequence by the temperature sensors T_{FR} , T_{SClow} and T_{NP} .

The amplitude of the temperature perturbation decreases with the distance from the cave entrance and cannot be detected at all by T_{MH} sensor. The air from the outside caused a visible decrease of carbon dioxide concentration in the main channel (C_{MC}).

External pressure variations can also result in air flow in caves. Caves where air flow is driven by pressure variations (instead of thermal differences) are often referred as barometric caves. Detail description of such cave behavior is given in the work of Badino (1995, pp. 95–100) and Pflitsch et al. (2010). Although in one cave, the thermal and barometric models are not mutually exclusive, frequently one

behavior can be assumed to be dominant over the other at least during large part of the year. At least three facts point toward a minority role played by barometric airflow in the studied cave:

- Barometric caves show small differences between summer and winter behaviour (Pflitsch et al. 2010). This is strongly in contrast with the dual seasonal behaviour recorded in Bijambare.
- Data shown in Fig. 7.2 show alternate periods of pressure decrease (expansion) and increase (compression) with a general trend towards a lower pressure. Under barometric cave conditions this would correspond to outward flow direction during expansion and inward during compression and the general trend should be toward outward flow. On the contrary field data (Fig. 7.2) shows only air velocity direction towards the internal section of the cave (Music hall).
- During the experiment, between 15:00 and 11:00 around 27,000 m³ of air passed through the narrow passage (average air velocity of 0.14 ms⁻¹ and cross section of 2.7 m²). In the same period the pressure decreases by about 5 mbar. Even without considering the incoherent flow direction, to achieve a change in volume of such magnitude (considered an ideal gas expansion at constant temperature) it would be necessary that the initial cave volume is around 5 × 10⁶ m³. Such a value is clearly unrealistic.

7.4 Modeling

7.4.1 *The Dynamics of Carbon Dioxide Release*

Before introducing modeling of experimental data, a short overview of the expected dynamics of carbon dioxide release from a tank is presented.

In case of storage of liquid carbon dioxide in a cylinder, at one given temperature and until there is liquid phase, the internal pressure is fixed at the equilibrium vapor pressure (e.g. at 5 °C the vapor pressure is around 40 atm). However, when vapor is released, carbon dioxide evaporation process happen initially at almost adiabatic conditions, cylinder temperature drops for several degrees until a dynamic equilibrium is established with surrounding environment (during first minutes from valve opening ice partially covered external part of the cylinder). When equilibrium is reached, the temperature gradient between the cylinder and the cave atmosphere provides a heat flux that balances the latent heat of evaporation. From this point the temperature stabilizes, the internal pressure achieves steady condition and consequently the discharge rate is constant until the last drop of liquid phase evaporates.

The cylinder used at Bijambare cave had a total volume of 20 L and an initial carbon dioxide mass of 10 kg. When last drop of liquid phase disappears, we can assume that pressure was around 40 atm. By using the ideal gas law, it can be estimated that around 1.5 kg of CO₂ are still inside the cylinder in the gas phase.

At this point, the internal pressure is not fixed anymore but starts decreasing. Consequently also the discharge rate diminishes following a rather complex function in which initially (as in the previous phases) the gas velocity through the nozzle is limited by the sound speed (choked flow). This does not imply that mass flow rate is constant because gas density changes. Description of the exact dynamic of gas outflow surpasses the scope and needs of this work but an example of detail analytical derivation can be found in the work of Jia and Wang (2001).

Since, for safety reason, during the experiment nobody resided in the “Music hall”, the gas discharge rate was not monitored and also the duration of the different discharge phases is unknown. However, based on the above mentioned mechanisms, it can be estimated that the constant discharge rate phase should account for more than 80 % of carbon dioxide released. Therefore, further in this chapter, it has been assumed a constant discharge rate during the whole emptying of the cylinder.

7.4.2 Modelling Approaches

In Chap. 6, a simple model has been proposed based on the main assumption that the atmosphere of the “Music hall” can be approximated by a perfectly mixed volume exchanging carbon dioxide by advection through the narrow passage leading to the “main channel”. Two inputs of CO₂ to the system have been considered:

- A natural input of carbon dioxide (J_S);
- An artificial contribution (J_A).

In the cases described in Chap. 6 only carbon dioxide concentration in the “Music hall” was known experimentally and therefore, in order to reduce the degrees of freedom of the model, several assumptions/simplifications have been made:

- The air flow (Q) and the terms J_S and J_A are constant during the integration time;
- The carbon dioxide concentration in the stream entering the “Music hall” can be obtained through a steady state mass balance through the cave (Eq. 6.7) under the assumption that Q and J_S are constant through the whole cave.

As described in Sect. 7.4.1, during the experiment duration, artificial carbon release and therefore J_A are constant during large part of cylinder emptying process except for the initial and final periods. Obviously, the first assumption of constant J_A is valid only if the model is applied separately to data belonging to the central part of the gas release period (accumulation curve) and to the period after the gas discharge ended (relaxation curve).

During the experiment with artificial release of carbon dioxide, CO₂ concentration in the “Music hall” and in the “Main channel” were monitored, Additionally, the air velocity through the narrow passage was recorded so that Q can be

calculated as product of air velocity and the cross section of the narrow passage, approximately equal to 2.7 m^2 .

Two different modeling approaches have been applied:

- *Approach 1*—Model described in Chap. 6 was directly applied and validated by comparing the predicted and measured values of C_{MC} and v_{air} ;
- *Approach 2*—Field data for inlet carbon dioxide concentration and airflow were used as measured parameters of the model so that two degrees of freedom were removed.

7.4.3 Approach 1

Equation 6.3 could be used as regression model for accumulation and relaxation segments of the experimental data (when the gas release rate can be assumed constant). Unfortunately, due to small amount of data and their large dispersion, there are not enough reliable points in the accumulation curve to fit the model. For this reason Approach 1 was applied only to data belonging to the relaxation curve. Least square regression of Eq. 6.3 with experimental data (C_{MH} from 9:23 PM to 11:03 AM) was performed using the same numerical algorithm (Solver add-in of Microsoft Excel software) as in Chap. 6. The volume V of “Music hall” and its surface S were fixed to $15,000 \text{ m}^3$ and 2500 m^2 respectively.

The best regression curve (R-squared = 0.784) and estimated carbon dioxide fluxes are presented in Fig. 7.3. The best fit is obtained adjusting the values of Q , J_S , C_0 and C_{in} to $1087 \text{ m}^3 \text{ h}^{-1}$, $17 \times 10^{-6} \text{ m h}^{-1}$, 819 ppm and 468 ppm respectively.

7.4.4 Approach 2

As described in Sect. 7.4.1, gas discharge rate is constant during the emptying of gas cylinder except for the initial and last part. Therefore we assume it constant during the whole gas release phase. The term J_A is defined in Chap. 6 as volumetric flow of carbon dioxide and, for the whole experiment duration, it can be expressed as follow:

$$\begin{aligned}
 J_A &= Q_{\text{CO}_2} & \text{for } t &\leq \frac{m_{\text{CO}_2-0}}{\frac{44}{22.4} Q_{\text{CO}_2}} \\
 J_A &= 0 & \text{for } t &> \frac{m_{\text{CO}_2-0}}{\frac{44}{22.4} Q_{\text{CO}_2}}
 \end{aligned} \tag{7.2}$$

where m_{CO_2-0} is the initial mass of carbon dioxide in the cylinder (10 kg) and Q_{CO_2} is the volumetric discharge rate of carbon dioxide from the cylinder ($\text{m}^3 \text{ h}^{-1}$) assumed constant. The time t is consequently expressed in hours.

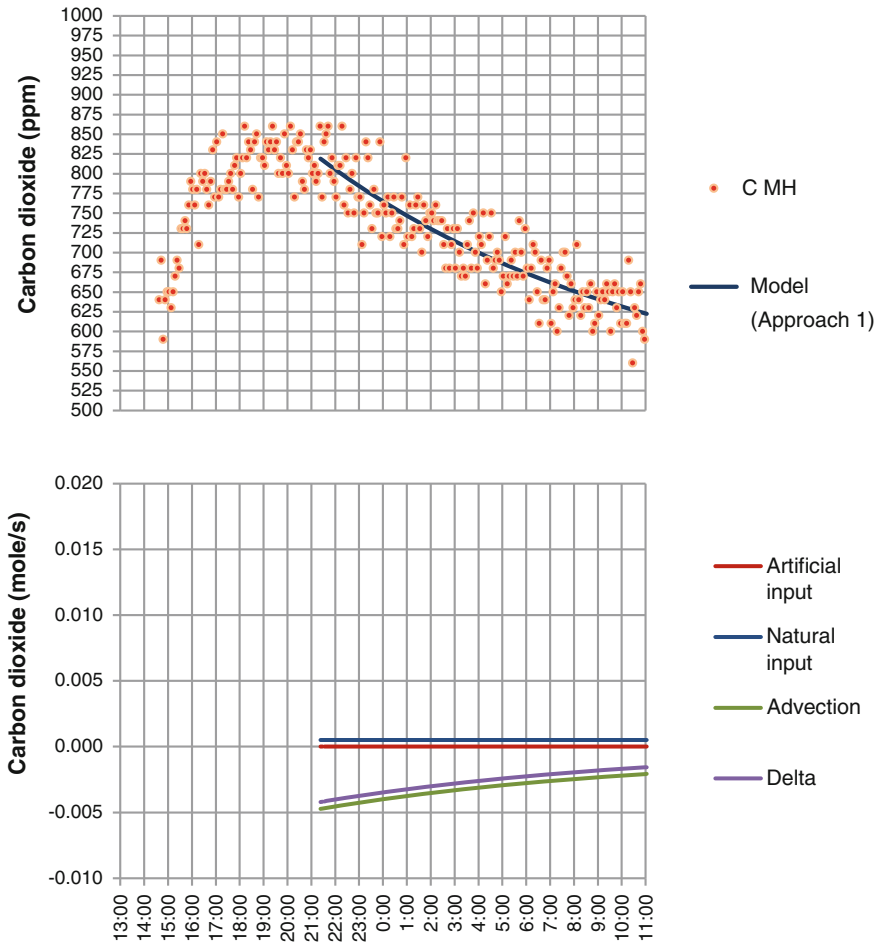


Fig. 7.3 Approach 1—experimental and modeled carbon dioxide concentrations (*upper graph*); modeled carbon dioxide fluxes (*lower graph*)

The terms J_A defined by the Eq. 7.2 has been introduced into Eq. 6.2. Alike to Chap. 6, the “Music hall” volume V and its surface S have been fixed to 15,000 m³ and 2500 m² respectively.

Hence this time the measured values of C_{in} and Q have been used. In detail, C_{in} is approximated by C_{MC} while Q is calculated from v_{air} .

Equation 6.2 was solved numerically using finite difference forward discretization scheme with a time step of 5 min. Since the values for the constant terms J_S , Q_{CO_2} and the initial concentration of CO₂ in the “Music hall” C_0 are initially

unknown, they were adjusted iteratively in order to provide the best fitting of predicted carbon dioxide concentrations in the “Music hall” and the experimental data (least square regression).

The best regression curve is obtained when the values for J_s , Q_{CO_2} and C_0 are $39.7 \times 10^{-6} \text{ m h}^{-1}$, $1.13 \text{ m}^3 \text{ h}^{-1}$ and 606 ppm respectively. The model results and experimental data are shown in Fig. 7.4.

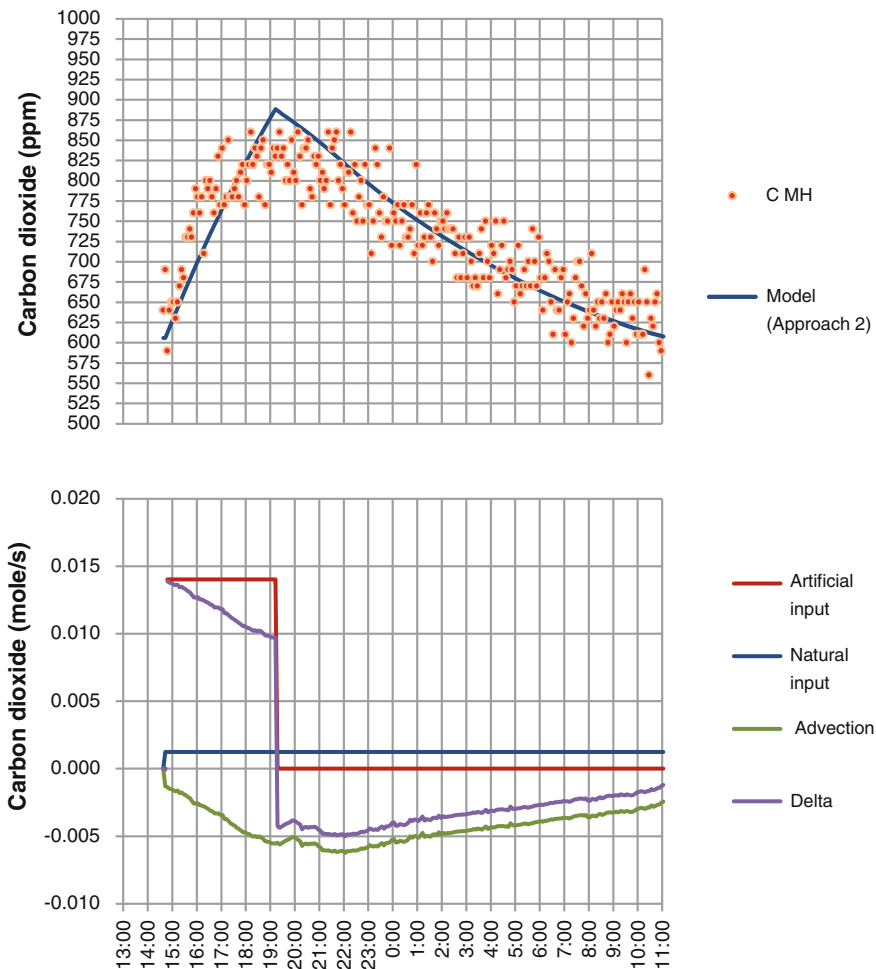


Fig. 7.4 Approach 2—experimental and modeled carbon dioxide concentrations (*upper graph*); modeled carbon dioxide fluxes (*lower graph*)

7.5 Discussion

7.5.1 Diffusion, Turbulence and Cave Atmosphere Mixing

All models presented so far are based on the assumptions that the “Music hall” is perfectly mixed and that advection is the dominant transport mechanism of CO₂ in the cave.

To validate these assumptions we will proceed through three steps:

- First, we use a simple model to demonstrate that the CO₂ transport between cave volumes by molecular diffusion can be neglected when compared to other mechanisms such as for example advection.
- Second, similar model and experimental data are used to show that homogenization of carbon dioxide concentration within the “Music hall” by molecular diffusion would require a long time incompatible with experimental data and dynamics observed in the field. Therefore, molecular diffusion is also ineffective to generate a perfectly mixed cave volume.
- Third, we will show that the low air velocities measured may be sufficient to create turbulent conditions within the “Music hall” volume and therefore providing means for rapid mixing.

As beginning, we set up a simple steady state 1-dimensional diffusion problem between the “Music hall” and the “Main channel”. The diffusion flux of carbon dioxide can be calculated by applying the Fick’s law:

$$J_{diff} = D \frac{dC}{dx} \quad (7.4)$$

where D is the diffusion coefficient for carbon dioxide in air and is approximately equal to $3.0 \times 10^{-6} \text{ m}^2 \text{ s}^{-1}$ (Baldini et al. 2006).

Conservatively, we can assume that concentration of carbon dioxide in the “Music hall” is 2100 ppm or 0.094 mol m^{-3} (summer maximum) and in the main channel is 600 ppm or 0.027 mol m^{-3} (winter minimum). These conditions produce the maximum concentration differential (0.067 mol m^{-3}) and therefore the maximum diffusion flux. The narrow passage connecting the two volumes has a length of 10 m and therefore the concentration gradient results to be $0.007 \text{ mol m}^{-3} \text{ m}^{-1}$. Using Eq. 7.4., a flux of $0.02 \text{ } \mu\text{mol m}^2 \text{ s}^{-1}$ can be estimated. If the flux is multiplied by the narrow passage cross section (around 2.7 m^2), a carbon dioxide flow of $0.05 \text{ } \mu\text{mol s}^{-1}$ is obtained. Carbon dioxide diffusion flow through the narrow passage is negligible if compared to other flows contributing to the CO₂ balance in the “Music hall” (see Figs. 7.3 and 7.4). Natural carbon dioxide input into the “Music hall” in Fig. 7.3, is the smaller contribution among all the others but yet it

amounts to hundreds of μmoles per second, more than thousand times higher than diffusion flow. Baldini et al. (2006) reach similar conclusion for Ballynamitra cave (Ireland) showing that by only diffusion process three years would be necessary to homogenize the concentration profile and that therefore diffusion is not a controlling factor for carbon dioxide transport along the cave.

The next step will give an answer to the question: how long would it take to a cave volume (in this specific case the “Music hall”) to reach a perfectly mixed condition by the only diffusion mechanism?

The solution can be obtained by analyzing the following idealized problem: an instantaneous point source emission is released in a perfectly quite isotropic medium, confined by two parallel boundaries on each direction. At these borders, a no-flux boundary condition is imposed. If mass is released in the center of the domain, the time-scales required to achieve uniform conditions in each dimension ($t_{mix,i}$) is given by Nepf (2008):

$$t_{mix,i} = \frac{L_i^2}{4D} \quad \text{where } i = x, y, z \quad (7.5)$$

L is the length-scale of interest and is defined as the full width of the domain in a given direction (i.e. the distance between the parallel boundaries).

In real conditions, the boundaries represent the walls, floor and ceiling of the cave room. However, in our case, it will be sufficient to analyze the problem along the direction where L is smaller (z direction). The other directions (x and y) will require an even longer time to achieve a null gradient of concentration.

In Bijambare, the “Music hall” ceiling height (L_z) can be considered to be 6 m while D for carbon dioxide in air, as already stated before, can be approximated by $3.0 \times 10^{-6} \text{ m}^2 \text{ s}^{-1}$. The resulting mixing time given by Eq. 7.5 is around 35 days. Although half of this time achieves already a mixing level that could be considered sufficient both values are still too high and contradictory with experimental data and dynamics observed in the field.

For example, in Fig. 6.9, it can be noticed that in both cases after an initial peak (during tourist visit) the concentration of carbon dioxide rapidly decrease (in less than one hour) and it reaches a flat or even slightly increasing trend. Although initial peak is surely related due to the not instantaneous mixing, after one hour there are no indications of further decrease of concentration due to additional expansion of the concentration profile within the “Music hall”.

In Fig. 7.2, although the C_{MH} probe was located around 5 m far from the release point and on the opposite direction of the generated gas plume, the increment of carbon dioxide concentration is almost immediate or at least much faster than what could be expected by molecular diffusion.

However, the strongest evidence that the volume can be approximate by a perfectly mixed system is given by a simple mass balance during the first 5 h of the

artificial release experiment. The discharge of 10 kg of CO₂ in a 15,000 m³ well-mixed volume produces, in absence of losses, an increase of concentration of 330 ppm. However, in the first 5 h of the experiment, around 3 kg of carbon dioxide were already lost by advection through the narrow passage (obtained as integral of experimental velocities in the narrow passage and difference of concentrations between the “Main channel” and “Music hall”). Hence, the expected increment of concentration in a perfectly mixed system is only around 240 ppm, in full agreement with experimental data.

These evidences support the idea that “Music hall” atmosphere is rapidly mixed and that molecular diffusion process cannot achieve this result.

Rapid mixing due to turbulent flow could be the mechanism able to fast spread carbon dioxide in the whole “Music hall”. However, this is possible only if air velocity is high enough to sustain this process.

Following the same approach as in Sect. 5.2.4 we can consider that the “Music hall” acts as the end of a convective cell and therefore that there is a net flux of air across its half cross section equal to the flow rate passing the narrow passage. Considering a cross section of 300 m² we can estimate an approximate diameter of 14 m and then, by using Eq. 5.3, a critical velocity for the transition to turbulent flow equal to $2.1 \times 10^{-3} \text{ m s}^{-1}$.

During the experiment, the minimum recorded wind velocity in the narrow passage of 0.12 m s^{-1} correspond to a flow of $0.325 \text{ m}^3 \text{ s}^{-1}$ and to an average velocity across the “Music hall” half cross section of $2.2 \times 10^{-3} \text{ m s}^{-1}$. Hence, despite large volumes and small velocities, conditions during minimum flow are already turbulent or at least very close the transition to turbulent flow. At higher flows detected during the experiment or calculated in Chap. 6 the fluid dynamic behavior should be even more chaotic.

The assumption of a well-mixed behavior of the “Music hall” is therefore justified and it is most probably caused by the air turbulence more than by diffusion process.

7.5.2 Model Results

By using the modelling “Approach 1”, the predicted value of Q is equivalent to an air velocity in the narrow passage of 0.11 m s^{-1} only slightly lower than experimentally recorded ($0.13\text{--}0.16 \text{ m s}^{-1}$). Similarly, the model estimates an average value for the concentration of carbon dioxide in the stream entering the “Music hall” (C_{in}) of 468 ppm in agreement with the range measured in the “Main channel” (C_{MC}) for the same period (450–500 ppm). The predicted natural input J_S equal to $17 \times 10^{-6} \text{ m h}^{-1}$ ($0.2 \mu\text{mol m}^2 \text{ s}^{-1}$) is lower but in the same order of magnitude than values from Chap. 6 for the autumn season (Fig. 6.7).

The “Approach 2” using directly the experimental values for air velocity and carbon dioxide concentration in “Main channel” predicts a natural input J_S equal to $39.7 \times 10^{-6} \text{ m h}^{-1}$ ($0.5 \mu\text{mol m}^2 \text{ s}^{-1}$), around double than the value obtained by using the “approach 1”.

7.5.3 Model Sensitivity to “Music Hall” Volume

In the model there two groups of input values:

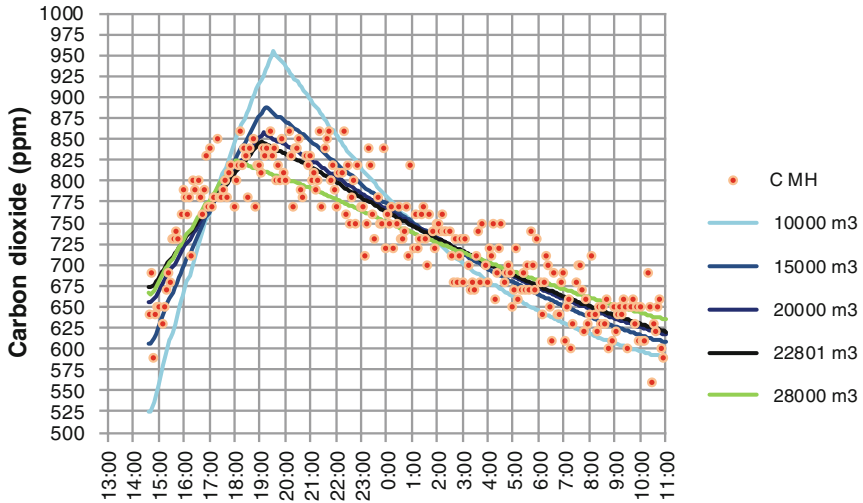
- (a) Fixed parameters (i.e. geometry of the system)
- (b) Adjusted parameters (e.g. natural carbon dioxide input flux J_S or gas release flow Q_{CO_2})

The values of parameters belonging to the first group are directly introduced in the model while, for the second group, the values are iteratively adjusted in order to achieve the best fit of results with experimental data. On the other hand, establish exact geometry of cave channels and rooms is difficult if not impossible and therefore the values provided to the model are only rough estimations based on simplified shapes. Hereafter, we will try to investigate the effects on model prediction caused by uncertainty in the “Music hall” volume.

It is important to notice that while in “Approach 1” different volumes of the “Music hall” affect only the value of the adjusted parameters but not the results and goodness of fit of the model (in other words regression using different volumes will always produce the same adjusted curve and will not change the R^2 residual), in the “Approach 2” the value of V modifies the shape of the model predictions and therefore the residual R^2 varies.

Figure 7.5 shows the results of “Approach 2” for different fixed volumes of the “Music hall”. J_S decreases from 51.9×10^{-6} to $17.6 \times 10^{-6} \text{ m h}^{-1}$ while carbon dioxide discharge rate rise from 1.05 to $1.57 \text{ m}^3 \text{ h}^{-1}$ as the volume increases from 10,000 to 28,000 m^3 .

The best model fit ($R^2 = 0.824$) has been obtained with the values for V , J_S , Q_{CO_2} and C_0 are 22,801 m^3 , $15.5 \times 10^{-6} \text{ m h}^{-1}$ and $1.17 \text{ m}^3 \text{ h}^{-1}$ and 673 ppm respectively. Reapplying the “Approach 1” using a volume of 22,801 m^3 the adjusted value for the parameters Q and J_S is $1652 \text{ m}^3 \text{ h}^{-1}$ and $25 \times 10^{-6} \text{ m h}^{-1}$ respectively. Concentration of carbon dioxide in the “main channel” (468 ppm) initial concentration in the “Music hall” (819 ppm) are unchanged. It should be noticed that for these conditions the predicted air velocity in the narrow passage of 0.162 m s^{-1} is equal to the maximum velocity experimentally recorded (0.16 m s^{-1}).



V	10000	15000	20000	22801	28000	m^3
J_s	51.9	39.7	24.1	15.5	17.6	$mh^{-1} \times 10^{-6}$
Q_{CO_2}	1.05	1.13	1.15	1.17	1.57	$m^3 h^{-1}$
C_0	524	606	655	673	666	ppm
R^2	0.310	0.732	0.817	0.824	0.806	

Fig. 7.5 Model results after optimization of “Music hall” volume

7.6 Conclusions

Following an experiment where 10 kg of carbon dioxide was released into the cave environment, and thanks to short but more controlled and detailed monitored conditions, several assumptions, hypothesis and results presented in Chaps. 5 and 6 have been tested. Srednja Bijambarska cave climate model presented in Chap. 5 proved able to describe also conditions during the carbon dioxide release experiment and cave barometric respiration appears to have only a marginal role in explaining air movements within the cave. Based on carbon dioxide concentration increase following the CO₂ introduction, it was possible to confirm that “Music hall” acts with good approximation as perfectly mixed volume. Based on data regression, the volume resulted as 22,800 m³ broad similar to the 15,000 m³

estimated by cave survey in Chap. 6. The mixing and transport processes between and inside cave sections appears to be related with air turbulence more than with diffusion phenomena. Application of model developed in Chap. 6 provides results comparable with experimental measured data (i.e. air velocity) although, in the future, more data should prove this conclusion to be valid on a longer period.

References

- Badino G (1995) *Fisica del Clima Sotterraneo*. Memorie dell'Istituto Italiano di Speleologia, Serie II, vol 7, Bologna
- Badino G (2009) The legend of carbon dioxide heaviness. *J Cave Karst Stud* 71:100–107
- Baldini JUL, Baldini LM, McDermott F, Clipson N (2006) Carbon dioxide sources, sinks, and spatial variability in shallow temperate zone caves: evidence from Ballynamindra cave, Ireland. *J Cave Karst Stud* 68:4–11
- Benavente J, Vadillo I, Carrasco F, Soler A, Liñán C, Moral F (2010) Air carbon dioxide contents in the vadose zone of a mediterranean karst. *Vadose Zone J* 9:1–11
- Bussani A (2007) Atmospheric tide effects in a Trieste karst cave: preliminary results. *Atti e Memorie della Commissione Grotte "E. Boegan"* 41:17–24
- Jia LX, Wang L (2001) Equations for gas releasing process from pressurized vessels in ODH evaluation, CEC/ICMC 2001 conference. Madison, Wisconsin
- Kowalczk AJ, Froelich PN (2010) Cave air ventilation and CO₂ outgassing by radon-222 modeling: how fast do caves breathe? *Earth Planet Sci Lett* 289:209–219
- Kowalski AS, Serrano-Ortiz P, Janssens IA, Sánchez-Moral S, Cuezva S, Domingo F, Were A, Alados-Arboledas L (2008) Can flux tower research neglect geochemical CO₂ exchange? *Agric For Meteorol* 148:1045–1054
- Liu Z, Zhao J (2000) Contribution of carbonate rock weathering to the atmospheric CO₂ sink. *Environ Geol* 39:1053–1058
- Liu Z, Dreybrodt W, Wang H (2010) A new direction in effective accounting for the atmospheric CO₂ budget: considering the combined action of carbonate dissolution, the global water cycle and photosynthetic uptake of DIC by aquatic organisms. *Earth Sci Rev* 99:162–172
- Nepf H (2008) Transport processes in the environment—lecture 4: boundary conditions [Online]. Available at http://ocw.mit.edu/courses/civil-and-environmental-engineering/1-061-transport-processes-in-the-environment-fall-2008/lecture-notes/lec_04.pdf. Accessed 27 July 2011
- Pflitsch A, Wiles M, Horrocks R, Piasecki J, Ringeis J (2010) Dynamic climatologic processes of barometric cave systems using the example Jewel cave and Wind cave in South Dakota, USA. *Acta Carsologica* 39:449–462
- Sanchez-Moral S, Cuezva S, Fernandez-Cortes A, Benavente D, Canaveras J (2010) Effect of ventilation on karst system equilibrium (Altamira cave, N Spain): an appraisal of karst contribution to the global carbon cycle balance. In: Bartolomé A, Carrasco F, Juan José J, James LW (eds) *Advances in research in karst media*. Springer, Berlin, pp 469–474
- Serrano-Ortiz P, Roland M, Sanchez-Moral S, Janssens IA, Domingo F, Goddérés Y, Kowalski AS (2010) Hidden, abiotic CO₂ flows and gaseous reservoirs in the terrestrial carbon cycle: review and perspectives. *Agric For Meteorol* 150:321–329

Chapter 8

From Soil to Cave: The Inorganic Carbon in Drip Water

Abstract Drip water at three sites appears to have been originated from a parent solution with an equilibrium carbon dioxide partial pressure ranging between 15,000 and 26,000 ppm. A large part of the variability in drip water composition observed in the cave can be explained by different stage of degassing. Water composition at several cave pools confirms that drip waters rapidly achieve equilibrium with the cave atmosphere after impact on the stalagmite apex, while oversaturation is retained longer. Water leaving the cave environment towards the phreatic zone has been estimated to be in equilibrium both with cave atmosphere and calcite during summer, while it retains some calcite oversaturation during winter. The difference of DIC between the solution entering and leaving the cave represents the total inorganic carbon lost by degassing into cave atmosphere and by precipitation of calcite. Separating these last two terms can be accomplished using the difference of calcium content of the two solutions. Once these concentrations have been defined, they were converted into fluxes by unit of surface using an average effective infiltration of 497 mm year^{-1} or $1.6 \times 10^{-5} \text{ L m}^2 \text{ s}^{-1}$. The resulting flux of carbon dioxide degassing from drip water is in the range of $0.03\text{--}0.06 \text{ } \mu\text{mol m}^{-2} \text{ s}^{-1}$. These values are similar to the results estimated by modelling of carbon dioxide variations in the cave atmosphere.

8.1 Introduction

Percolating water plays a key role in transferring inorganic carbon from soil through the vadose zone of a karst massif. Infiltration rates and water composition are controlled by external climatic conditions and by soil and epikarst settings. Further on, changes in composition occurs when percolating water enters in ventilated voids (i.e. caves) where degassing and advection of carbon dioxide produce solution

Material from this chapter has been originally published in Milanolo S, Gabrovšek F (2015) Estimation of carbon dioxide flux degassing from percolating waters in a karst cave: case study from Bijambare cave, Bosnia and Herzegovina. *Chemie Erde—Geochemistry* 75(4):465–474. DOI:10.1016/j.95chemer.2015.10.004

oversaturation and calcite precipitation. Ventilation, and therefore advection of carbon dioxide, is controlled by geometry of conduits and again by the interaction with the external climate.

Modern paleoclimate studies using stalagmites rely on the capacity of a climatic signal to be recorded as change in percolating water quantity and/or composition, transferred underground to a drip site in a cave and then recorded by progressively deposited carbonate layers. This transfer function (and also its inverse function) is however still partially unknown. One of the reasons lies in the complexity of drip water dynamics that have been shown to be highly variable in flow and composition both in time and space.

Inorganic carbon released by drip water degassing represents the major input source of carbon dioxide to a cave atmosphere. Another contribution is the direct molecular diffusion from soil or epikarst, which is effective only through epikarst fractures and voids that are not water filled.

In this chapter we assess the change of DIC in percolating water as it passes the cave. The estimation is based on monitoring of flow rates at drip sites and composition and of water at drip sites and in pools. By the difference of these two concentrations, the flux of carbon dioxide entering the cave atmosphere can be estimate and compared with estimation from Chap. 6.

8.2 Results

8.2.1 Drip Sites

Water for chemical analysis has been sampled at four sites: at three drip points above actively forming stalagmites and over a flowstone at site four (result presented in Fig. 8.1). Sampling frequency was maintained generally within 1–6 weeks, but at least two gaps are present due to monitoring interruption. A detailed description of sampling position and methodology is given in Sect. 3.3 and Fig. 3.11. Site 3 during sampling operation is depicted in Fig. 3.9a.

The mean flow rate is different for each drip site. Site 1 registers the lowest average flow of 0.18 L h^{-1} , peak value of 0.49 L h^{-1} and minimum flow of 0.08 L h^{-1} . Site 2 records the maximum mean flow of 1.15 L h^{-1} , a peak flow of 4.00 L h^{-1} and minimum of 0.63 L h^{-1} while site 3 has intermediate mean flow (mean 0.60 L h^{-1} , peak 1.00 L h^{-1} and minimum 0.35 L h^{-1}). Site 4 has a strongly intermittent behaviour and for the majority of the time it is dry. During short periods when it is active, it delivers water flow as high as 6.00 L h^{-1} .

As average, all sites show two main flow peaks: the first during April and the second during December while a third less pronounced maximum is located in June. Hence, the drip flow rate appears to be correlated with external average precipitation with a delay of the main peak of maximum 1 month. The two drip flow peaks at the beginning and end of winter could be attributed to snow melting periods (early snow falling in November is rapidly melted by the following rain events).

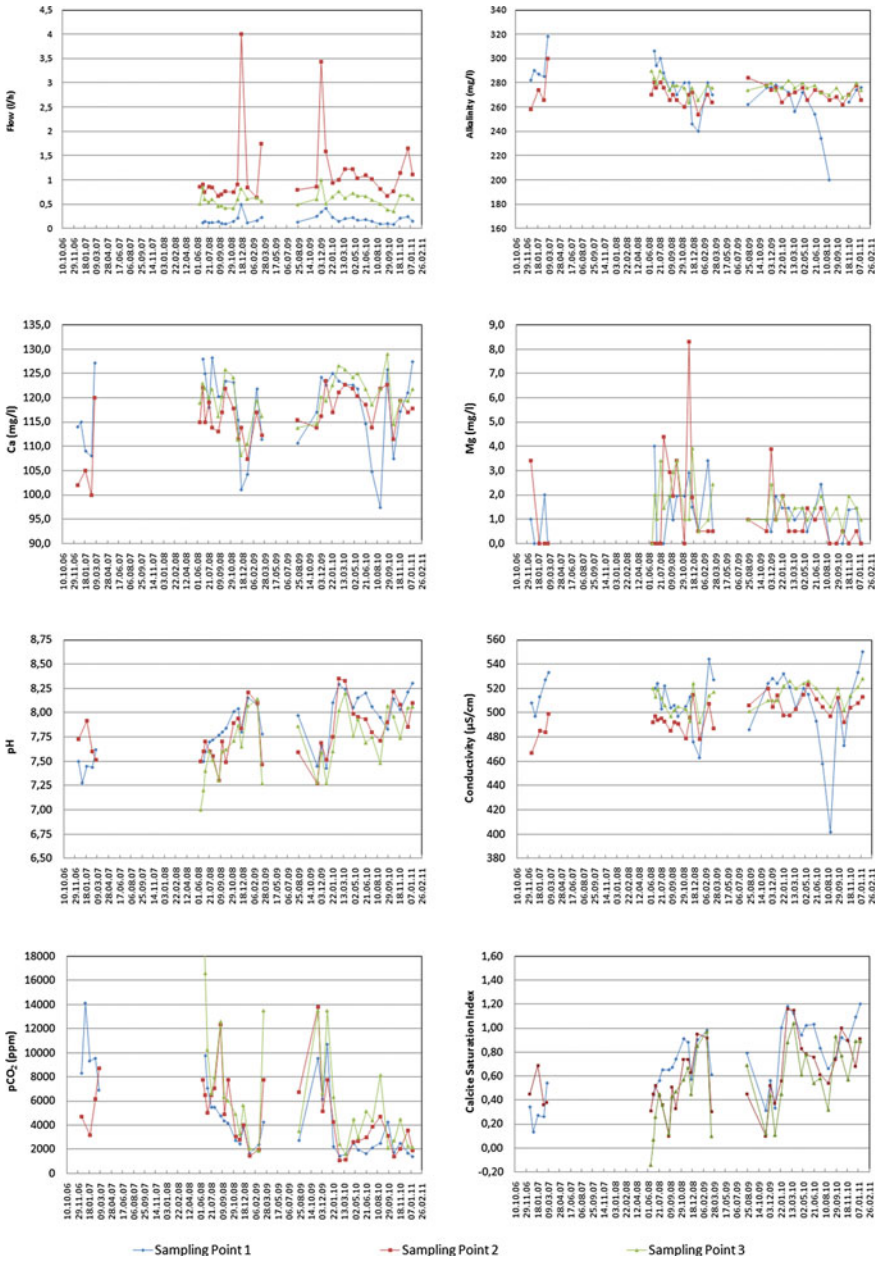


Fig. 8.1 Results from drip water analysis

The majority of water alkalinity values lie between 260 and 280 mg L⁻¹ with few exceptions reaching up to almost 320 mg L⁻¹, and at least two visible depletions in alkalinity at Site 1 during December 2008 and August 2010. During this last event, the minimum alkalinity value of 200 mg L⁻¹ has been recorded. With the exception of this behaviour at Site 1, there are no apparent differences of alkalinity between Sites 1, 2 and 3 and no evident seasonal behaviour. By contrast, alkalinity at Site 4 varies between 86 and 200 mg L⁻¹ (average 116 mg L⁻¹), significantly lower than at the other sites.

Similarly to alkalinity, calcium concentration was mostly within the narrow range of 110–125 mg L⁻¹, very similar between Sites 1, 2 and 3. Also in this case there are two episodes of calcium concentration drop correlated with alkalinity decreases. These events are visible at all sites but are most evident at Site 1. The few calcium concentration values recorded during the 2006–2007 period may also belong to a third episode but, due to the small sample population, this cannot be confirmed. The minimum calcium concentration recorded was 97 mg L⁻¹. Site 4, when is active, delivers water with a calcium concentration value around half that of Sites 1, 2 and 3 (37–72 mg L⁻¹ with an average of 49 mg L⁻¹).

Magnesium analyses show very low concentrations reflecting the weak dolomitization of the rock. Almost all detected concentrations are within the expected analytical error and therefore results cannot be discussed. The only exception may be a single peak slightly over 8 mg L⁻¹ that occurs at the same time as a drip flow peak and alkalinity and calcium concentration drop event in November 2008.

The pH signal presents a complex behaviour at all sites. However, for Sites 1, 2 and 3 there is a general tendency for higher values during the early months of the year. With the exclusions of 4 values the remaining 101 measurements, present a range of variation for this parameter from 7.25 to 8.25.

The specific electric conductivity (SEC) mimics calcium concentrations time-series with typical values in the range 460–540 μS cm⁻¹ for Sites 1, 2 and 3. Similarly to calcium concentration behaviour, also SEC shows at least one depletion episode, reaching a minimum of 400 μS cm⁻¹ in August 2010. Site 4 records lower SEC values in the range 184–320 μS cm⁻¹ (Fig. 8.2).

8.2.2 Pool Water

In order to investigate the evolution of water composition after the drip point, water from several pools has been analysed during different visits. The sampling points are located along two different sides of the stalagmite (Site 2, see Fig. 3.11). Water was sampled from pools with approximate volumes of 0.3–1.0 L on one side and from few millilitres to a couple of litres on the other side. The majority of water feeding all pools is originated from Site 2. Based on visual inspection, only a few drops, during the almost two hours pool water sampling procedure, did not belong to Site 2. During summer months most of the pools completely dry up and although

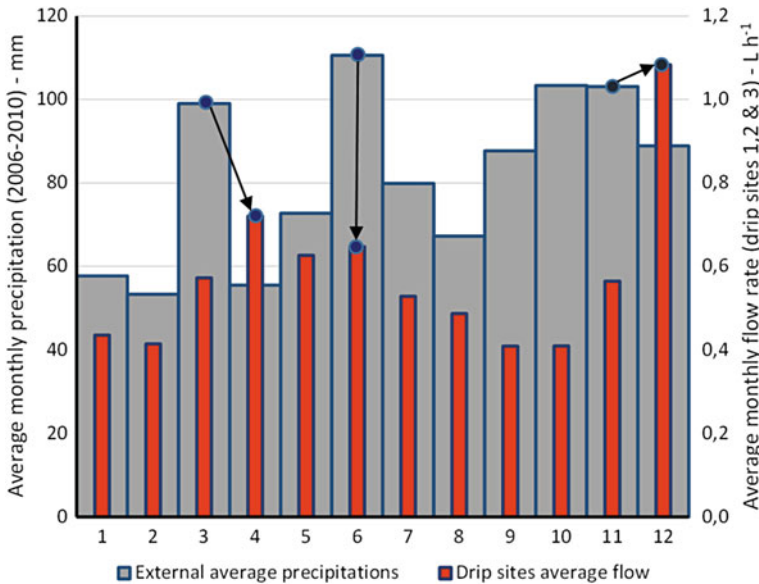


Fig. 8.2 Comparison between external average monthly precipitation for the period 2006–2010 and the average monthly drip flow rate for the same period (sum of drip site 1, 2 and 3)

few samples have been collected from remaining active pools, the results are presented in Fig. 8.3 only for months where a complete profile could be sampled.

Based on these analyses, calcium concentrations decrease rapidly from around 120 mg L⁻¹ at Site 2 to around 60 mg L⁻¹ at one meter distance. At distances greater than 1 m from the impingement point the calcium level appears to asymptotically stabilize in the range from 40 to 60 mg L⁻¹. Similar behaviour is recorded for alkalinity and SEC. pH appears to exhibit two general behaviours: during winter, the pH at drip site is usually higher than 8.0 and tends to stay rather constant or even increase with distance from the drip site. Conversely, in late spring (summer months are not available) pH at the drip site is below 8.0 and further decreases away from drip point. Temperature raises by about 0.5 °C, from values of 5.0–5.5 °C at Site 2 to 5.5–6.0 °C at the most distant pool.

Based on these data, values of *p*CO₂ in equilibrium with the concentration of CO₂ in the water and calcite Saturation Index have been calculated. Concentration of carbon dioxide in equilibrium with solution changes during the year. At the drip site, it increases from slightly more than 1000 ppm during cold months up to more than 4000 ppm in late spring. The CO₂ in pool water decreases rapidly with distance from Site 2 down to about 500 ppm in winter. The values of CO₂ in summer months are higher. Values recorded in May and June appears to converge asymptotically in the range between 2000 and 2500 ppm. Saturation indices decrease as well from 0.6 to 1.2 at Site 2 to values typically from 0 to 0.6 in the farthest pool. The lower half of the range is typical in warmer months, while higher values are more common during the winter months.

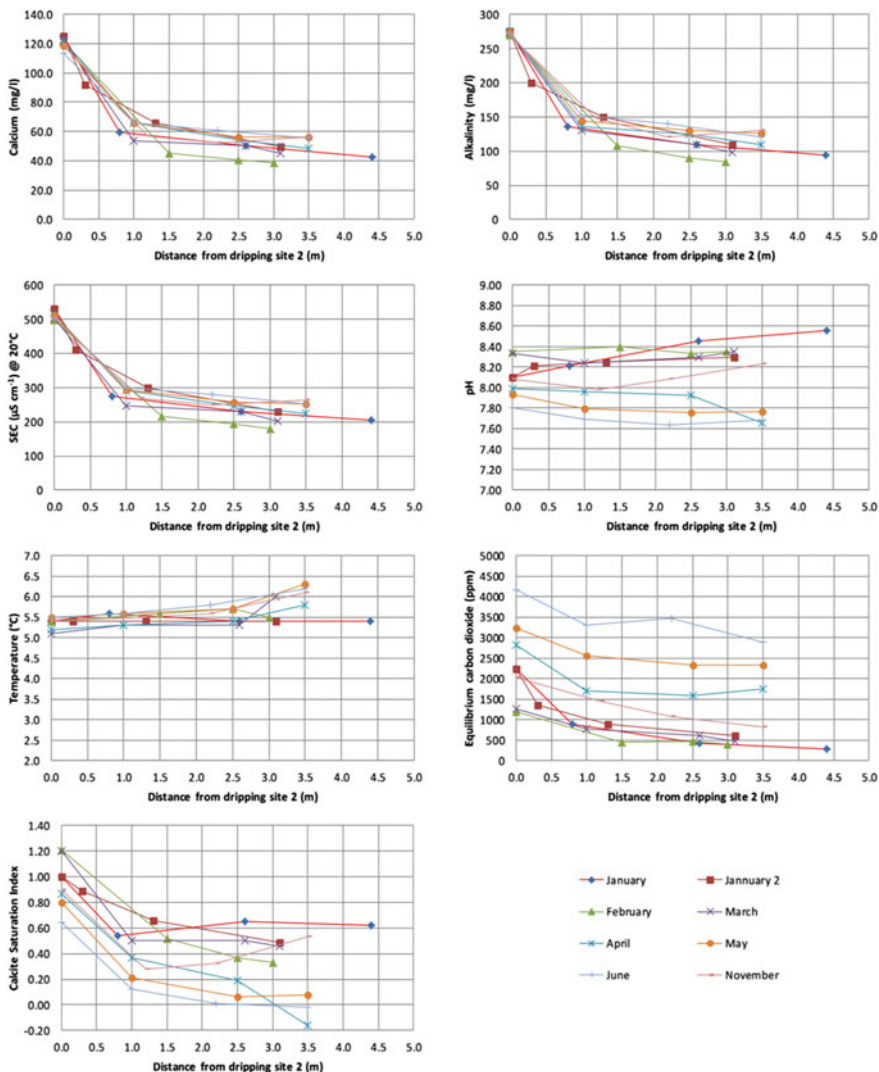


Fig. 8.3 Results from pool water analysis

8.3 Discussion

8.3.1 The Characteristics and Classification of Drip Sites

The selected sampling sites present contrasting hydrological behaviour. The sites have been sorted using the classification of Smart and Friederich (1987), dividing waters into 5 main categories based on their flow rate and coefficient of variation of

discharge (Fig. 8.4). A conceptual illustration of six vadose flow categories has been previously provided by Gunn (1981). Based on this approach, Sites 1 and 3 can be considered in terms of predominant seepage flow with Site 1 showing lower dripping rate but higher relative variability with respect to Site 3. Site 2 shows almost one order of magnitude higher discharge rate than Site 1, and should be considered border line to vadose flow. Site 4 represents an exception since it is not fed from a stalactite but by water running over a flowstone. This site is dry for most of the year, but reacts vigorously to precipitation events. Based on above classification it should be classified as subcutaneous flow.

Nowadays most of the drip sites used for geochemical, isotopic or paleoclimate analyses have lower discharge than Site 1 in Bijambare (Mickler et al. 2004; Spötl et al. 2005; Beddows et al. 2008; Verheyden et al. 2008). In carbonate waters the SEC directly relates to total hardness (Vokal 1999; Krawczyk and Ford 2006). In Bijambare, this correlation (Fig. 8.5) is indeed strong ($R^2 = 0.92$) and therefore

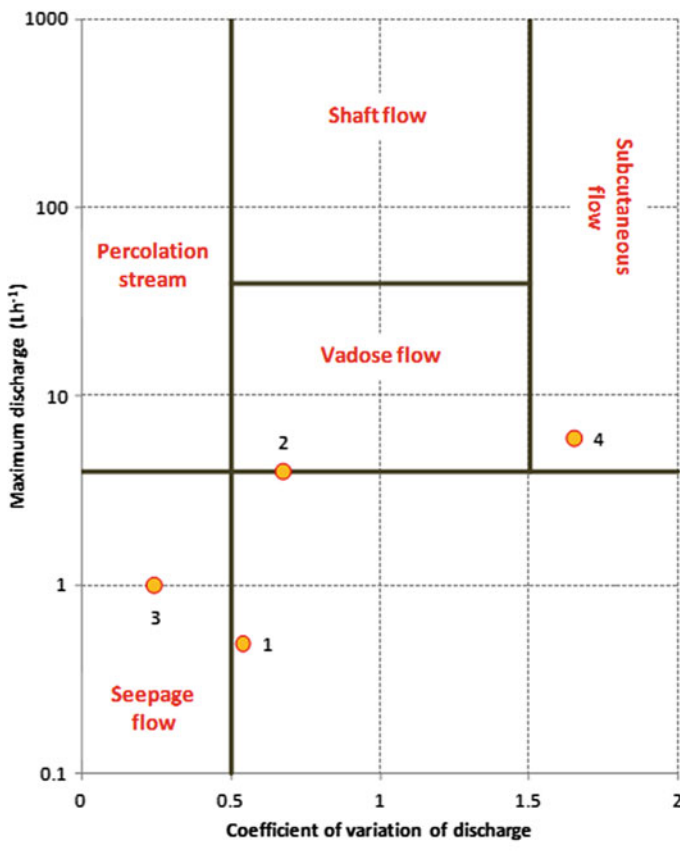


Fig. 8.4 Variability of flow components in the vadose zone with over impressed characteristics of the investigated drip sites in Bijambare. Adapted from Smart and Friederich (1987)

contribution of foreign ions is probably very limited. The small misfit between the data and regression line shown in Fig. 8.5 could result from the limited presence of magnesium ions (poorly present also in the hosting limestone), pH (hydro-carbonate equilibrium) differences and analytical error.

The sampling profiles at Bijambare can be divided clearly in two groups based either by their calcium concentration or by SEC:

- Sites 1, 2 and 3
- Site 4 and pool water

Although this is already clearly visible from Fig. 8.5, an Anova test (based on calcium concentrations) proved that there is no statistically difference between the Sites 1, 2 and 3 ($p = 0.056$), but there is high difference with Site 4 and pool water ($p \ll 0.01$). Hence there is again no significant difference between Site 4 and pool water ($p = 0.132$).

By the analysis of three fast dripping sites in Postojna cave, Vokal (1999) found a strong linear relationship between average Ca^{2+} or SEC and average dripping rate at different dripping sites, but the same author also suggests that this correlation needs to be confirmed using a larger number of profiles. Since Sites 1, 2 and 3 at Bijambare have no significant difference in average Ca^{2+} concentration but they have considerably different discharge rate, it can be concluded that the inter-site relationship between calcium concentration and discharge rate in this case is weak or completely absent.

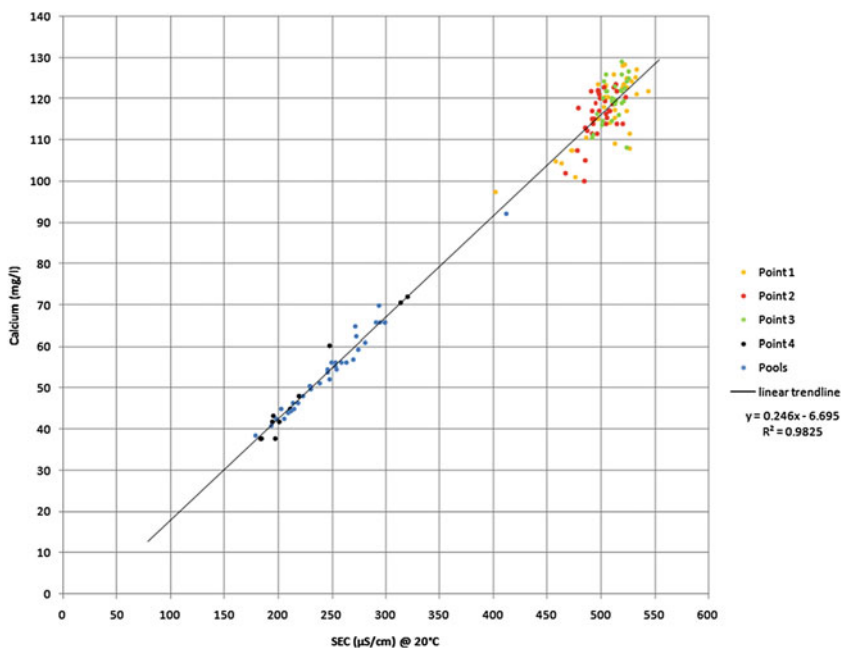


Fig. 8.5 Specific electric conductivity and calcium concentration relationship

The large difference between the compositions of water at the drip site and in the pools can be explained by the precipitation of calcite along the path. It appears that along 1 m long path over stalagmite surface (from Site 2 to the first sampled pool), the concentration of calcium in solution drops for 50 %. Site 4, collecting water running over a flowstone, presents characteristics similar to pool water.

8.3.2 *The Evolution from Soil to Sampling Point*

The carbon dioxide concentration shown in Fig. 8.1 describes the equilibrium situation frozen at the moment and place of sampling, but it does not provide information about the evolution in composition that occurred along the pathway from soil to the sampling point. To track back the CO₂ content in the soil it is necessary to identify a sufficiently reliable proxy for the amount of carbon dioxide lost before the sampling point.

Two mechanisms are responsible for the reduction of inorganic carbon in the solution: degassing of CO₂ in the cave atmosphere and precipitation of calcium carbonate.

If carbon dioxide lost by degassing is not balanced by calcite deposition, the overall effect is an increase of SI_C of the solution. Therefore, under the assumption that there is no prior precipitation, the calcite saturation index of the sample provides an indication for the amount of carbon dioxide lost by degassing before the sampling point. The assumption of no prior precipitation requires that no calcite has been deposited during the percolation of drip water from soil-epikarst boundary to the stalactite tip. While from the moment of droplet detachment to immediately after the impact on stalagmite, time scale of degassing process is much shorter (requiring only few seconds to equilibrate drip solution with cave atmosphere) and is largely predominant over calcite deposition (Dreybrodt 2008). We will therefore overall assume that Ca²⁺ is a conservative ion and its concentration invariant during degassing. At usual cave drip water pH range of 7–8, the inorganic carbon is mostly in the form of HCO₃⁻ (Appelo and Postma 2006) and OH⁻ and H⁺ are negligible. Combining a simplified electric charges balance:

$$\begin{aligned} (\text{HCO}_3^-) + 2(\text{CO}_3^{2-}) + (\text{OH}^-) &= 2(\text{Ca}^{2+}) + (\text{H}^+) \\ (\text{HCO}_3^-) &\cong 2(\text{Ca}^{2+}) \end{aligned} \quad (8.1)$$

with definition of SI_C and log(pCO₂) as given in Chap. 4 (Eqs. 4.9 and 4.10) we get:

$$\text{SI}_C \cong -\log(\text{pCO}_2) + 3 \log(\text{Ca}^{2+}) + \log\left(\frac{4K_2}{K_C K_1 K_H}\right) \quad (8.2)$$

If calcium concentration and temperature are constant during degassing then the Eq. 8.2 describes the relationship between SI_C and $\log(pCO_2)$ as a set of lines with slope -1 . Roberge (1979) used such plot to describe the evolution of spring water composition as a mixture between allogenic and autogenic recharge (Ford and Williams 2007, p. 50).

Figure 8.6 presents the theoretical evolution of a solution initially in equilibrium with calcite and with an infinite gas phase containing 20,000 ppm of carbon dioxide ($\log(pCO_2) = -1.7$) in an open system. The figure also presents the experimental results for the samples collected during this study.

The experimental results (Sites 1, 2 and 3) show a relatively small spread around the theoretical line and the results of an Univariate Analysis of Variance test (performed with SPSS software v.15) also demonstrate that there are no significant differences ($p > 0.05$) between the three sampling points in terms of intersection of their linear regression line with the horizontal axis. This good fit was expected and it reflects the small differences in calcium concentration recorded within a single Site and between different Sites.

Normally, around 70 % (from 50 to 90 % depending on specific conditions) of limestone dissolution occurs along the first ten meters of vertical water percolation (Ford and Williams 2007, p. 93). After 30–40 m (the thickness of ceiling above Srednja Bijambarska cave) it is reasonable to assume that the solution achieved almost the equilibrium with calcite ($SI_C \cong 0$).

This is of course only an approximation because switch from linear to non-linear rate law for systems close to saturation results in a very slow approaching to the complete equilibrium allowing a residual aggressiveness to propagate deeper in a limestone massif (Palmer 2002).

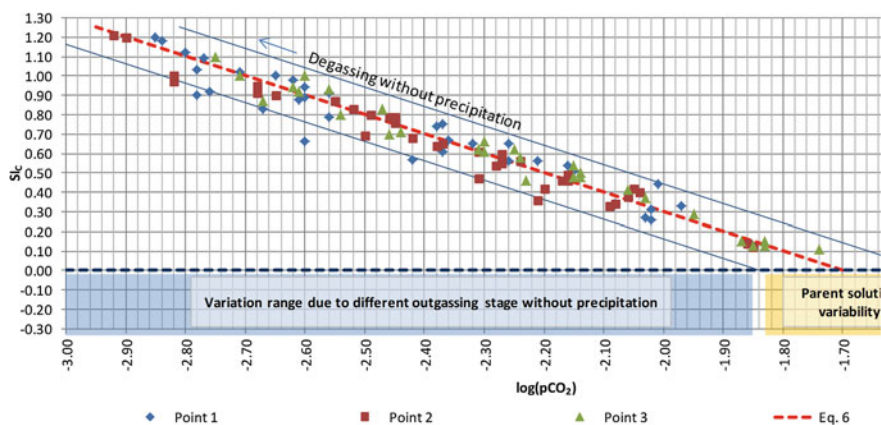


Fig. 8.6 Calcite saturation index versus carbon dioxide partial pressure in equilibrium with the solution. *Points* represent the experimental samples collected after drop fall and just before impact on stalagmite

As a result, the intersection of the set of lines shown in Fig. 8.6, representing the samples evolution, with the horizontal axis ($SI_C \cong 0$) provides an estimate of the range of conditions in the epikarst region before carbon dioxide degassing occurred.

Variation of equilibrium pCO_2 obtained from samples composition during the investigated period can be largely explained by different degassing stage of the dripping in the unsaturated zone (different position along the same line given by Eq. 8.2), while another fraction of variability is caused by parent solution equilibrium pCO_2 changes (changing Ca^{2+} concentration and therefore moving between different parallel lines with horizontal axis intercept between -1.82 and -1.58 with an average value of -1.70 and corresponding roughly to the range 15,000–26,000 ppm with average value of 20,000 ppm).

This range of equilibrium carbon dioxide partial pressure, under several assumptions, may be used to approximate carbon dioxide concentration variations in epikarst/soil interface.

Figure 8.7 schematically presents the consequences of prior calcite precipitation, incomplete saturation and closed system equilibrium on the estimation of soil/epikarst pCO_2 from drip water samples. In Fig. 8.7a, point A represents the

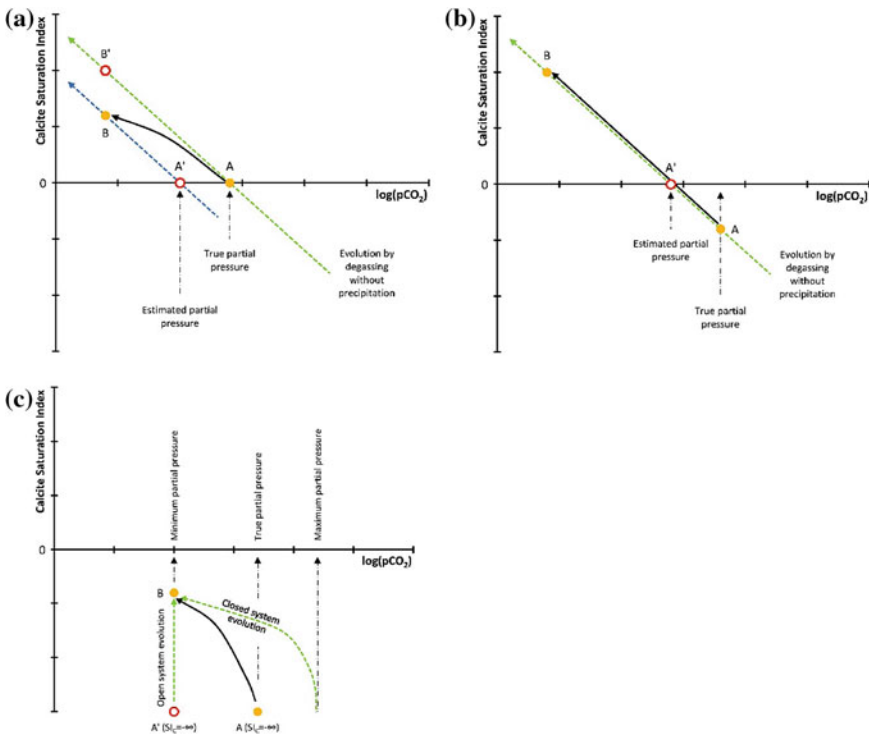


Fig. 8.7 Effects of prior precipitation, incomplete dissolution equilibrium in the epikarst and open or closed system in the soil-epikarst interface on the evolution of solution calcite Saturation Index and equilibrium carbon dioxide partial pressure

composition of a hypothetical percolating solution in equilibrium with calcite. Degassing without calcite precipitation would follow a -1 slope line leading to an ideal sampled composition in the cave denoted by the point B'. However, if calcite precipitation occurred before sampling, the resulting final calcite saturation index measured in the sample is lower due to the lost calcium carbonate (point B). Hence, looking backward from point B and neglecting the effect of prior precipitation, the estimated equilibrium partial pressure of the parent solution (point A') is located at a lower value than the real conditions. Similarly, in Fig. 8.7b, point A represents the composition of an hypothetical percolating solution which has not yet reached complete equilibrium with calcite at the moment when degassing started ($SI_C < 0$). Degassing without calcite precipitation would still follow the same -1 slope line leading to a composition denoted by the point B. By assuming that original solution was in equilibrium with calcite, the estimated equilibrium partial pressure of the parent solution (point A') is located at a lower value than the real conditions. Proceeding of calcite dissolution under open system conditions is described by an increase of SI_C from $-\infty$ to zero (if complete equilibrium is achieved) at a constant pCO_2 . On the other hand, in a closed system, because the consumption of carbon dioxide in the reaction for hydrocarbonate formation cannot be replenished by new carbon dioxide from the gas phase, the equilibrium pCO_2 of the solution is decreasing along with the increment of the saturation level. In Fig. 8.7c, the percolating solution represented by the point B is originated by intermediate soil/epikarst conditions (point A) comprised within the open system (minimum required pCO_2) and closed system (maximum required pCO_2) end members.

Therefore, assuming no prior calcite precipitation, complete saturation and open system equilibrium, the obtained partial pressure range is always an under estimation of real conditions in the soil/epikarst.

The range estimated at Bijambare falls within the typical carbon dioxide concentrations (0.1–6 %) reported for soil air of temperate zones (Ford and Williams 2007, p. 50; Jassal et al. 2004; Atkinson 1977). Several authors (Faimon et al. 2012; Faimon and Ličbinská 2010; Bourges et al. 2001; Atkinson 1977), comparing measurements of carbon dioxide concentration in shallow karst soils with CO_2 in caves or with drip water hydrochemistry have put under question the role of soil layer as primary source of carbon dioxide in favor of a deeper source caused by organic material biodegradation in the epikarst. This idea appears to be further supported by the high CO_2 concentrations (up to 6 %) found in piezometers extending deeply into the karst vadose zone (Benavente et al. 2010).

8.3.3 The Evolution from Dripping Site to the Equilibrium with Cave Environment

In the previous paragraph we have shown that variation in the chemical composition of sampled water at sites 1 to 3 can be attributed mainly to different stage of degassing with very limited deposition of calcite. After droplet detachment from

cave ceiling, degassing strongly prevails over deposition (i.e. during droplet falling and impact on the stalagmite) in this period the calcite Saturation Index reaches high values usually in the range 0.6–1.2.

After impact, dripping water is spread into a thin film flowing on stalagmite surface, degassing still proceeds fast and is expected to bring the solution into equilibrium with the cave atmosphere within around 10 s (Dreybrodt 2008). On the stalagmite apex also calcite precipitation occurs at a high rate but, the time scale of the process is about an order of magnitude higher than degassing. Hence the oversaturation with respect to calcite phase is retained at longer distance from drip site than CO₂ oversaturation with respect to the cave atmosphere. Although degassing from thin films is expected to be fast, the same process in thick solution layers rapidly slow down. Dreybrodt (2008) estimates a decay time for carbon dioxide outgassing from cave pools in the range of several hours up to days depending of depth of water.

Limited results in terms of equilibrium carbon dioxide partial pressure and Saturation Index versus distance given in Fig. 8.3 partially confirm this evolution.

During the first instant, dripping water evolves by degassing following a pseudo exponential decrease of equilibrium carbon dioxide concentration over distance, decreasing from the level recorded at drip site to equilibrium with cave atmosphere (500–600 ppm during winter up to 2000–2500 ppm during summer) in around two to four meters.

At the same time, calcite deposition also occurs at a high rate, and therefore Saturation Index is decreasing from the initial value at drip site to an infinite distance asymptotic value which appears to change during the year. During winter, after 3–4 m distance from drip site, the solution preserves an oversaturation level equal to $SI_C = 0.3\text{--}0.6$. Hence, it is possible that oversaturation may still decrease proceeding further with solution residence. During summer when drip flow is reduced and pools are progressively drying up, the residence time increases enough for the solution to completely equilibrate.

8.3.4 The Fluxes of Carbon Dioxide

As described in Paragraph 4.5 drip water entering the cave has an initial amount of dissolved inorganic carbon originated by the contact with a carbon dioxide rich gas phase in the soil-epikarst voids and from dissolution of carbonate rock.

From Sect. 8.3.2 we know that soil-epikarst pCO₂ has to be at least in the range of 15000–26000 ppm. We can reasonably assume that, by percolating through the epikarst, the solution achieved almost open system equilibrium with limestone with a constant temperature of 6 °C. The DIC concentration can be easily calculated by PHREEQC software v.2.17 (Parkhurst and Appelo 1999) and it amount to 6179–8034 μmol L⁻¹ (depending on the above mentioned concentration range). Calcium content varies between 2630 and 3218 μmol L⁻¹ (105–129 mg L⁻¹).

Similarly, after degassing and precipitation in the cave, the solution leaving towards the phreatic zone still contains a certain amount of dissolved inorganic carbon.

Section 8.3.3 shows that after a relatively short time from impingement on stalagmite apex, drip water reaches an almost completely equilibrium with the cave atmosphere. CO_2 concentration in the “Music hall” has been shown to vary during the year between a minimum of 550 ppm in winter and a maximum of 2200 ppm in summer (Sect. 5.2.7). Paragraph 8.3.3 also shows that deposition process is much slower and some oversaturation is retained far from the drip site. The residual SI_C in pools at almost 4 m from drip site has been found to vary from a minimum of 0 during summer, to 0.6 during winter. Hence, the DIC concentration in the solution leaving the cave environment at these conditions (temperature is fixed at 6 °C) can be estimated to range between 2680 (winter) and 2764 $\mu\text{mol L}^{-1}$ (summer) while calcium concentration varies from 1319 $\mu\text{mol L}^{-1}$ during summer to 1344 $\mu\text{mol L}^{-1}$ in winter (53–54 mg L^{-1}).

The difference of DIC concentration between the solutions entering and leaving the cave environment is the amount of inorganic carbon lost in the form of calcite deposit and carbon dioxide released to cave atmosphere. Two end member cases have been considered:

- Case 1: maximum CO_2 concentration in the soil-epikarst and minimum concentration in the cave atmosphere.
- Case 2: minimum CO_2 concentration in the soil-epikarst and maximum concentration in the cave atmosphere.

These cases give the widest range of DIC amount lost by the solution (3415–5354 $\mu\text{mol L}^{-1}$). Similarly, the difference of calcium concentration between the two solutions is in the range 1311–1874 $\mu\text{mol L}^{-1}$ and it is equivalent to the amount of inorganic carbon lost by calcite deposition. Hence, the amount of carbon dioxide degassing from the solution (2104–3480 $\mu\text{mol L}^{-1}$) can easily be calculated by subtracting the amount lost by calcite precipitation from the total DIC lost by the solution within the cave. The results for both cases are summarized in Fig. 8.8.

Previously calculated concentrations can be converted into fluxes by multiplying them by the amount of percolating water for unit of plan surface.

The average amount of water percolating through the soil and reaching the cave environment per unit of plan surface can be approximate by the annual average precipitation rate (917 mm year^{-1}) minus the water lost by evapotranspiration (420 mm year^{-1}) estimated by Turc’s equation (Turc 1961) and it amount to 497 mm year^{-1} or $1.6 \times 10^{-5} \text{ L m}^2 \text{ s}^{-1}$. This of course assumes that horizontal transport of water in soil and epikarst can be neglected and therefore that percolation from soil to cave is strictly vertical.

The resulting flux of carbon dioxide degassing from drip water is in the range of 0.03–0.06 $\mu\text{mol m}^{-2} \text{ s}^{-1}$. These values are similar to the results estimated in Chap. 6, where we used non-linear regression to model data of CO_2 monitoring in the cave atmosphere. There we estimated that even if during large carbon dioxide concentration variations episodes, the input of carbon dioxide in the Srednja

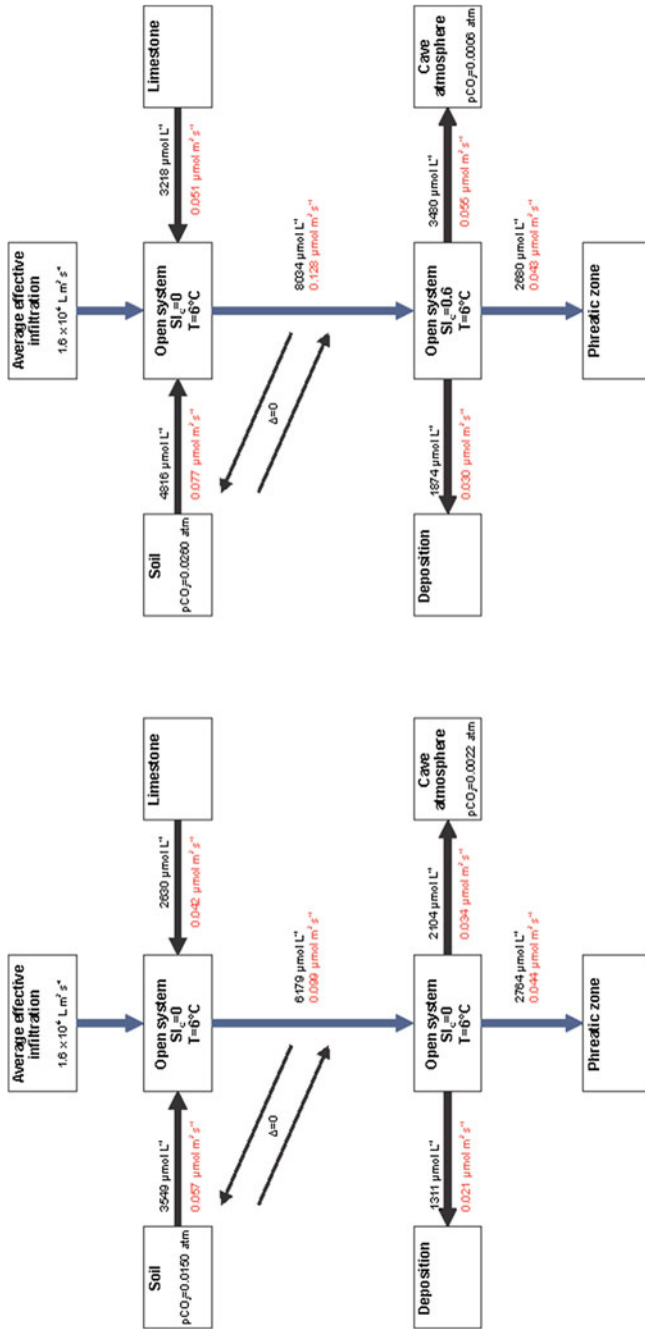


Fig. 8.8 Schematic sketch of the estimated carbon dioxide fluxes

Bijambarska cave environment may reach $12.40 \mu\text{mol m}^{-2} \text{s}^{-1}$, the average carbon dioxide flux is the range of few hundredths of $\mu\text{mole m}^{-2} \text{s}^{-1}$. Between 5 July and 26 August, 2007 the CO_2 concentration in the cave atmosphere increased from 1500 to 2100 ppm with very low advection losses due to the high external temperature. Therefore the average value of incoming carbon dioxide flux was found to be $2.9 \times 10^{-6} \text{ m h}^{-1}$ or $0.04 \mu\text{mol m}^{-2} \text{s}^{-1}$. These values are in close agreement with the range found in this study by drip water analysis. The match between the results of these two independent methods can be considered an indicator that the assumptions made in both works are reasonably fulfilled.

It should be noticed that moles of calcium in the inlet solution are equivalent to the amount of DIC initially introduced into the percolating water by limestone dissolution. This accounts for around 50 % of total DIC. However, in an open system, dynamic equilibrium allows for a continuous exchange of inorganic carbon between solution (including carbon derived from limestone dissolution) and the gas phase.

These fluxes do not affect the overall amount of DIC in the solution. However, by replacing most of the carbon atoms originally sourced from limestone dissolution with an identical quantity from voids atmosphere they change DIC isotopic composition (Hendy 1971; White 2007). The residual fraction of DIC originated from limestone dissolution is often referred to as “dead carbon” (to highlight its oldness and therefore lack of ^{14}C for dating) and its amount typically from 10 to 20 % (Genty et al. 2001; Oster et al. 2010).

8.4 Conclusions

Drip water at three sites appears to have been originated from a parent solution with an equilibrium carbon dioxide partial pressure in the range 15,000–26,000 ppm. Under no prior calcite precipitation and perfect open system equilibrium assumptions, this range reflects also the carbon dioxide pressure in the soil-epikarst voids. These assumptions, if not satisfied, will lead to higher equilibrium partial pressures. A large part of variability in drip water composition observed in the cave is explained by different degassing stages.

Water composition at several cave pools confirms that drip water rapidly achieves equilibrium with cave atmosphere after impact on the stalagmite apex, while oversaturation is retained longer. Water leaving cave environment towards the phreatic zone has been estimated to be in equilibrium with cave atmosphere and calcite during summer but retaining an oversaturation equal to $\text{SI}_\text{C} = 0.6$ during winter.

The difference of DIC between the solution entering and leaving the cave represents the total inorganic carbon lost by the solution in form of calcite precipitate and carbon dioxide degassed to cave atmosphere. Splitting between these last two terms can be accomplished using the difference of calcium content of the two solutions.

Once defined the concentrations these have been converted into fluxes by unit of surface using an average effective infiltration of 497 mm year^{-1} or $1.6 \times 10^{-5} \text{ L m}^2 \text{ s}^{-1}$.

The resulting flux of carbon dioxide degassing from drip water is in the range of $0.03\text{--}0.06 \text{ } \mu\text{mol m}^{-2} \text{ s}^{-1}$. These values are similar to the results estimated in Chap. 6 confirming that despite large number of assumptions made in both approaches there is confidence that results are correct.

References

- Appelo CAJ, Postma D (2006) *Geochemistry, groundwater and pollution*. AA Balkema Publishers, Leiden
- Atkinson TC (1977) Carbon dioxide in the atmosphere of the unsaturated zone: An important control of groundwater hardness in limestones. *J Hydrol* 35:111–123
- Beddows PA, Schwarcz HP, Zhang R, Ford DC (2008) Cave-drip monitoring as a foundation for better paleoclimate reconstruction. In: Elliott WR (ed) *Proceedings of the 18th national cave and karst management symposium*, St. Louis, Missouri, 8–12 Oct 2007, pp 204–211
- Benavente J, Vadillo I, Carrasco F, Soler A, Liñán C, Moral F (2010) Air carbon dioxide contents in the Vadose Zone of a Mediterranean Karst. *Vadose Zone J* 9:1–11
- Bourges F, Mangin A, d’Hulst D (2001) Le gaz carbonique dans la dynamique de l’atmosphère des cavités karstiques : l’exemple de l’Aven d’Ornac (Ardèche). *Comptes Rendus de l’Académie des Sciences - Series IIA - Earth and Planetary Science* 333:685–692
- Dreybrodt W (2008) Evolution of the isotopic composition of carbon and oxygen in a calcite precipitating $\text{H}_2\text{O}\text{--}\text{CO}_2\text{--}\text{CaCO}_3$ solution and the related isotopic composition of calcite in stalagmites. *Geochim Cosmochim Acta* 72:4712–4724
- Faimon J, Ličbinská M (2010) Carbon dioxide in the soils and adjacent caves of the Moravian Karst. *Acta Carsologica* 39:463–475
- Faimon J, Ličbinská M, Zajíček P (2012) Relationship between carbon dioxide in Balcarka Cave and adjacent soils in the Moravian Karst region of the Czech Republic. *Int J Speleol* 41:1–8
- Ford DC, Williams PW (2007) *Karst hydrology and geomorphology*. Wiley, London
- Genty D, Baker A, Massault M, Proctor C, Gilmour M, Pons-Branchu E, Hamelin B (2001) Dead carbon in stalagmites: carbonate bedrock paleodissolution vs. ageing of soil organic matter. Implications for ^{13}C variations in speleothems. *Geochim Cosmochim Acta* 65:3443–3457
- Gunn J (1981) Hydrological processes in karst depressions. *Zeitschrift fur Geomorphologie* 25:313–331
- Hendy CH (1971) The isotopic geochemistry of speleothems—I. The calculation of the effects of different modes of formation on the isotopic composition of speleothems and their applicability as palaeoclimatic indicators. *Geochim Cosmochim Acta* 35:801–824
- Jassal RS, Black TA, Drewitt GB, Novak MD, Gaumont-Guay D, Nesic Z (2004) A model of the production and transport of CO_2 in soil: predicting soil CO_2 concentrations and CO_2 efflux from a forest floor. *Agric For Meteorol* 124:219–236
- Krawczyk WE, Ford DC (2006) Correlating specific conductivity with total hardness in limestone and dolomite karst waters. *Earth Surf Proc Land* 31:221–234
- Mickler PJ, Banner JL, Stern L, Asmerom Y, Edwards RL, Ito E (2004) Stable isotope variations in modern tropical speleothems: evaluating equilibrium vs. kinetic isotope effects. *Geochim Cosmochim Acta* 68:4381–4393
- Oster JL, Montañez IP, Guilderson TP, Sharp WD, Banner JL (2010) Modeling speleothem $\delta^{13}\text{C}$ variability in a central Sierra Nevada cave using ^{14}C and $^{87}\text{Sr}/^{86}\text{Sr}$. *Geochim Cosmochim Acta* 74:5228–5242

- Palmer AN (2002) Speleogenesis in carbonate rocks, in: Gabrovsek, F. (Ed.), Evolution of karst: from prekarst to cessation. Institut za raziskovanje krasa, Ljubljana, Slovenia, pp 43–59
- Parkhurst DL, Appelo CAJ (1999) User's guide to PHREEQC (version 2)—a computer program for speciation, reaction-path, 1D-transport, and inverse geochemical calculations. US Geological Survey
- Roberge J (1979) Geomorphologie du karst de la Haute-Saumons, Ile d'Anticosti, Quebec, Hamilton, Ontario
- Smart PL, Friederich H (1987) Water movement and storage in the unsaturated zone of a maturely karstified carbonate aquifer, Mendip Hills, England. In: Proceeding of conference on environmental problems in Karst terranes and their solutions. National Water Wells Association, Dublin, pp 59–87
- Spötl C, Fairchild IJ, Tooth AF (2005) Cave air control on dripwater geochemistry, Obir Caves (Austria): implications for speleothem deposition in dynamically ventilated caves. *Geochim Cosmochim Acta* 69:2451–2468
- Turc L (1961) Estimation of irrigation-water requirements, potential evapotranspiration: a simple climatic formula evolved up to date. *Ann Agron* 12:13–49
- Verheyden S, Genty D, Deflandre G, Quinif Y, Keppens E (2008) Monitoring climatological, hydrological and geochemical parameters in the Père Noël cave (Belgium): implication for the interpretation of speleothem isotopic and geochemical time-series. *Int J Speleol* 37:221–234
- Vokal B (1999) The carbon transfer in karst areas—an application to the study of environmental changes and paleoclimatic reconstruction, Nova Gorica
- White WB (2007) Paleoclimate records from speleothems in limestone caves, studies of cave sediments—physical and chemical records of paleoclimate. Springer, Dordrecht, pp 135–175

Chapter 9

Calcite Deposition

Abstract Calcite precipitation rates on glass tablets located under three drip sites have been recorded monthly for around one year. Recorded rates range from 0.2 to 4.7 mg d⁻¹. Results are compared with several potential predictors including external temperature, rainfall, drip rate and composition. Differences between sites have been found to be correlated mainly to drip flow rate while only within one site correlation with calcium concentration is significant. Theoretical predicted values overestimate experimental values on average by a factor two, and fail to predict the observed correlation with drip rate. It is therefore proposed to modify the standard theory by considering an effective drip rate lower than measured drip rate by a factor Φ_1 . This factor accounts for drip water by-passing the glass tablet due to drop splashing. Best fit of experimental data is obtained when about 99.9 % of water is considered to be ejected during drop impingement. The order of magnitude is confirmed by additional laboratory experiment and comparison with literature data.

9.1 Introduction

Speleothems and more generally cave sediments are considered important proxies of terrestrial climatic conditions from late Pleistocene to Holocene. They potentially provide complementary information to other widely used paleoclimate reconstruction records such as ice and deep sea cores (White 2007; Baldini 2010).

On the other hand, the function that transform the external climate signal into stalagmite growth rate and isotopic composition is only partially understood and many factors that potentially influence the interpretation of results have still to be properly addressed.

Theoretical and experimental results on precipitation kinetics of calcium carbonate provides estimate on precipitation rates which could be expected also in natural environment (Curl 1973; Plummer et al. 1978; Buhmann and Dreybrodt 1985a, b; Dreybrodt and Buhmann 1991; Dreybrodt 1999; Kaufmann 2003;

Baldini et al. 2008; Dreybrodt 2008; Dreybrodt and Romanov 2008). However there are relatively few works focused on cross-validation of these models prediction (i.e. growth rates) with experimental results (Baker and Smart 1995; Baker et al. 1996, 1998; Genty et al. 2001a). The main obstacle is the lack of simultaneous long term data on growth rates and factors influencing it (e.g. drip water temperature, flow and chemical composition). In fact most comparisons assume that present parameters have been valid for the growth in the recent history. This difficulty is even more severe when high resolution annual and seasonal fluctuations need to be investigated.

The theory can successfully predict growth rates and shapes of stalagmites. Recent efforts have been made towards relating the model of calcite deposition to the evolution of isotopic composition and thus providing even more sophisticated tools for interpretation of paleoclimate signals (Mühlinghaus et al. 2007; Baldini et al. 2008; Dreybrodt 2008).

In this chapter we compare almost one year of sub-seasonal measurements of calcite precipitation rate and predicted growth rate estimated from the flow rate and chemical composition of drip water. At the same time, specific conditions of experimental set-up introduce the effect of droplet splash as one of the potential ways to enhance model prediction.

9.2 Precipitation Rate Theory

The basic theory behind modelling stalagmite growth rate and shape has been detailed developed by several works of Dreybrodt and co-authors spanning several decades (Buhmann and Dreybrodt 1985a, b; Dreybrodt and Buhmann 1991; Dreybrodt 1998) and founded on the rate laws of calcite precipitation presented by Plummer et al. (1978) and early work of Franke (1965) and Curl (1973).

Based on numerical modelling of kinetics applied to different environmental conditions, precipitation rates have been estimated for laminar flow (Buhmann and Dreybrodt 1985a, b) and turbulent flow (Dreybrodt and Buhmann 1991). Calcite precipitation rate from a supersaturated film at stagnant or slow motion conditions can be approximated by the simple equation (Dreybrodt 1999; Dreybrodt and Romanov 2008):

$$R = \alpha(c - c_{eq}) \quad (9.1)$$

where R is the precipitation rate ($\text{mol cm}^{-2} \text{s}^{-1}$), c is the present concentration of calcium in the solution (mol cm^{-3}), c_{eq} is the final equilibrium concentration of calcium in the solution (mol cm^{-3}), α is the rate constant (cm s^{-1}).

Equilibrium calcium concentration depends on temperature and carbon dioxide partial pressure in the gas phase while α is a function of temperature and film thickness, but not of the partial pressure of carbon dioxide in the cave atmosphere.

Precipitation rate R can be expressed in mm per year (R') by using a molecular weight of 100, a calcite density of 2.7 g cm^{-3} and computing for the number seconds in one year:

$$R'[\text{mm year}^{-1}] = 1.168 \times 10^{10} R[\text{mol cm}^2\text{s}^{-1}] \tag{9.2}$$

In some works (Dreybrodt 1999; Kaufmann 2003), calcium equilibrium concentration is replaced by the apparent calcium concentration at equilibrium (c_{app}) in order to reflect inhibition of precipitation caused by real mineral surfaces at natural conditions. The relationship between the two calcium concentrations is given by Dreybrodt (1999):

$$c_{app} \approx \frac{c_{eq}}{\sqrt{f}} \tag{9.3}$$

In the same work is reported that the correction factor f has a typical value of 0.8.

Considering α (in laminar condition) approximated by the following temperature function valid for the range 0–30 °C (Romanov et al. 2008):

$$\alpha = (0.52 + 0.04 \cdot T + 0.004 \cdot T^2) \times 10^{-5} \tag{9.4}$$

where α is the rate constant (cm s^{-1}) and T is the temperature in centigrade.

In the case of a deposition over a finite surface wetted by a solution film originated by an unsteady source (i.e. a stalagmite under a drip site), the decrease of precipitation rate in the time and space domains have to be introduced (see Fig. 9.1).

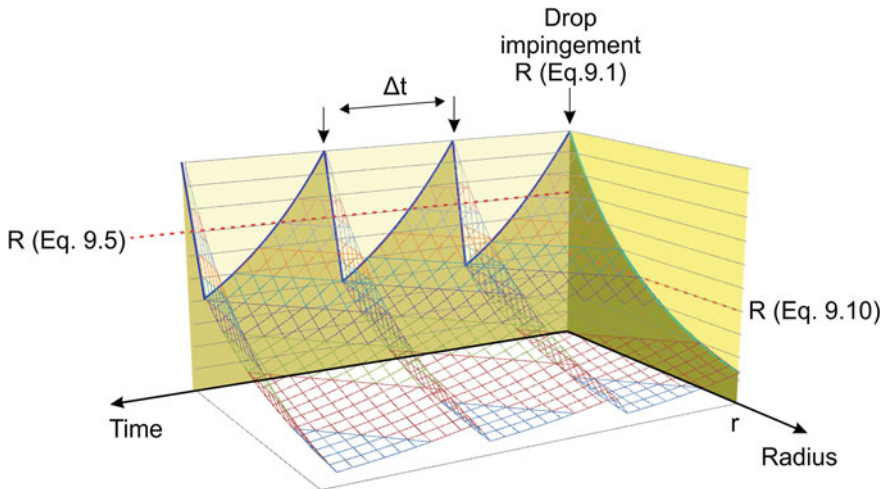


Fig. 9.1 Concept comparison of maximum precipitation rates from Eq. 9.1 and corrections for finite circular surface (Eq. 9.10) and periodic flow (Eq. 9.5)

In the time domain, Eq. 9.1 can approximate real precipitation rate only if drip rate is fast enough that a decrease in calcium concentration during the time between two successive drops of water can be neglected.

If the drip rate is slow, one has to account for the decrease of concentration in the water film at the apex of the stalagmite between two drops. Assuming the time interval between two drops is Δt and the film thickness δ , the average precipitation rate at the apex becomes (Dreybrodt 1988):

$$R = (c - c_{eq}) \frac{\delta}{\Delta t} \left(1 - e^{-\frac{\alpha}{\delta} \Delta t} \right) \quad (9.5)$$

One can easily show that when $\frac{\alpha}{\delta} \Delta t$ is small, Eq. 9.5 becomes Eq. 9.1.

Both Eqs. 9.1 and 9.2 represent a maximum precipitation rate in an infinitesimal surface around the point of droplet impact. In the case of finite surfaces, the calcium concentration in the solution decreases moving away from the drip point due to the precipitation of calcite and therefore also precipitation rates diminish.

In the case of a flat circular tablet where a pseudo continuous flow (Q_d) is spread uniformly from the centre to the periphery, assuming Eq. 9.1 valid (not turbulent flow), a general solution can be found by balancing calcite precipitation rate and calcium lost by the solution over the tablet surface. In detail we can state that for an infinitesimal small circular ring element of radius r and width dr the following mass balance must be valid:

$$\alpha(c - c_{eq})2\pi r dr = -Q_d dc \quad (9.6)$$

This differential equation can be integrated along the tablet radius:

$$\int_{c_0}^{c(r)} \frac{dc}{c - c_{eq}} = -\frac{2\pi\alpha}{Q_d} \int_0^r r dr \quad (9.7)$$

Solution of this integral gives the profile of calcium concentrations in function of the tablet radius:

$$c = c_{eq} + (c_0 - c_{eq})e^{-\frac{2\pi\alpha r^2}{Q_d}} \quad (9.8)$$

The precipitation rate is defined as amount of calcium carbonate deposited per unit of surface and per unit of time. An average precipitation rate for the whole tablet can be defined as:

$$R = \frac{Q_d(c_0 - c)}{\pi r^2} \quad (9.9)$$

Combining together Eqs. 9.8 and 9.9 we get:

$$R = \frac{Q_d}{\pi r^2} (c - c_{eq}) \left(1 - e^{-\frac{\delta}{Q_d} \pi r^2}\right) \quad (9.10)$$

In order to obtain R in moles $\text{cm}^2 \text{s}^{-1}$ than Q_d should be expressed in L s^{-1} and r in cm. Note the similarity between the Eqs. 9.5 and 9.8. If Δt is defined as the residence time of water in the film wetting the tablet surface:

$$\Delta t = \frac{V_{film}}{Q_d} = \frac{\delta \pi r^2}{Q_d} \rightarrow \frac{Q_d}{\pi r^2} = \frac{\delta}{\Delta t} \quad (9.11)$$

then Eq. 9.10 becomes Eq. 9.5.

Hence, while Eq. 9.5 represents an average precipitation rate during the interval between two drops when spatial profile can be neglected, Eq. 9.10 is an average precipitation rate over a disk surface when time evolution can be neglected.

9.3 Results

Calcite growth rates were measured for one year at three sites in Bijambare cave. The glass tablets were exposed to precipitating trickles and the deposition rates were determined based on a monthly weight measurement. Results are shown in Fig. 9.2. A few tablets were found out of correct position and therefore results are not available. Site 1 shows the slowest deposition rates with initial value of $0.013\text{--}0.015 \text{ mm year}^{-1}$ during winter season and a first peak slightly over $0.04 \text{ mm year}^{-1}$ in April. After winter season, deposition trend appears to decrease with a minimum in October ($0.005 \text{ mm year}^{-1}$) followed again by a fast rising to values over $0.04 \text{ mm year}^{-1}$ in January.

Site 2 displays a monotonous rise from initial value of $0.042 \text{ mm year}^{-1}$ to the peak of $0.126 \text{ mm year}^{-1}$ in December, and then decreasing to some extent during the following two months. It should be noted that though this site does not record any minimum in the autumn season it presents a change in the deposition rate trend during October.

Site 3 shows a positive trend from $0.027 \text{ mm year}^{-1}$ at the beginning of records to a peak of $0.083 \text{ mm year}^{-1}$ in September followed by a fast decrease to $0.043 \text{ mm year}^{-1}$ in November and then a second peak in January ($0.089 \text{ mm year}^{-1}$).

In terms of calcium carbonate the above values are equivalent to mass rate of $0.2\text{--}1.7 \text{ mg d}^{-1}$ for site 1, $1.6\text{--}4.7 \text{ mg d}^{-1}$ for site 2 and $1.0\text{--}3.3 \text{ mg d}^{-1}$ for site 3.

Early deposition is most probably influenced by initial surface conditioning and steady deposition can be assumed only when a first layer of calcite is covering the

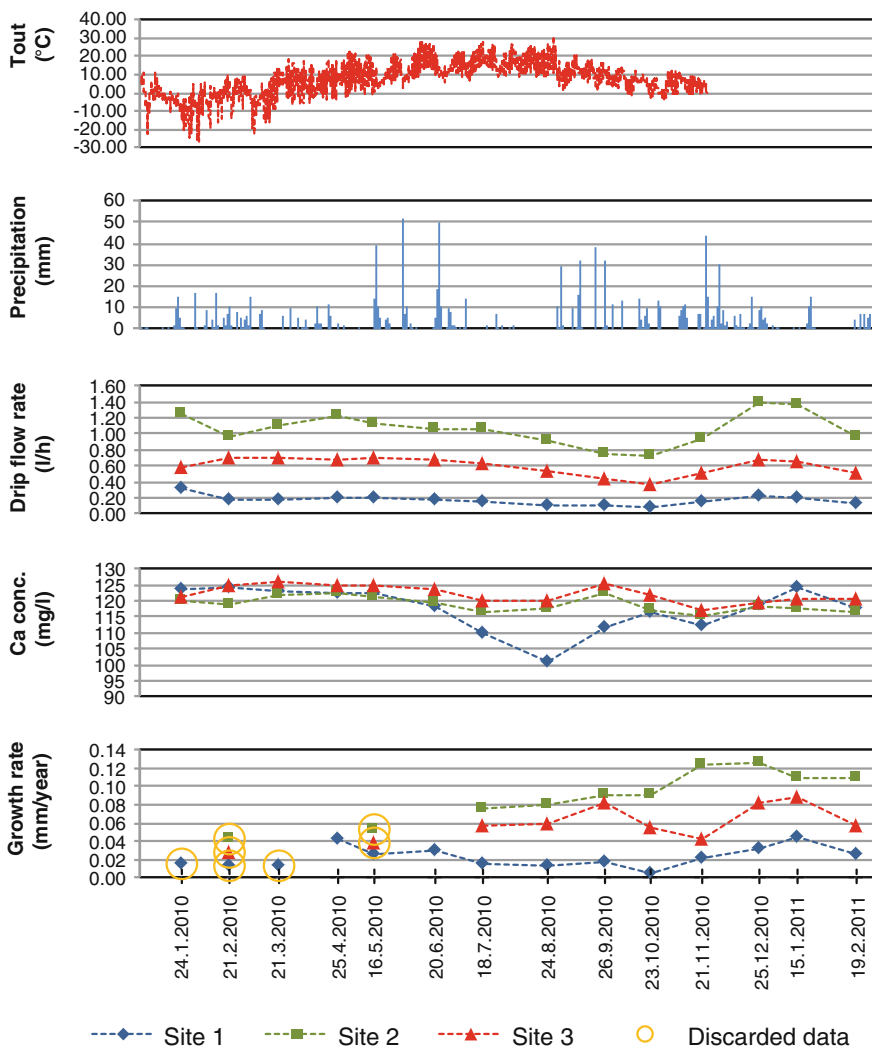


Fig. 9.2 Observed growth rates together with potential controlling factors: external temperature (T_{out}), precipitation, drip flow rate and calcium concentration in drip water

glass surface. Therefore the first three results from site 1 and first two values for sites 2 and 3 have been discarded and not further considered in this work. Descriptive statistics for deposition rate results are given in Table 9.1.

Our analysis is based on 8 reliable precipitation rate values for drip sites 2 and 3 and 11 for drip site 1 (total of 27 valid samples).

Table 9.1 Descriptive statistics for the observed growth rates

Growth rate (mm year ⁻¹) descriptive statistics	N	Minimum	Maximum	Mean	Std. deviation
All drip sites					
All samples	34	0.005	0.126	0.05332	0.034703
Without discarded samples	27	0.005	0.126	0.05967	0.035577
Drip site 1					
All samples	14	0.005	0.045	0.02271	0.011783
Without discarded samples	11	0.005	0.045	0.02518	0.012205
Drip site 2					
All samples	10	0.042	0.126	0.09020	0.028217
Without discarded samples	8	0.075	0.126	0.10087	0.019075
Drip site 3					
All samples	10	0.027	0.089	0.05930	0.020271
Without discarded samples	8	0.043	0.089	0.06588	0.016462

9.4 Discussion

9.4.1 Parameters Controlling Calcite Deposition

In this section we compare results of drip water analysis from Sect. 8.2.1 and surface climatic conditions from Sects. 2.1.4 and 5.2.2 to the available deposition rates. The determined deposition rate is cumulative result of several varying parameters acting during the entire exposition time of the tablet.

For our analysis we have taken the average values of hourly temperatures and daily amount of rain between two weightings of the tablets. Average drip flow and calcium concentration at two consecutive weightings is taken for these two parameters.

For a screening of statistical dependence between growth rates and potential predictors we have used the Spearman’s rank correlation coefficient. The use of this statistical method does not limit the relationship to a linear function and does not imply assumptions on population distribution (e.g. normal distribution). A time shift (delay) is reported to enhance correlation between external and underground parameters (Baldini et al. 2008). This transfer function has not been considered in this study.

The correlation coefficients and their significance between all potential predictors and the growth rate as dependent variable are presented in Table 9.2.

The statistical analysis indicates a high significant correlation between growth rates (samples from all sites) and the drip flow rates. On the other hand, when researching for control factors within a single drip site data series (intra-site), this relationship is retained only for drip site 1.

Sites 2 and 3, based on available data, show no significant correlation with flow. Similarly, Banner et al. (2007) found a direct correlation between mean growth rate

Table 9.2 Spearman's rank correlation coefficient and significance between growth and several predictors

		All drip sites	Site 1	Site 2	Site 3
T _{out} (average between sampling)	Correlation coef.	-0.045	-0.357	-0.872	0.700
	Sig. (2-tailed)	0.860	0.385	0.054	0.188
	N	18	8	5	5
Rain (average between sampling)	Correlation coef.	0.033	-0.041	0.181	0.000
	Sig. (2-tailed)	0.872	0.905	0.668	1.000
	N	27	11	8	8
Ca (average of two sampling)	Correlation coef.	0.210	0.863	-0.129	0.361
	Sig. (2-tailed)	0.294	0.001	0.761	0.379
	N	27	11	8	8
Flow (average of two sampling)	Correlation coef.	0.929	0.826	0.446	0.405
	Sig. (2-tailed)	<0.001	0.002	0.268	0.320
	N	27	11	8	8

and mean drip rate at several sites in central Texas (U.S.A), but only weak dependency when intra-site data were analysed. Drip site 1, when considered alone, shows also a highly significant correlation with calcium concentration. In contrast with Banner's work, at Bijambare, measured growth rates do not appear to be directly correlated with external climatic conditions. However this can depend by the fact that the number of observation in this study is much lower.

It should be noted again that flow and calcium concentration are obtained averaging only two measurements during a period of 20–30 days and therefore the obtained value may be not representative of the real conditions during the whole tablet residence in the cave. This may create large scattering and therefore hide significant correlation under a random error.

9.4.2 Predicted Growth Rates

The available data also allow direct comparison of measured and theoretically predicted growth rates at the three sites. The latter can be calculated from Eqs. 9.1, 9.5 and 9.10 (depending if time and spatial evolutions have to be considered) using the results of chemical analysis of the drip water.

We will proceed first by showing that, based on drip frequency and flow recorded at Bijambare sites and the glass tablets dimension used in the experiment,

the corrections introduced by Eqs. 9.5 and 9.10 to the precipitation rates given by Eq. 9.1 are negligible.

The assumption that the drip rates are high enough to neglect the temporal variations of concentration in the water film at the apex can be exactly tested verifying that:

$$\Delta t \ll \frac{\delta}{\alpha} \tag{9.12}$$

For a drip interval that is 20 % of the decay period $\delta\alpha^{-1}$, the difference between Eqs. 9.1 and 9.5 is already within 10 % (Baker et al. 1998). Considering a film thickness of 0.01 cm and $\alpha = 8.8 \times 10^{-6} \text{ cm s}^{-1}$ (calculated by Eq. 9.4 at 5.7 °C) it results a characteristic decay period of 1136 s. Typical drip intervals recorded at the sites never exceed 10 s and therefore Eq. 9.5 can be safely simplified into Eq. 9.1.

Equation 9.10 foresees a dependency of growth rate on the drip flow rate but only for relatively low dripping rates. Figure 9.3 depicts dependency of growth rate towards flow considering the ratio between Eq. 9.10 and Eq. 9.1 for $\alpha = 8.8 \times 10^{-6} \text{ cm s}^{-1}$ and $r = 4 \text{ cm}$. It should be noticed that also in this case, considering that recorded flow at Bijambare cave was always higher than 0.08 L h^{-1} , the rates provided by Eq. 9.1 should be acceptable.

We have shown that, for the conditions investigated, the Eqs. 9.5 and 9.10 can be approximated by Eq. 9.1. Hence by applying Eq. 9.1, the predicted growth rates are independent from drip flow and therefore in contrast with the strong correlation found between measured deposition rate and flow.

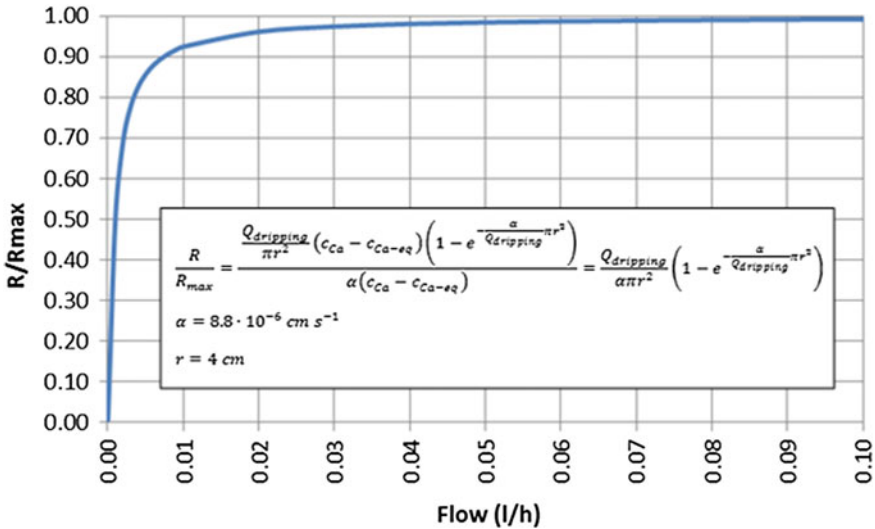


Fig. 9.3 Ration between precipitation rates foreseen by Eqs. 9.10 and 9.1 at different drip flow. Tablet radius is fixed to $r = 4 \text{ cm}$ and rate constant is fixed for all points to $\alpha = 8.8 \times 10^{-6} \text{ cm s}^{-1}$

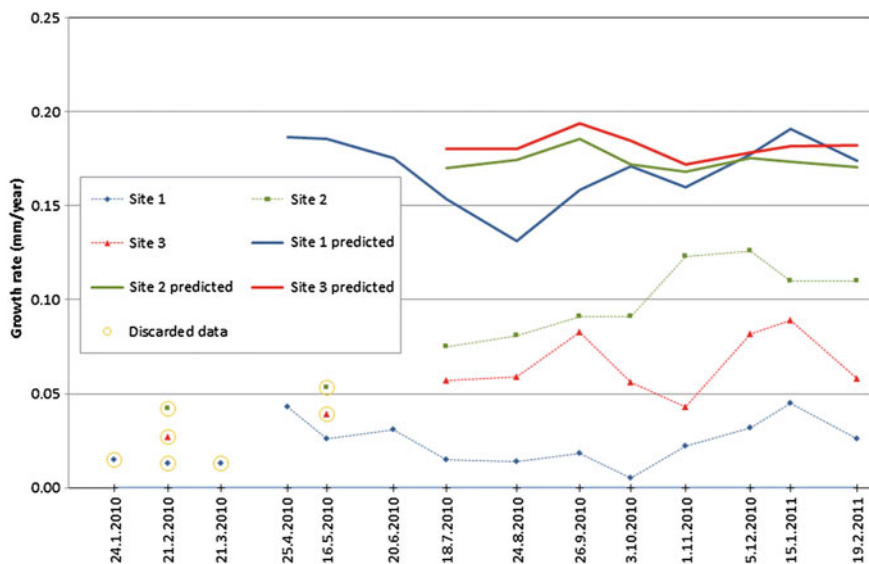


Fig. 9.4 Measured growth rates and theory predictions versus time. Expected growth rates have been calculated by Eq. 9.1 from field data of calcium concentration and drip rate. Tablet radius is fixed to $r = 4$ cm and calcium equilibrium concentration is set to $c_{eq} = 50$ mg L⁻¹. Rate constant is constant for all points to $\alpha = 8.8 \times 10^{-6}$ cm s⁻¹

Precipitation rates can be obtained from Eq. 9.1 using an equilibrium Ca concentration (corrected by Eq. 9.3) at equilibrium of 50 mg/L (average between corrected concentrations at equilibrium with carbon dioxide partial pressure equivalent to 600 and 2000 ppm) and α equal to 8.8×10^{-6} cm s⁻¹ are in the range of 0.15–0.20 mm year⁻¹ with almost no difference between drip sites (see Fig. 9.4).

These results are almost double than values recorded experimentally. Although 2–3 times overestimation error is reported in literature (Baker et al. 1996) and it is also comparable with original error stated for kinetics coefficients in Plummer et al. (1978), it is clear that other factors are controlling the calcite deposition rate during the experiments with tablets.

9.4.3 Impact of Droplet Splashing on the Measured Deposition Rates

Although early introduced by Curl (1973) and then reminded by other authors (Baker et al. 1996; Mühlinghaus et al. 2007) the effect of drop splashing on stalagmite apex remains still nowadays largely understudied and its impact neglected.

Based on field observations (Fig. 9.5a, b), during the impact of a water drop on the glass surface, a certain amount of water is immediately splashed away having short if not at all time for calcite deposition.

In order to partially account for this phenomenon we propose a simple modification of Eq. 9.10 by reducing the measured drip rates for a constant factor \varnothing_1 , so that $Q_{d-eff.} = \varnothing_1 \cdot Q_d$. Considering this new effective drip flow $Q_{d-eff.}$ we get:

$$R = \frac{Q_{d-eff.}}{\pi r^2} \cdot (c - c_{eq}) \left(1 - e^{-\frac{\alpha}{Q_{d-eff.}} \pi r^2} \right) \tag{9.13}$$

where \varnothing_1 is considered constant and it represents the “first splash function” in the sense of Curl (1973). Rigorously, Eq. 9.13 assumes that flow over the surface is constant. It does not consider that, by proceeding far from the point of impingement, solution ejected due to drop impact gradually returns to merge with the remaining flowing stream. However, due to the small dimensions of plates used in the experiment, this process is negligible and almost totality of ejected solution ends outside the tablet. In his work, Curl (1973) also foresaw a “second splash function” accounting for partial mixing of the drop and thin layer solutions during impact and consequently originating a solution with an intermediate concentration. This second

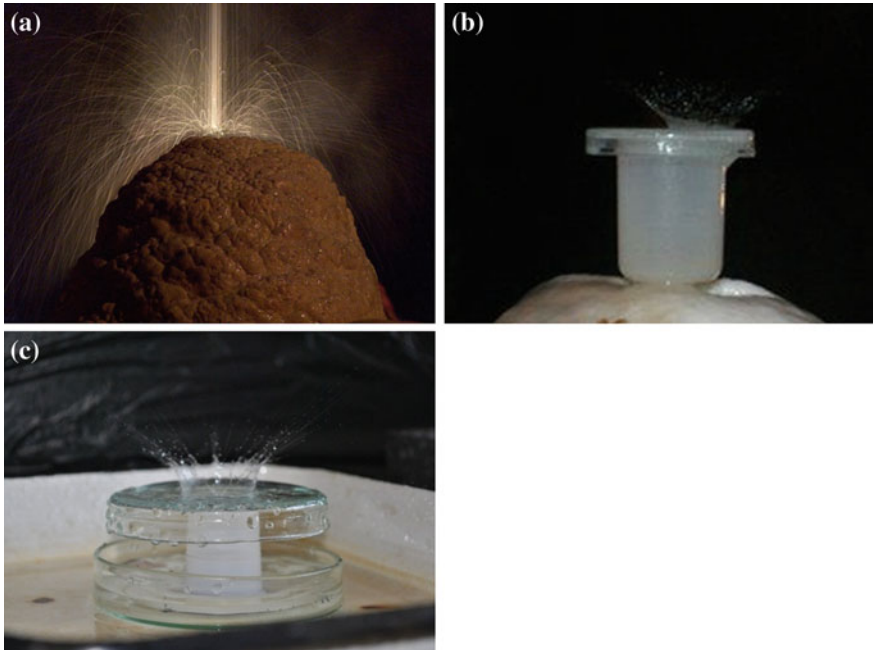


Fig. 9.5 Droplet impingement: **a** Natural conditions: drip water over a stalagmite. **b** Cave experimental set-up: drip water over a glass tablet. **c** Laboratory experimental set-up: water over a glass tablet

splash function has not been considered for the interpretation of Bijambare cave results but it is for example implemented by Mühlinghaus et al. (2007) in a model attempting to link stalagmite growth and isotopic fractionation.

In the present work, it has been assumed that, though Eq. 9.13 is developed from Eq. 9.1 and therefore it strictly applies only to stagnant or slow motion films it can be extended to turbulent conditions (at least in a narrow range of variation of calcium concentration) by considering an adequate increase of the α value.

It should be noted that by decreasing the effective flow, the dripping time period has not been changed and therefore Eq. 9.12 is still satisfied and decay of growth rate between two subsequent drops can be neglected.

The best fitting of experimental results ($R^2 = 0.83$) with Eq. 9.13 (see Figs. 9.6 and 9.7) is obtained for values of \varnothing_1 of 1.0×10^{-3} and α equal $10.7 \times 10^{-6} \text{ cm s}^{-1}$. It is evident how the new predictions are now able to describe differences between sites and partially reflect also intra-site seasonal dynamics. As comparison, Genty et al. (2001a) found agreement between several measured and predicted growth rates with a R^2 in the range of 0.69 and 0.81.

The required value of the rate constant in order to best fit results is only 20 % higher than values predicted by Eq. 9.4, and this increase is fully justified by better mass transfer created by highly turbulent conditions. For turbulent flows, Dreybrodt (1999) reported increase in deposition rate up to one order of magnitude.

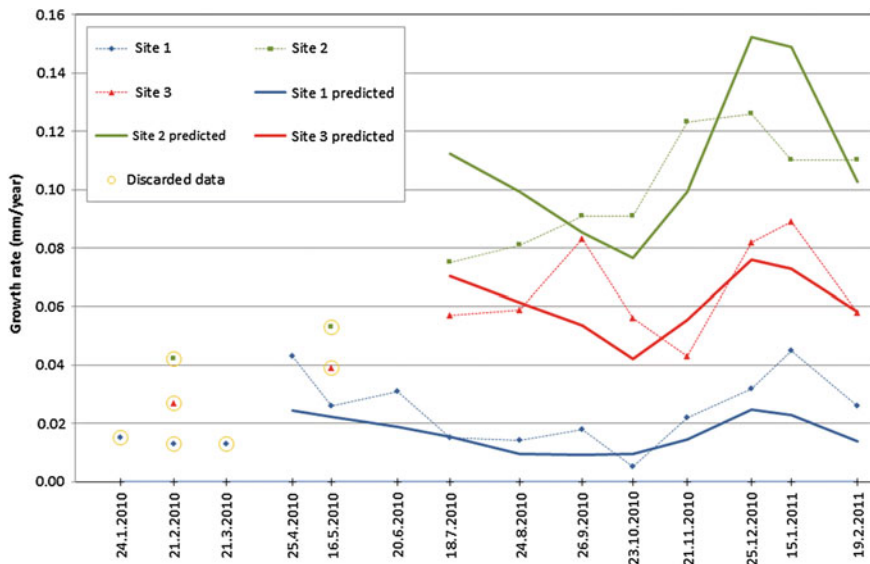


Fig. 9.6 Measured growth rates and theory predictions versus time. Expected growth rates have been calculated by Eq. 9.13 from field data of calcium concentration and drip rate. Tablet radius is fixed to $r = 4 \text{ cm}$ and calcium equilibrium concentration is set to $c_{\text{eq}} = 50 \text{ mg L}^{-1}$. Best fitting with experimental data ($R^2 = 0.83$) is obtained for \varnothing_1 of 1.0×10^{-3} and α equal $10.7 \times 10^{-6} \text{ cm s}^{-1}$

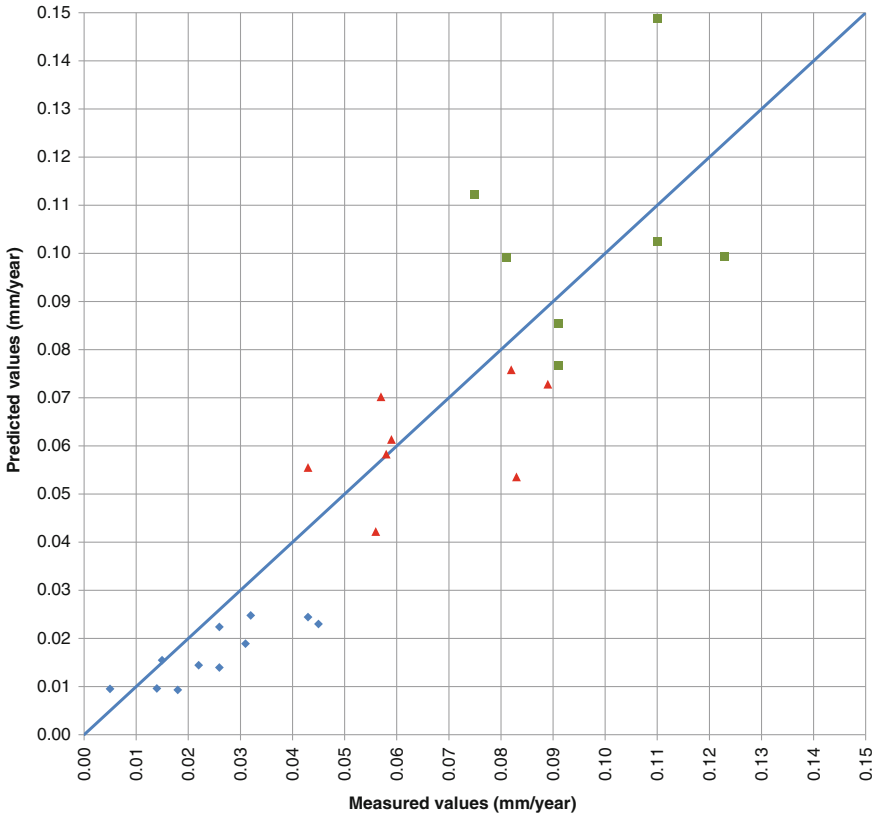


Fig. 9.7 Theory predictions versus measured growth rates. Presented values are the same as for Fig. 9.5

The ratio between effective and total dripping flow as low as one to thousand is unexpected. To verify the relevance of this we performed a set of experiments. To do this we created an artificial drip site in the laboratory (Fig. 9.5c), with variable drop height and discharge.

As targets, the same tablets were used as in the cave (not sand blasted). An additional set of tests has been performed using a convex glass tablet ($r = 4.5$ cm and approximate curvature radius $r_c = 11$ cm). Below a tablet another reversed tablet (i.e. container) with slightly larger diameter was placed to collect the water.

Flow rates and corresponding \varnothing_{1-lab} were calculated from the collected and total volumes and the duration of the experiment. The tests have been performed at different fall heights and they have been conducted at laboratory temperature (20 °C).

The value of \varnothing_{1-lab} factor (see Fig. 9.8) depends on drop impingement dynamics and it is influenced by several parameters (van Hinsberg 2010, p. 10) among which the most important for the studied conditions are:

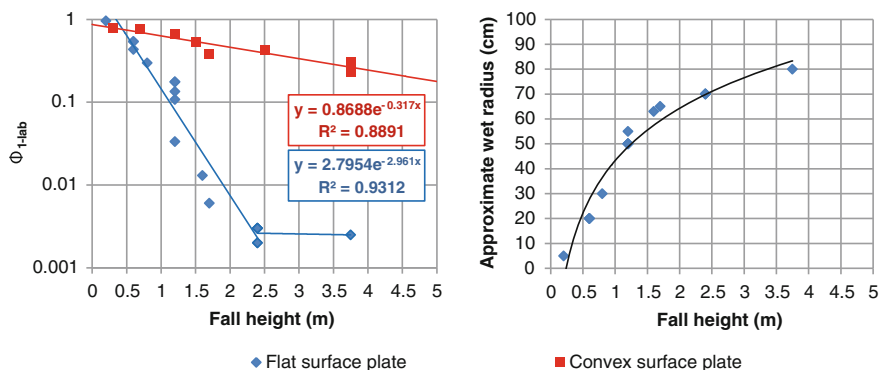


Fig. 9.8 Laboratory values for the parameter ϕ_{1-lab} using flat and convex glass tablets. Approximate wet radius is given for information only and it is obtained by visual identification of the radius containing majority of fallen secondary droplet after splashing

- Fall height
- Convex or flat tablet surface
- Tablet diameter
- Drip rate

Fall height

Increasing the vertical path of the droplet raises drop kinetic energy to be dissipated during the impact and therefore it increases the amount of ejected water and the distance at which this is projected. However at very high elevation, droplet velocity will approach terminal velocity making further increase in fall height irrelevant. Based on cave measured flow rates ($0.08\text{--}4.00\text{ L h}^{-1}$) and dripping frequency (from roughly $0.2\text{--}5\text{ drop s}^{-1}$), the resulting drop volume is between 0.1 and 0.2 mL equivalent to a droplet radius of around 3 mm. A typical drop volume of 0.1 mL has been assumed in several works (Dreybrodt 1999; Kaufmann 2003; Dreybrodt and Romanov 2008). Verheyden and co-authors analyzed 5-years data on drip rate and flow and concluded that for 94 % of cases drop volume was constant at 0.14 mL (Verheyden et al. 2008). A radius larger than 1 mm has limited influence on the falling drop velocity (Wang and Pruppacher 1977) unless for much higher radius when droplet become unstable. Terminal velocity is around 9 m s^{-1} and already by falling from 3–4 m height, the droplet reaches around 80 % of the final velocity (Wang and Pruppacher 1977). To further increase to 99 % of terminal velocity are necessary in total around 12 m. Since distance between stalactite and stalagmite at selected cave drip sites is in the range of 4–5 m it has been expected that differences in splash behavior between the sites are negligible and therefore the same value of ϕ_1 can be used for all three sites.

In laboratory tests, an exponential decrease of ϕ_{1-lab} with fall height has been obtained. For a flat tablet, the values for the ratio between runoff water and total

dripping water from vertical falls of 4–5 m (the values in Bijambare cave) are in the magnitude of 10^{-3} . This result is in agreement with the value obtained from analysis of calcite precipitation rates by Eq. 9.13. Drop impingement dynamics are frequently correlated to the drop Weber number. This non-dimensional parameter compares drop kinetic energy with its surface energy and is defined as follow:

$$We_d = \frac{\rho v^2 2r}{\sigma} \quad (9.14)$$

where ρ is the liquid density, v is the impact velocity, r the drop radius and σ is the liquid surface tension.

Kalantari (2006, p. 88) performed several experiments to define the dynamics of spray impact onto flat wet surfaces. He measured the secondary-to-incident mass ratio (equivalent to $1 - \varnothing_{1-lab}$) for different constant impact Weber numbers and film thickness. It results an average decrease of \varnothing_{1-lab} from 0.9 ($We_d = 40$) to 0.2 ($We_d = 141$). At Bijambare, considering a water drop with density of 1000 kg m^{-3} , $r = 3 \text{ mm}$, surface tension of 0.075 N m^{-1} and impact velocity of approximately 8 m s^{-1} (5 m fall), we get a value for We_d of 5120. These conditions are largely outside the range investigated by Kalantari but considering the general trend, values presented in Fig. 9.8 appear to be reasonable.

Convex or flat tablet surface

If the ratio of the drop diameter to the radius of curvature of the impact surface (convex tablet) is very small, then the effect of the surface curvature on the impingement dynamic over a dry surface can be neglected. Under these conditions, surface curvature should not be a factor influencing impingement process (van Hinsberg 2010, p. 12). Conversely, impingement process on a wet surface depends in a rather complex way to the liquid film thickness (Kalantari 2006, p. 88) and this depends from surface curvature.

In fact, the use of a convex tablet surface instead of a flat surface enormously affects the results of laboratory tests by increasing the underflow collection (see Fig. 9.8). Apparently this is related to a more readily evacuation of liquid from the drop impact point in convex tablets leaving less amount of available water to be ejected during the following drop impingement. Non perfect centering of convex tablet apex with the drop impact point causes drop to hit a slightly inclined instead of a perpendicular surface and may introduce another factor reducing total ejected water.

Tablet diameter and drip rate

Although increase of diameter should be beneficial in intercepting again part of the splashed water, this for small diameters under examination appeared to be almost negligible (few tests performed with 7 and 9 cm diameter did not held significant differences from the standard 8 cm tablet).

The experiments have been performed at different drip (and flow) rates. The result, namely \varnothing_{1-lab} , does not depend strongly on the flow rate. However, based

on limited available data, it cannot be excluded that there is an influence of drip rate on \varnothing_{1-lab} but surely, if it exists, it is less important compared to changes caused by increase fall or tablet shape.

9.4.4 Impact of the Incomplete Solution Equilibration Process on the Measured Deposition Rates

There is another mechanism that can potentially affect the experimental growth rates, decreasing them with respect to the maximum values given by the theory described in Sect. 9.2. As suggested by Dreybrodt (2012) commenting the experimental results published by Day and Henderson (2011), the oversaturation level of the solution has to be sufficiently high in order to sustain maximum precipitation rates. Because initial degassing of carbon dioxide from the solution takes several seconds before it completes and equilibration of the ionic species requires a time one order of magnitude greater, high saturation conditions may not be achieved at drop impingement point but later during the radial film flowing. There is no sufficient data to exclude completely or to quantify the importance of this phenomenon during the performed experiments in Bijambare cave. However, as evident from Fig. 8.1, the measured calcite Saturation Index of the impinging solution appears to be rather high and generally double than other experiments where such phenomenon has been suggested as explanation for low precipitation rates (Hansen et al. 2013).

9.5 Conclusions

Deposition rates between 0.2 and 4.7 mg d⁻¹ have been recorded in one year period based on regular monthly measurements of glass tablets weight under three drip sites. These values (equivalent to 0.05–0.126 mm year⁻¹ growth) show significant correlation with drip flow and only for the site with lowest drip rate, also with calcium concentration. This comes to a conflict with the theoretical predictions, which predict that the growth rate is independent on the drip rate in conditions like ours (high drip frequency and small tablet radius). This inconsistency has been solved by introducing a correction factor accounting for the water lost by droplet splashing due to high falling distance. Best fit of experimental deposition rate data is obtained with $\alpha = 10.7 \times 10^{-6}$ cm s⁻¹, which is in good agreement with the literature. The introduced correction coefficient requires that 99.9 % of water is by-passing the glass tablet due to droplet splash. This result is in agreement with our laboratory results, which gave correction factor with the same order of magnitude for a 4–5 m high drop on a flat glass tablet. For convex surface water lost factor could be as low as only few tens of per cent.

References

- Baker A, Smart PL (1995) Recent flowstone growth rates: field measurements in comparison to theoretical predictions. *Chem Geol* 122:121–128
- Baker A, Genty D, Barnes WL (1996) Recent stalagmite growth rates: cave measurements, theoretical predictions and the environmental record, climate change: the karst record. *Karst Waters Inst Spec Publ* 2:7–9
- Baker A, Genty D, Dreybrodt W, Barnes WL, Mockler NJ, Grapes J (1998) Testing theoretically predicted stalagmite growth rate with recent annually laminated samples: implications for past stalagmite deposition. *Geochim Cosmochim Acta* 62:393–404
- Baldini JUL (2010) The geochemistry of cave calcite deposits as a record of past climate. *Sediment Rec* 8(2):4–9
- Baldini JUL, McDermott F, Hoffmann DL, Richards DA, Clipson N (2008) Very high-frequency and seasonal cave atmosphere PCO₂ variability: implications for stalagmite growth and oxygen isotope-based paleoclimate records. *Earth Planet Sci Lett* 272:118–129
- Banner JL, Guilfoyle A, James EW, Stern LA, Musgrove M (2007) Seasonal variations in modern speleothem calcite growth in central texas, U.S.A. *J Sediment Res* 77:615–622
- Buhmann D, Dreybrodt W (1985a) The kinetics of calcite dissolution and precipitation in geologically relevant situations of karst areas: 1. Open system. *Chem Geol* 48:189–211
- Buhmann D, Dreybrodt W (1985b) The kinetics of calcite dissolution and precipitation in geologically relevant situations of karst areas: 2. Closed system. *Chem Geol* 53:109–124
- Curl RL (1973) Minimum diameter stalagmites. *Bull Nat Speleol Soc* 35:1–9
- Day CC, Henderson GM (2011) Oxygen isotopes in calcite grown under cave-analogue conditions. *Geochim Cosmochim Acta* 75:3956–3972
- Dreybrodt W (1988) Processes in karst systems—physics, chemistry and geology, vol 5., Springer Series in Physical Environment, Springer, Berlin
- Dreybrodt W (1998) Limestone dissolution rates in karst environments. *Bull d’Hydrogeologie* 16:167–183
- Dreybrodt W (1999) Chemical kinetics, speleothem growth and climate. *Boreas* 28:347–356
- Dreybrodt W (2008) Evolution of the isotopic composition of carbon and oxygen in a calcite precipitating H₂O–CO₂–CaCO₃ solution and the related isotopic composition of calcite in stalagmites. *Geochim Cosmochim Acta* 72:4712–4724
- Dreybrodt W (2012) Comment on “Oxygen isotopes in calcite grown under cave-analogue conditions” by C.C. Day and G.M. Henderson. *Geochim Cosmochim Acta* 85:383–387
- Dreybrodt W, Buhmann D (1991) A mass transfer model for dissolution and precipitation of calcite from solutions in turbulent motion. *Chem Geol* 90:107–122
- Dreybrodt W, Romanov D (2008) Regular stalagmites: the theory behind their shape. *Acta Carsologica* 37:175–184
- Franke WH (1965) The theory behind stalagmite shapes. *Stud Speleol* 1:89–95
- Genty D, Baker A, Vokal B (2001) Intra- and inter-annual growth rate of modern stalagmites. *Chem Geol* 176:191–212
- Hansen M, Dreybrodt W, Scholz D (2013) Chemical evolution of dissolved inorganic carbon species flowing in thin water films and its implications for (rapid) degassing of CO₂ during speleothem growth. *Geochim Cosmochim Acta* 107:242–251
- Kalantari D (2006) Characterization of liquid spray impact onto walls and films. TU Darmstadt, Darmstadt
- Kaufmann G (2003) Stalagmite growth and palaeo-climate: the numerical perspective. *Earth Planet Sci Lett* 214:251–266
- Mühlinghaus C, Scholz D, Mangini A (2007) Modelling stalagmite growth and δ¹³C as a function of drip interval and temperature. *Geochim Cosmochim Acta* 71:2780–2790

- Plummer LN, Wigley TML, Parkhurst DL (1978) The kinetics of calcite dissolution in CO₂—water systems at 5° to 60 °C and 0.0 to 1.0 atm CO₂. *Am J Sci* 278:179–216
- Romanov D, Kaufmann G, Dreybrodt W (2008) $\delta^{13}\text{C}$ profiles along growth layers of stalagmites: comparing theoretical and experimental results. *Geochim Cosmochim Acta* 72:438–448
- van Hinsberg N (2010) Investigation of drop and spray impingement on a thin liquid layer accounting for the wall film topology. TU Darmstadt, Darmstadt
- Verheyden S, Genty D, Deflandre G, Quinif Y, Keppens E (2008) Monitoring climatological, hydrological and geochemical parameters in the Père Noël cave (Belgium): implication for the interpretation of speleothem isotopic and geochemical time-series. *Int J Speleol* 37:221–234
- Wang PK, Pruppacher HR (1977) Acceleration to terminal velocity of cloud and raindrops. *J Appl Meteorol* 16:275–280
- White WB (2007) Paleoclimate records from speleothems in limestone caves, studies of cave sediments—physical and chemical records of paleoclimate. Springer, Dordrecht, The Netherlands, pp 135–175

Chapter 10

The Isotopic Imprint

Abstract Stable isotope ratios (such as $^{13}\text{C}/^{12}\text{C}$) change slightly between the main compartments of an element earth cycle because of fractionation processes. These changes, although small, are statistically significant and they can be nowadays clearly distinguished by mass spectrometry. When this tool is used in conjunction with concentration or flux measurements, further insights can be gained into the sources and sinks of CO_2 in the ecosystem. A preliminary investigation of the carbon stable isotopic composition of the DIC from drip water samples show similar results from two campaigns realized during summer and winter respectively. The calcite deposited over glass tablets left in place almost one year under the same drip sites returns $\delta^{13}\text{C}$ values around 1.5 ‰ higher than in the drip water DIC. $^{13}\text{C}/^{12}\text{C}$ ratios measured directly in samples of the cave air is significantly different during winter and summer sampling campaign, due to the different cave ventilation conditions. A simple mass balance of the cave system applied to carbon dioxide and carbon isotopes predicts that cave air isotopic composition is a linear function of the inverse of carbon dioxide concentration (Keeling's plot). Observed summer and winter $\delta^{13}\text{C}$ values can be explained by an ideal mixing between a typical canopy air and a pure carbon dioxide source (degassing) with average $\delta^{13}\text{C}$ of -16.2 ‰.

10.1 Introduction

An isotope is “one of two or more atoms with the same atomic number but with different numbers of neutrons” (Anon., n.d.). If the decay half-life is extremely long such that it has never been observed then the isotope can be considered stable. Although the chemical properties of an atom are governed mainly by the number of protons and therefore do not change in large extent between isotopes of the same element, the slight dissimilarities in mass have a minor influence on physical-chemical properties with differences in kinetics and equilibrium constants.

Therefore, the proportion between stable isotopes concentrations changes slightly between the main compartments of an element earth cycle because of

fractionation processes. These changes, although small, are statistically significant and they can be nowadays clearly distinguished using specialized instrumentation.

As stated by Ghosh and Brand, “*the oxygen and carbon isotopic compositions of individual components, in particular air-CO₂, provide a potentially powerful tool towards quantifying the contribution of different components to ecosystem exchange. When this is used in conjunction with concentration or flux measurements, further insight can be gained into the sources and sinks of CO₂ in the ecosystem*” (Ghosh and Brand 2003).

The aim of this chapter is to present the basic mechanisms at the origin of the ¹³C stable isotope signatures in the composition of carbon dioxide in the cave atmosphere, DIC in drip water and calcium carbonate in speleothems. The results of a small set of isotope analyses are also presented and discussed and despite the limited extension they provide further understanding on inorganic carbon path within the karst vadose zone integrating results discussed in previous chapters.

10.2 The Carbon Stable Isotopic Composition of Drip Water

Carbon dioxide originated by biodegradation and root respiration in soil layer is depleted of the heavier stable isotope ¹³C. The shift toward a lighter composition depends on the metabolic pathway used by different vegetation types. C3 plants, that follow the Calvin photosynthetic cycle and they are typical of temperate climate, produce a soil air carbon dioxide with $\delta^{13}\text{C}$ usually ranging between -26 and -20 ‰ as reported and reviewed by several works (Hendy 1971; Cerling 1984; Spötl et al. 2005; Benavente et al. 2010; Frisia et al. 2011). Conversely, C4 vegetation species diffused in arid climatic conditions generate lower ¹³C depletion in the range -16 to -10 ‰ (Hendy 1971; Cerling 1984). The variations of measured isotopic concentrations in soil atmosphere are often attributed to the invasion of external atmosphere (isotopic heavier) and described by a two components mixing model (Spötl et al. 2005; Benavente et al. 2010; Frisia et al. 2011).

Water in contact with the carbon dioxide rich atmosphere in the soil layer dissolves CO₂ and equilibrates its DIC content both in terms of chemical and isotopic species. Proceeding downstream, this original isotopic imprint is then transformed by the limestone dissolution process occurring between soil and cave.

The isotopic composition of dissolved carbon in percolating water depends largely if the solution equilibrium with gas phase and limestone is reached through open or closed system conditions (see Sect. 4.3). In the first case the solution isotopic composition tends to equilibrate continuously with isotopic light gas phase, largely counteracting the changes driven by the introduction of isotopic heavier carbon from limestone dissolution. Theoretically, if enough contact time is allowed, no residual imprint from bedrock composition should be left in the percolating solution (Baker et al. 1997; McDermott 2004).

Conversely, in a closed system, the inorganic carbon introduced in the solution by limestone dissolution cannot be exchanged any longer with the isotopic light gas phase and therefore the final solution will achieve a higher $\delta^{13}\text{C}$. Of course transitional conditions between the “open system” and “closed system” end members will originate intermediate isotopic compositions.

Once solution enters in contact with an atmosphere characterized by a lower $p\text{CO}_2$, degassing of dissolved carbon dioxide rapidly starts followed by the re-equilibration of ionic species in the solution and in particular by the slow conversion of HCO_3^- into CO_2 (Buhmann and Dreybrodt 1985a, 1985b; Dreybrodt 1988; Dreybrodt and Scholtz 2011). Degassing provides enrichment of solution in the heavier ^{13}C isotope due to kinetic and equilibrium fractionation.

Recently Dreybrodt and Scholtz (Dreybrodt and Scholtz 2011) have modelled the processes governing the evolution of ^{13}C isotopic composition from soil atmosphere to the calcite precipitate on speleothem. They have found that, for a perfectly closed system, the final isotopic composition after degassing to equilibrium with the cave atmosphere is almost invariant with the concentration of calcium in the solution. In other words, incomplete equilibrium between limestone and water will not affect the final isotopic composition. Furthermore isotopic composition is also not significantly influenced by soil carbon dioxide partial pressure. However, in an open or partially closed system the dependence of final composition on the calcium concentration has to be considered.

The first fast release of carbon dioxide to cave atmosphere occurs without changes in calcium concentration in the solution but with an increase of the calcite saturation index because both bicarbonate conversion and calcium carbonate deposition are much slower processes. It follows that on the apex of a stalagmite or immediately after splashing of the drop, when first precipitation of calcite occurs, the fast degassing of carbon dioxide and therefore the related ^{13}C enrichment is already completed. Therefore the first calcite left on the stalagmite tip will be in isotopic equilibrium with this “degassed” solution. Because for each molecule of calcite a molecule of carbon dioxide has to be released further slow concomitant precipitation and degassing occurs moving away from apex along the stalagmite profile. This process drives further ^{13}C enrichment and creates a $\delta^{13}\text{C}$ increase along one deposition layer.

10.3 Results

Stable isotopic analyses (^{13}C and ^{18}O) have been performed on:

- water samples collected at Drip Sites 1, 2, 3 (same as for chemical analyses in Chap. 8) and at one drip site located in the Main Channel;
- air samples collected in proximity to the above mentioned drip sites;

Table 10.1 Results of isotopic analysis performed on air, water and carbonate samples during summer and winter sampling campaigns

	$\delta^{13}\text{C}$		$\delta^{18}\text{O}$	
	August	December	August	December
<i>Water</i>				
Drip site 1	-11.72	-11.75	-10.97	-
Drip site 2	-	-11.89	-	-
Drip site 3	-12.28	-12.01	-10.99	-
Drip site Main Channel	-12.07	-	-11.04	-
	August	December	August	December
<i>Air</i>				
Drip site 1	-	-11.71	-	-
Drip site 2	-13.93	-10.86	-	-
Drip site 3	-15.88	-11.49	-	-
Drip site main channel	-14.52	-	-	-
<i>Calcium carbonate</i>				
Glass plate at drip site 1 a	-10.20		-7.73	
Glass plate at drip site 1 b	-10.21		-7.64	
Glass plate at drip site 2 a	-10.65		-7.87	
Glass plate at drip site 2 b	-10.66		-7.81	
Glass plate at drip site 3 a	-10.75		-7.84	
Glass plate at drip site 3 b	-10.81		-7.77	
Bed rock	2.57		-3.13	

- two series of three tablets used for calcite precipitation experiments described in Chap. 9 and
- One sample of limestone bedrock.

Sampling (except for bedrock and tablets which are representative of almost yearly cumulative conditions) have been repeated twice, one during August 2010 (summer conditions) and one during December 2010 (winter conditions). Results are given in Table 10.1. Stable oxygen isotope results are presented but not discussed.

10.4 Discussion

Drip water samples have an average $\delta^{13}\text{C}$ value of -12.0‰ (6 measurements; standard deviation 0.2‰). Based on the figures provided by Dreybrodt and Scholtz (Dreybrodt and Scholtz 2011) for a perfectly closed system at 10 °C (and a limestone with $\delta^{13}\text{C} = 1\text{‰}$), this drip water isotopic composition would be derived from a soil $\delta^{13}\text{C}$ of around -22.0‰ with negligible influences by soil and cave pCO_2 (400–2000 ppm in Bijambare) and degree of calcium carbonate saturation achieved

by the solution. This soil composition appears realistic considering that in Bijambare only C3 vegetation is present. This value represents the minimum $\delta^{13}\text{C}$ in the soil because moving toward an open system the heavy ^{13}C isotope enrichment will be lower.

It is interesting to note that, although the number of samples is limited, there is no evident difference between summer and winter values of $\delta^{13}\text{C}$ in percolating water, at least not manifest as found by other authors (Spötl et al. 2005).

On the other hand it can be noticed in both series (winter and summer), a weak correlation between drip site and isotopic composition, where $\delta^{13}\text{C}$ increases moving from Site 3, Site 2 and Site 1. This could be related to site-specific paths in the soil-epikarst or, considering that this drip site order reflect also the increase drip flow rate, it may be inferred a positive correlation between heavier isotope concentration and flow (the drip site on the Main Channel has flow rate intermediate between Site 3 and Site 1). This later correlation could be explained for example with a lesser residence time available at the soil/limestone interface where open system conditions occurs, and consequently lesser time to achieve isotopic re-equilibration.

The carbonate deposit on the glass plates has an average $\delta^{13}\text{C}$ value of -10.5‰ (6 measurements; standard deviation 0.3‰). Also in this case, in analogy with drip water, a trend with the concentration of heavier isotope increasing moving from Site 3 to Site 2 and then Site 1 is recorded.

The isotopic composition recorded on glass tablets, considering the fast dripping interval, represents calcite in equilibrium with the drip water. Fractionation coefficient between bicarbonate and calcite is rather small, and in accordance with the approach used by Frisia et al. (2011), can be neglected.

The difference between drip water (-12.0‰) and calcite (-10.5‰) isotope composition can be attributed to the fact that drip water collected have not yet completed the degassing of all dissolved carbon dioxide to equilibrium with cave atmosphere pCO_2 . Therefore further degassing will occur during drop splashing driving additional ^{13}C isotopic enrichment. This is supported by drip water data presented in Fig. 8.1 where most of results show equilibrium partial pressure of carbon dioxide above cave atmosphere maximum (in average around 5500 ppm). Extrapolating figures given by Dreybrodt and Scholtz (Dreybrodt and Scholtz 2011), the ^{13}C enrichment promoted by differences in cave atmospheres carbon dioxide concentration between 5500 ppm and 600 ppm is in the order of magnitude of 1‰ .

The cave atmosphere has an average $\delta^{13}\text{C}$ value of -13.1‰ with significantly larger seasonal variations than drip water and calcite deposits (6 measurements; standard deviation 2.0‰). There are important differences between sampling sites but the relationship between isotopic composition and spatial distribution is unclear and mostly related to local air flow paths.

On the other hand it is evident that the winter sampling campaign provided samples more enriched in heavier ^{13}C isotope. This is in agreement with the more intense cave ventilation and consequent mix of cave air (^{13}C depleted) and external atmosphere (^{13}C rich).

A ^{13}C steady state balance in the cave is formulated below, introducing few important simplifications and using notation wherever possible in accordance to Chap. 6.

J_S (the natural input of carbon dioxide per unit of cave plan surface) is assumed uniform over the whole cave and Q (the volumetric air flow rate entering the “Music Hall”) equal to the flow entering the cave from the external atmosphere. The whole balance can be written as:

$$J_S S_{cave} = Q(C_{cave} - C_{atm}) \quad (10.1)$$

where S_{cave} is the total cave plan surface and by using the $\delta^{13}\text{C}$ notation:

$$\delta^{13}\text{C}_{input} J_S S_{cave} = Q(\delta^{13}\text{C}_{cave\ air} C_{cave} - \delta^{13}\text{C}_{atm\ air} C_{atm}) \quad (10.2)$$

Where $\delta^{13}\text{C}_{input}$ is the isotopic enrichment of the carbon dioxide entering the cave degassing from drip water, $\delta^{13}\text{C}_{cave\ air}$ and $\delta^{13}\text{C}_{atm\ air}$ are the isotopic enrichment in the cave atmosphere and external atmosphere respectively. By coupling the two balances (Eq. 10.1 and Eq. 10.2) results:

$$\delta^{13}\text{C}_{input} = \frac{(\delta^{13}\text{C}_{cave\ air} C_{cave} - \delta^{13}\text{C}_{atm\ air} C_{atm})}{C_{cave} - C_{atm}} \quad (10.3)$$

That can be expressed as:

$$\delta^{13}\text{C}_{cave\ air} = (\delta^{13}\text{C}_{atm\ air} - \delta^{13}\text{C}_{input}) \frac{C_{atm}}{C_{cave}} + \delta^{13}\text{C}_{input} \quad (10.4)$$

Equation 10.4 describes a linear dependence of cave air $\delta^{13}\text{C}_{cave\ air}$ with the inverse of carbon dioxide concentration in the cave atmosphere $\left(\frac{1}{C_{cave}}\right)$. This linear relationship represents the mixing of two end members: from one side the external atmosphere (with its carbon dioxide concentration C_{atm} and isotopic composition $\delta^{13}\text{C}_{atm\ air}$) and on the other side a pure carbon dioxide source from degassing (with isotopic composition $\delta^{13}\text{C}_{input}$). This is the theoretical base of a Keeling’s mixing plot (Pataki et al. 2003). According to data presented in Chap. 6, it has been assumed that during sampling in august, carbon dioxide concentration in the cave atmosphere was 2000 ppm while in December was 600 ppm. The relative Keeling’s plot is presented in Fig. 10.1 together with similar plots from several works presented in literature (Spötl et al. 2005; Kowalczyk and Froelich 2010; Benavente et al. 2010; Frisia et al. 2011; Tremaine et al. 2011).

The linear regression of Bijambare data in the Keeling’s plot gives information of the two end members expected composition. Regarding the external atmosphere composition the line is passing through the typical range of variation for a canopy air centred around 505 ppm and $\delta^{13}\text{C} = -10.7\text{‰}$ (Tremaine et al. 2011). On the other extreme, Bijambare data predict a significantly heavier isotope composition

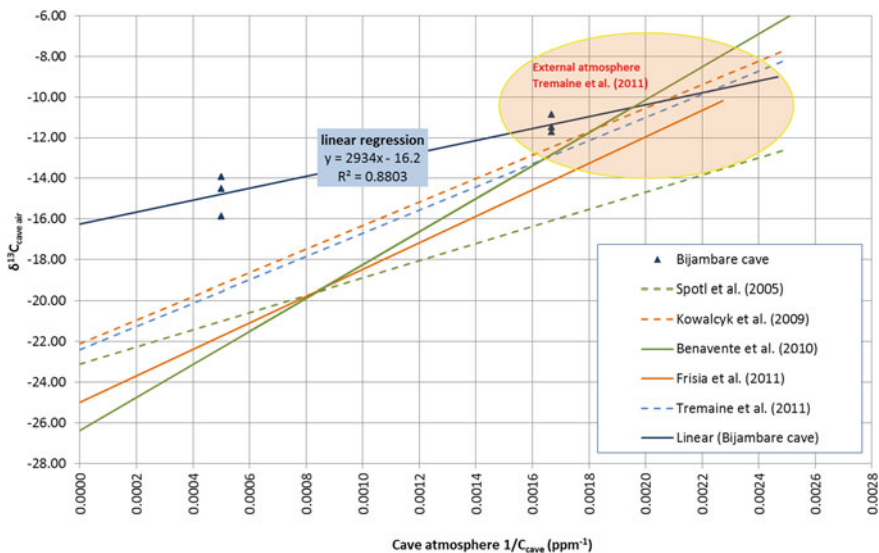


Fig. 10.1 Keeling’s mixing plot ($\delta^{13}C$ vs. $1/C_{\text{cave}}$). Together with Bijambare data and their linear regression, are reported results from several available literature sources

(-16.2 ‰) for a pure carbon dioxide source ($C = \infty$) than other literature works (from -22 to -26 ‰).

Although there is no evident reason why the isotopic composition of the carbon dioxide source for soil atmosphere and cave atmosphere should be the same, almost all authors found that composition of soil, cave and external atmospheres lies on the same line in the Keeling’s plot (Kowalczyk and Froelich 2010; Benavente et al. 2010; Frisia et al. 2011; Tremaine et al. 2011). Assuming that this is valid also for Bijambare, it can be expected a soil atmosphere isotopic composition around -16 ‰ . This is not unrealistic. It has been shown before that in closed system DIC isotopic composition found in drip water can be originated by soil atmosphere with $\delta^{13}C = -22.0 \text{ ‰}$. If the uncompleted degassing is considered and therefore the heavier isotopic composition of calcite layer on glass tablet is used instead of drip water DIC composition, the soil atmosphere should be around -19 ‰ . The remaining difference to -16 ‰ could be explained by the presence of partially open system conditions.

10.5 Conclusions

A preliminary investigation of carbon stable isotopes composition in DIC from drip water samples show similar results from two campaigns completed during summer and winter respectively. The calcite deposited over glass tablets left in place almost

one year under the same drip sites returns $\delta^{13}\text{C}$ values around 1.5 ‰ higher than in the drip water DIC. This difference could be explained by the fact that sampled water has not fully completed the degassing of dissolved carbon dioxide to equilibrium with cave atmosphere.

^{13}C content in cave air is significantly different during winter and summer sampling campaign due to the different cave ventilation conditions. A simple mass balance of the cave system applied to carbon dioxide and ^{13}C predicts that cave air isotopic composition is a linear function of the inverse of carbon dioxide concentration (Keeling's plot). Obtained values summer and winter values for $\delta^{13}\text{C}$ can be explained by an ideal mixing between a typical canopy air and a pure carbon dioxide source (degassing) with average $\delta^{13}\text{C}$ of -16.2 ‰.

References

- Anon (n.d.) WordNet search [Online]. Available at <http://wordnetweb.princeton.edu/perl/webwn?s=isotope>. Accessed 18 April 2012
- Baker A, Ito E, Smart PL, McEwan RF (1997) Elevated and variable values of ^{13}C in speleothems in a British cave system. *Chem Geol* 136:263–270
- Benavente J, Vadillo I, Carrasco F, Soler A, Liñán C, Moral F (2010) Air carbon dioxide contents in the Vadose Zone of a Mediterranean Karst. *Vadose Zone J* 9:1–11
- Buhmann D, Dreybrodt W (1985a) The kinetics of calcite dissolution and precipitation in geologically relevant situations of karst areas: 1. Open system. *Chem Geol* 48:189–211
- Buhmann D, Dreybrodt W (1985b) The kinetics of calcite dissolution and precipitation in geologically relevant situations of karst areas: 2. Closed system. *Chem Geol* 53:109–124
- Cerling TE (1984) The stable isotopic composition of modern soil carbonate and its relationship to climate. *Earth Planet Sci Lett* 71:229–240
- Dreybrodt W (1988) Processes in karst systems—physics, chemistry and geology. Springer series in physical environment, vol 5. Springer, Berlin
- Dreybrodt W, Scholz D (2011) Climatic dependence of stable carbon and oxygen isotope signals recorded in speleothems: from soil water to speleothem calcite. *Geochim Cosmochim Acta* 75:734–752
- Frisia S, Fairchild IJ, Fohlmeister J, Miorandi R, Spötl C, Borsato A (2011) Carbon mass-balance modelling and carbon isotope exchange processes in dynamic caves. *Geochim Cosmochim Acta* 75:380–400
- Ghosh P, Brand WA (2003) Stable isotope ratio mass spectrometry in global climate change research. *Int J Mass Spectrom* 228:1–33
- Hendy CH (1971) The isotopic geochemistry of speleothems—I. The calculation of the effects of different modes of formation on the isotopic composition of speleothems and their applicability as palaeoclimatic indicators. *Geochim Cosmochim Acta* 35:801–824
- Kowalczk AJ, Froelich PN (2010) Cave air ventilation and CO_2 outgassing by radon-222 modeling: how fast do caves breathe? *Earth Planet Sci Lett* 289:209–219
- McDermott F (2004) Palaeo-climate reconstruction from stable isotope variations in speleothems: a review. *Quatern Sci Rev* 23:901–918
- Pataki DE, Ehleringer JR, Flanagan LB, Yakir D, Bowling DR, Still CJ, Buchmann N, Kaplan JO, Berry JA (2003) The application and interpretation of Keeling plots in terrestrial carbon cycle research. *Global Biogeochem Cycles* 17:22/1–22/14

- Spötl C, Fairchild IJ, Tooth AF (2005) Cave air control on dripwater geochemistry, Obir Caves (Austria): Implications for speleothem deposition in dynamically ventilated caves. *Geochim Cosmochim Acta* 69:2451–2468
- Tremaine DM, Froelich PN, Wang Y (2011) Speleothem calcite farmed in situ: Modern calibration of $\delta^{18}\text{O}$ and $\delta^{13}\text{C}$ paleoclimate proxies in a continuously-monitored natural cave system. *Geochim Cosmochim Acta* 75:4929–4950

Chapter 11

General Conclusions

11.1 Summary of the Inorganic Carbon Fluxes in the Unsaturated Zone

Figure 11.1, presents the conceptual scheme early described in Sect. 4.5 with a summary of data obtained during this work directly by field measurements or indirectly through modeling and mass balances.

Drip water appears to have been originated from a parent solution with an equilibrium carbon dioxide partial pressure in the range 15,000–26,000 ppm. By assuming an effective infiltration of 497 mm year^{-1} the consequent DIC flux in the percolating water is around $0.10\text{--}0.13 \mu\text{mol m}^{-2} \text{ s}^{-1}$. By stoichiometry, DIC should be composed in almost equal part by carbon from carbon dioxide originated by biological degradation of organic matter and carbon originally in the form of calcium carbonate (limestone rock). However, even if the overall fluxes do not change, due to partial re-equilibration under open conditions the final DIC is likely to be enriched of carbon from organic origin (only visible due to different isotopic imprint).

This solution approaches equilibrium with the cave atmosphere (carbon dioxide around 550–2200 ppm) by degassing $0.03\text{--}0.06 \mu\text{mol m}^{-2} \text{ s}^{-1}$ of carbon dioxide and precipitating $0.02\text{--}0.03 \mu\text{mol m}^{-2} \text{ s}^{-1}$ of calcium carbonate. The remaining solution feeds the karst aquifer and eventually the karst spring with a residual flux of DIC of $0.04 \mu\text{mol m}^{-2} \text{ s}^{-1}$.

By modeling of variations of carbon dioxide concentration in the cave atmosphere, the natural input of CO_2 in the cave atmosphere is estimated at around $0.62 \mu\text{mol m}^{-2} \text{ s}^{-1}$ during the winter season, and up to more than $12.40 \mu\text{mol m}^{-2} \text{ s}^{-1}$ during the first temperature falls at the end of summer. These peak values have been found to be related to the cave ventilation rate (ultimately linked to the external climatic conditions) and dependent on the availability of CO_2 in the surrounding environment. For airflow close to zero, the values of J_S seem to converge to a few $0.01 \mu\text{mol m}^{-2} \text{ s}^{-1}$. This last value can be used to estimate the average input flux and

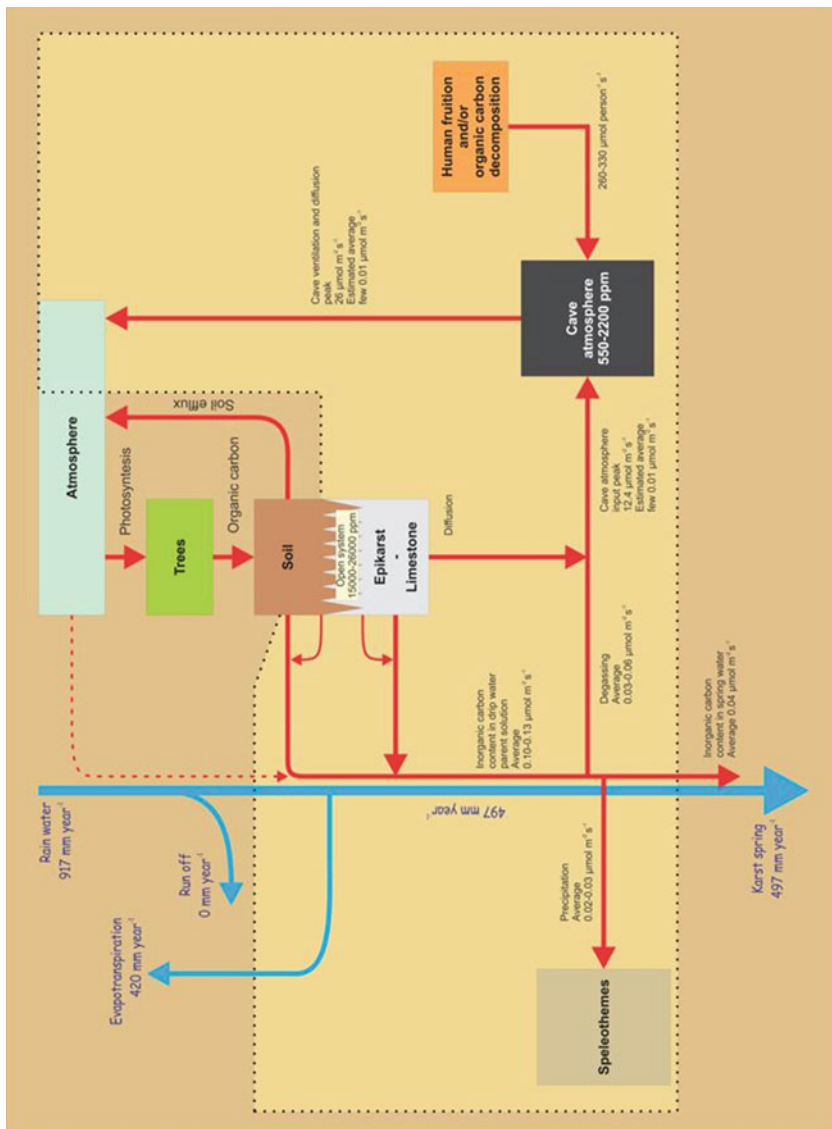


Fig. 11.1 Summary plot of inorganic carbon fluxes at Bijambare cave

is in good agreement with values found from dripping water degassing and confirming that despite large number of assumptions made in both approaches there is confidence that results are fundamentally corrected. Potential anthropogenic contribution is estimated around 0.45 and 0.35 $L_{CO_2} \text{ min}^{-1} \text{ person}^{-1}$.

11.2 Scale-Up to Global Level

The set of data obtained in this work refers to only a specific location while the processes involved are sensitive to climatic conditions, geology and several other factors so that a generalization to a global scale is rather speculative. However, Bijambare cave should not be far from typical average conditions, and the field measurements are well within the variability published in literature for other caves, therefore, despite anisotropy and uneven characteristics of worldwide karst, it is assumed that obtained carbon fluxes can be used as average values for global karst areas. The extension of karst worldwide is around $20\text{--}22 \times 10^6 \text{ km}^2$. Based on extrapolation of fluxes obtained at Bijambare, the amount of carbon which evades the unsaturated zone due to caves or cracks respiration is around $0.3 \text{ PgC year}^{-1}$ in the same order of magnitude of several other inland carbon fluxes.

Likewise, the expected flux of carbon released at karst springs is also $0.3 \text{ PgC year}^{-1}$ not far from the estimation of $0.4 \text{ PgC year}^{-1}$ for the global DIC flowing in the world due to carbonate rock weathering (Farquhar et al. 2001).

What it should be noticed is that carbon evasion due to unsaturated zone respiration is a different flux than the soil efflux because of different governing processes, occurring more concentrated (at point sources such as caves or rock discontinuities) and often emerging after a medium to long underground path. It is largely unlikely that sites aimed to measure soil efflux would catch also unsaturated zone respiration and therefore this flux is probable mostly unaccounted in the global carbon balance.

11.3 Open Questions and Further Research Possibilities

In this work the whole cave atmosphere was modeled as a perfectly mixed volume. This large oversimplification was mainly caused by the availability of only one carbon dioxide measurements point.

During the last decade we have seen to a rapid growth in the availability and performance of carbon dioxide probes based on infrared technology and a parallel drop of their costs. The long term deployment in remote underground regions coupled with a high sampling rate is still challenging due to relatively high energy consumption but the development of new generation of light and high storage capacity batteries is also solving this issue. It is therefore expected that soon, will be feasible to install underground a large network of carbon dioxide sensors which will

provide information on cave atmosphere composition with high space and time resolution. This will allow more complex modeling of air exchange dynamics to be tested.

In fact, complexity of model describing carbon dioxide input, transport and storage within complex geometries rapidly rises requiring a larger amount of data in order to calibrate and validate the results.

During model implementation several groups of parameters, which are difficult to be measured accurately, had to be estimated. Among this, geometrical dimensions of underground passages are the most evident. Speleological survey can provide only a rough estimation of these numbers but more sophisticated techniques involving 3D laser scanning may prove to be more reliable.

Volume of compartments or other remaining undetermined factors in models can be estimated by using ad hoc experiments where known quantities of carbon dioxide (or eventually other tracers) are released underground under controlled conditions. The experiment performed during this work provided usefully information to test model predictions and the correctness of assumptions. However, similar tests in different settings and more controlled environment will prove to be even more useful in future.

The analysis of carbon dioxide concentration in the cave atmosphere suggested that variations are mainly related to the air exchange between cave and external atmosphere (and therefore related with cave climate) or at least that variations induced by changes in the input flux of carbon dioxide from epikarst play a minor role (mostly only at seasonal level). One of the interesting features is that the model predicts a clear dependence of the input carbon dioxide in the cave atmosphere by the ventilation rate suggesting the presence of a variable buffer zone surrounding the cave passages. This zone provides means for fast carbon dioxide replenishment and it is involved in the underground atmosphere dynamics at different extent depending on ventilation penetration capacity. This buffer zone appears also to have a finite regeneration capacity so that contribution in function of ventilation rate follows a hysteresis curve linked with replenishment and depletion events history. Further studies and data are surely needed to prove this process and they may provide useful information on carbon dioxide storage and transport in the region surrounding the cave atmosphere.

Drip water analyses provided an invaluable tool to investigate conditions in the epikarst region by reconstructing the parent solution composition. Unfortunately, differently from air, continuous analysis of water is still limited to few parameters. Therefore sampling has to be carried out manually at relatively large time intervals and most of analysis performed offsite. The relatively small amount of data collected during this study allow to compare carbon dioxide released to cave atmosphere by degassing with air exchange model prediction only on average level and based on a very small spatial mesh. In order to appreciate seasonal effects and spatial distribution it will be necessary a much longer (multiple years) sampling campaign duration, a high sampling rate and larger number of investigated sites.

Investigation of calcite deposition on glass plates put in evidence deposition rates much lower than predicted by present theory. In this study it has been shown

how experimental results may be fitted by theory if water lost by drop splashing is taken into account. These results, if confirmed may open new questions on the impact of drop impingement dynamics on the calcite deposition profile and consequently on the theoretical equilibrium shape of a stalagmite. Falling of secondary (generated by primary drop splashing) droplets which retain original oversaturation at variable distance away from stalagmite apex may originate flat top stalagmites and provide a different isotopic profile along a deposition layer.

Reference

Farquhar GD, Fasham MJR, Goulden ML, Heimann M, Jaramillo VJ, Khashgi HS, Le Quéré C, Scholes RJ, Wallace DWR (2001) The carbon cycle and atmospheric carbon dioxide. In: Houghton JD, Ding Y, Griggs DJ, Noguer M, van der Linden PJ, Dai X, Maskell K, Johnson CA (eds) *Climate change 2001: the scientific basis. Contribution of working group I to the third assessment report of the intergovernmental panel on climate change*. Cambridge University Press, Cambridge, p 881